High Density Microelectrode Arrays for *In vitro* Retinal Studies

Deborah Gunning

UNIVERSITY
of
GLASGOW

Department of Physics and Astronomy

Thesis submitted for the degree of Doctor of Philosophy in the subject of physics

July 10, 2007

To my family

Abstract

Neurophysiologists traditionally studied the behaviour of individual neurons by measuring their extracellular signalling on a single electrode. This PhD has involved developing a technology to enable the behaviour of populations of neurons in the retina to be studied. By recording simultaneously from hundreds of neurons a much greater insight into retinal processing and encoding is achievable. To this end, a large area, high density, transparent microelectrode array, of unprecedented dimensions, was manufactured on a glass/indium tin oxide (ITO) substrate. This state-of-the-art device has 519 hexagonally close-packed, 5 μm diameter electrodes spaced by 30 μm. All channels are electrically well isolated with typical interchannel resistance and capacitance values of $\sim$200 GΩ and 1 pF respectively. Electrodes are electroplated with platinum to form a low impedance (200 kΩ at 1 kHz) interface between the electrodes and electrolyte. Fabrication and modelling tests also proved the electrical and physical feasibility of future larger area and higher density arrays. Investigations were carried out to establish an electrode/electrolyte interface capable of delivering enough charge to directly stimulate neurons in the retina. Iridium oxide films formed by an electrochemical activation technique were found to create 5 μm diameter electrodes with 4 mC/cm^2 charge capacity and 150 kΩ (at 1 kHz) impedance which are ideal characteristics for direct electrical stimulation of neurons. The state-of-the-art microelectrode array technology developed in this thesis has allowed

amongst the most complete datasets from primate retina to be produced.

Acknowledgements

Declaration

Except where explicit reference is made to the work of others, this dissertation is the result of my own work. None of this material has been submitted for any other degree at the University of Glasgow or any other institution.

Deborah Gunning

Contents

7   Conclusions   **149**

List of Figures

List of Tables

Chapter 1

Introduction

"It is in the brain that everything takes place...it is in the brain that the poppy is red, that the apple is odorous, that the skylark sings".

A very poetic statement made by Oscar Wilde, however, it should not mislead us to believe that *"everything"* consists purely of our primary senses such as vision, hearing and olfaction. To elaborate, therefore, and delve further into science, the brain is an organ of thought. It is in the brain that reason and intelligence originate in the forms of cognition, perception, attention, memory, learning, conscience, behaviour and emotion. Without the need for conscious awareness, it has the incredible ability to perform actions such as walking, coordination of sensory systems and homeostatic bodily functions including heart rate, blood pressure and body temperature. The brain is also responsible for control of movement (motor function) and posture. Thinking carefully about the immenseness of these combined tasks, we must be amazed at the extraordinary ability and complexity of the human brain. It is hardly surprising that for millennia scientists from a variety of research fields worldwide have felt compelled and challenged to try and understand the workings of the brain.

Amongst these disciplines, psychology examines human behaviour and mental processes. Psychiatry and neurology apply knowledge obtained through neuroscience and psychology to medicine. Cognitive science seeks to unify neuroscience and psychology with other fields that concern themselves with the brain, such as computer science (artificial intelligence and similar fields) and philosophy. Neuroscience, however, is the scientific discipline concerned with studying the brain and central nervous system at a cellular level. It attempts to understand the complexity of the brain's chemical, physical and electrical structure. To this end, branches of biological (anatomy, physiology, molecular biology and biochemistry) and computational sciences are combined.

This thesis is ultimately concerned with developing a state-of-the-art enabling technology for neuroscience applications, in particular, studying the retina. To understand the requirements of this device, it is important to know and understand its application. To this end, the following paragraphs briefly describe neural systems and approaches to their study.

The human brain is a complex, 3-dimensional network of approximately 10^{10} - 10^{12} neurons or nerve cells, hence the term "neuroscience". Neurons are electrically excitable cells in the nervous system that function to process and transmit information. In vertebrate animals, neurons are the core components of the brain, spinal cord and peripheral nerves. They are typically composed of a soma, or cell body, a dendritic tree and an axon (see Figure 1.1). The majority of vertebrate neurons receive input on the cell body and dendritic tree, and transmit output via the axon.
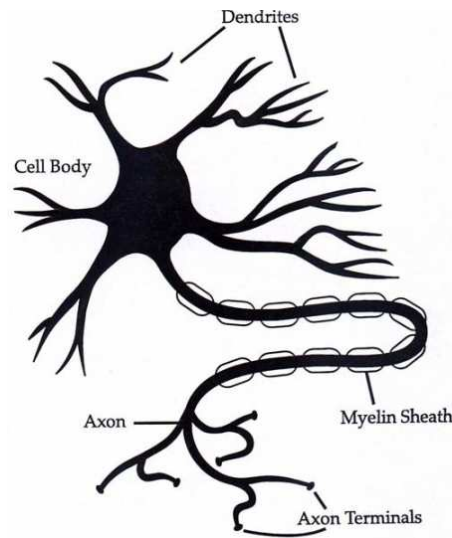
Figure 1.1: A schematic showing the components of a typical neuron: the soma (or cell body), dendrites and axon [3].

There is, however, great heterogeneity throughout the nervous system and the animal kingdom, in the size, shape and function of neurons. Neurons communicate via chemical and electrical synapses, in a process known as synaptic transmission. The fundamental process that triggers synaptic transmission is the action potential, a propagating electrical signal that is generated by exploiting the electrically excitable membrane of the neuron.

During the past century, much information has been discovered about the behaviour of individual neurons: how they carry information, transmit information and receive stimuli. Significantly less, however, is known about the interactions between these neurons in the brain and how they result in meaningful patterns of neural activity. The most prominent problem in such an investigation is the enormous number of neurons ($\sim 10^{11}$) which are networked together in the brain. Further to this, each neuron can make between

10^3 and 10^4 synaptic connections. It seems inconceivable, therefore, that we could even begin to understand such a complex structure.

Two main approaches have been adopted to simplify the task. Firstly, simpler systems are studied. Invertebrates typically have far fewer neurons than vertebrates and in some species, neurons are in fact distributed throughout the nervous systems according to their function. Also, invertebrate neurons are frequently larger than those in vertebrate systems and this supports intracellular recording [1]. A drawback, however, to this type of investigation is that only a limited insight into neural and behavioural phenomena of higher order organisms can be achieved. The second approach involves studying simpler parts of more complex brains. Regions which have been subject to significant investigation include the olfactory bulb, cerebellum (a small part of the brain responsible for fine-tuning of motor movement) and the visual system. Of these three, the visual system is probably the most thoroughly studied.

The visual system is the part of the central nervous system which is responsible for sight and Figure 1.2 shows it in schematic form. A component of this system is the retina, a thin ($\sim$200 μm in humans), flexible tissue which lines the back of the eye. Its function is to convert the visual scene into processed electrical signals which are sent to the brain via the optic nerve. It is a neural network with a planar, layered cellular structure and providing strict physiological conditions are maintained, it will remain healthy and function normally for up to 12 hours after extraction from the eye. It is also possible to excite the retina using light, its natural stimulus, unlike studies of other regions of the brain where it is difficult to recreate the exact natural

stimulus. These combined qualities lend the retina to extracellular recording studies both *in-vivo* and *in-vitro* and because of these properties, the retina is thought of as an approachable part of the brain and is of great scientific interest.
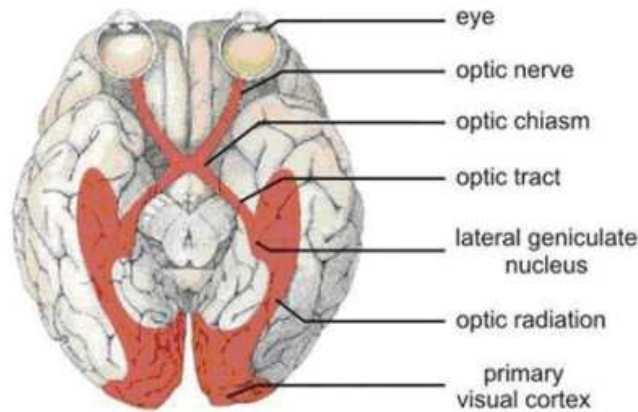
Figure 1.2: A schematic showing how the visual system is incorporated into the human head and how connections are made between the eye and the brain [4].

Historically, retinal cell recordings were made from individual cells [2]. More recent investigations [7] [8] show that neurons act in a connected fashion rather than as independent sources of information. This would suggest the need for a multichannel recording device to study the connectivity of the neurons. Preferably, a device would be required which could record over a relatively large area of the retina and from sites with a density and size similar to those of the cells being studied. Neurobiologists did not have access to this level of technology previously. However, the possibility of this research has now been realised with the emergence of interdisciplinary studies which involve the collaboration of scientists from different academic disciplines working together in pursuit of a common goal. This union of very

specialised knowledge from different research fields commonly arises in an attempt to solve a scientific problem which is beyond the limitations of each individual field.

Many research groups have adopted an interdisciplinary approach to neuronal studies. They are manufacturing microelectrode arrays for the recording, stimulation and culture of neural tissues to more fully understand the behaviour of populations of neurons. Research by Y. Jimbo is an example of leading work in this field. This work realises the benefits of planar microelectrodes for long term chronic stimulation and culturing of neurons. Arrays of 64 indium tin oxide electrodes are made on glass substrates with each electrode being 10-50 μm^2 and separated by 50-250 μm [5] [6]. Glass plates coated with transparent thin films of indium tin oxide have also been successfully used to record spike potentials from neural cultures by G.W Gross et al. To form the electrodes, 100μm^2 areas of ITO are exposed and coated with gold to reduce impedance [8] [9] [10]. Work performed by J. Pine involves growing neural cultures on thin-film microcircuits each of which provides 32 microelectrodes. The electrodes are 8 x 10 μm and have been used to record extracellular action potentials from individual neurons. Action potentials have also been evoked by stimulating neurons via these electrodes [11]. Other approaches involve active pixel sensor based electrode arrays. L. Berdondini et al. developed and use an array of 64 x 64 pixels to image *in-vitro* neuronal network electrophysiological activity. Each pixel has a dimension of 40 x 40 μm^2 and includes a gold microelectrode of 20 x 20 μm^2 [14]. Kovacs, Borkholder et al. have made and used planar 6 x 6 arrays of 10 μm diameter iridium electrodes electroplated with platinum with 100 μm pitch to study neural tissue preparations. These electrode ar-

rays were used to stimulate acutely prepared slices of spinal cord and record neuron responses and thereby study the interconnectivity of neural processes [12] [13].

An advancement on the planar electrode technologies described, is the use of arrays of silicon based probes in neural studies. The state-of-the-art in devices of this nature are manufactured by researchers at the University of Utah Health Sciences Centre (P.A. House et al.). Arrays of 10 x 10 electrodes, 1.5 mm in length and spaced by 0.4 mm, have been used successfully to probe neural tissues, recording and stimulating from populations of neurons [16]. For a similar application, K.D. Wise is involved in research which groups together devices, each with four probes, to form an array. The probes are 2 mm long and each have four microelectrodes. The probes are spaced by 150 μm and the microelectrodes by 100 μm [15].

The retinal readout project at the University of Glasgow is another prime example of interdisciplinarity. It is an international collaboration between the University of Glasgow, the University of California, Santa Cruz, the University of Krakow, Poland, and the Salk Institute for Biological Studies, San Diego. It successfully integrates semiconductor fabrication techniques, particle physics detection techniques and neurobiology in an attempt to gain a greater understanding of neural processing through retinal cell recordings.

For the past three years I have undertaken my PhD as a member of the retinal readout project in the Department of Physics and Astronomy, University of Glasgow. My part in this collaboration has been the development, manufacture and characterisation of large area, high density, planar microelectrode

arrays for *in-vitro* retinal cell studies. These form the interface between the biological tissue and the readout electronics. The following paragraphs will describe in brief, the content of this thesis.

Background theory, which is integral to understanding this work and its applications, is covered in Chapter 2. A description is firstly given of how light travels through the eye and ultimately, how the retina converts a visual image into processed electrical signals which are received by the brain. The morphology and function of the various classes of cell that comprise the retina are described. Following this, specifications of the electronics system developed at the University of California, Santa Cruz (UCSC) for simultaneous multi-channel readout from the electrode arrays are given. Information is then given on the technique for biological experimentation developed by collaborators at UCSC and the Salk Institute for Biological Studies. There are very strict conditions and precise methods which are used by the neurobiologists at the above institutions and these are described in Section 2.5.

Chapter 3 is divided into two main parts. The first part describes the principles of standard semiconductor fabrication techniques which are essential to the work undertaken in this thesis. These techniques were manipulated and combined to develop processes for the manufacture of large area, high density microelectrode arrays, of varying dimensions, on transparent glass/indium tin oxide (ITO) substrates. Initially, the process for the fabrication of arrays of 61-electrodes, with inter-electrode spacings of 60 μm, was optimised. To study a larger area of tissue and also to best imitate the density of cells in the retina, the array dimensions were altered to 519 electrodes spaced by 30 μm. Due to the significant difference in feature sizes of these arrays, different pro-

cessing techniques were needed. The processes developed to produce both types of array are described. A description of problems encountered during process development are also included.

There are many characteristics, mechanical and electrical, of a microelectrode array which contribute toward its success as a neural signal recording tool. In Chapter 4, these characteristics and methods of their measurement are described. The device of importance in this thesis is the 30 μm spacing 519-electrode array. Since, during this PhD, the 61-electrode array fabrication process was fine tuned and these arrays had previously been manufactured, characterised and used to effectively record retinal signals, it serves as a benchmark for the performance of the 30 μm spacing 519-electrode array. All measurements were therefore made for both the 61- and 519-electrode arrays to allow a suitable comparison to be made. After considerable process development, a 30 μm spacing 519-electrode array was made with characteristics entirely suitable to record electrical pulses generated by retina. The 5 μm diameter platinum electrodes on this array typically have a 200 kΩ impedance at 1 kHz. All channels are electrically well isolated with typical interchannel resistance and capacitance values of 200 GΩ and $\sim$1 pF respectively. Pilot experiments were performed with monkey retina at the Salk Institute using this array. Evidence of the arrays success as a recording device and improvement in the detection efficiency of OFF-small midget ganglion cells in these experiments is shown in the form of recorded action potentials, electrophysiological images and receptive field mappings in the final section of this chapter.

More recently, many neuroscientists have focused their studies on the stimu-

lation of retinal cells via arrays of microelectrodes, aiming to fully understand retinal cell functions as well as having applications for a retinal prosthesis. Since a current substantial enough to stimulate cells must be supplied, new problems arise. The electrodes are of small dimensions and therefore are required to repeatedly handle large current densities without exhibiting any deterioration. Chapter 5 investigates the suitability of platinum black and iridium oxide as materials for small diameter electrodes for cell stimulation. The deposition and characterisation techniques needed to form and qualify the electrode for this use are described. Iridium oxide films formed by an electrochemical activation technique were found to create 5 μm diameter electrodes with 4 mC/cm^2 charge capacity and 150 kΩ (at 1 kHz) impedance which are ideal characteristics for the direct stimulation of neurons.

The final chapter looks at further work and possible applications of the work presented in this thesis. Arrays of 60 μm spacing 1027 electrodes and 15 μm spacing 519 electrodes were fabricated and characterised as proof of principle future arrays. An electrical model of the electrode/electrolyte was adapted and used to predict electrical characteristics of future higher density and larger area arrays and promised the feasibility of arrays of thousands of electrodes. Applications of the arrays produced in this thesis were also discussed and these included cortical slice, transgenic mouse and iridium oxide electrical stimulation studies.

Chapter 2

Background theory

2.1   Introduction

The work in this thesis involves the development of a process to manufacture a high density microelectrode array for use recording, via an electronic readout system, extracellular signals from cells in the retina. This system is capable of extracting information from retinal tissue in order to understand more completely the operations of the different classes of output retinal ganglion cell.

To appreciate fully the research and its applications, this chapter provides background information on all the relevant subjects. A description of the elements constituting the electronic readout system, developed by collaborators at UCSC [17] and the University of Krakow [18], is given. The biological procedure followed to perform the retinal experiments (conducted at the Salk Institute for Biological Studies, San Diego [19]) is illustrated and described. A guide to the analysis of data produced is also given. With reference to "The First Steps in Seeing" by R.W. Rodieck [20] and "The Retina: An Ap-

proachable Part of the Brain" by J.E. Dowling [21], a concentrated narration of the functions and anatomy of the eye and its components, in particular the retina, is given.

2.2 The visual system

Ancient Greek scientists (Ptolemy and Euclid) believed our eyes to emit rays allowing us to sense our surroundings [22]. With extensive optical research, however, a 10th century Islamic mathematician, astronomer and physicist, Ibn al-Haitham, contradicted this theory of vision suggesting correctly that the rays originate from the object being observed as opposed to being from the eye of the observer [23]. Ibn al-Haitham's theory was the first step in understanding how the visual system performs and in following centuries was elaborated upon forming an accurate model of the eye and an almost complete understanding of its operation.

Since this work aims to understand aspects of the visual system, an overview of the known structure and functions of both the eye and its components is given. In particular, the retina will be discussed in detail as it is the subject of the biological experiments described in this thesis.

2.2.1 The eye

A convenient way to comprehend the operation of the eye is to journey with light as it travels from objects in our surroundings, through the eye to the brain, where it is received as electrical signals. Figure 2.1 shows the structure of a human eye and its internal components and throughout this chapter only human eyes are discussed unless otherwise stated.
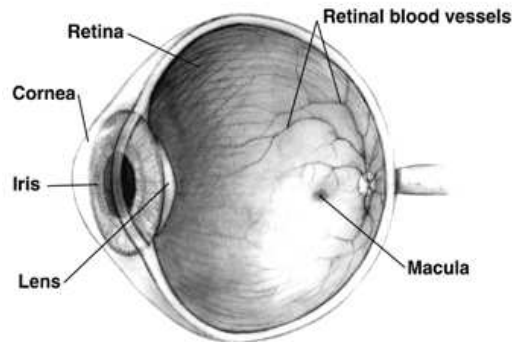
Figure 2.1: A cross sectional view of a human eye showing its components and structure [24].

The eye is an almost perfect sphere of approximately 25 mm (anterior to posterior) diameter [25] and varies only within ~1 mm between individuals. The outer surface, the sclera (white of the eye), is a tough, fibrous tissue. On the inner surface of the sclera are layers of blood vessels, named the choroid, which nourish the back of the eye. Before light from the outside world can enter, it is refracted by the cornea, a transparent layer covering the front of the eye, providing ~80% of its focusing power. This refracted light then travels through the pupil, the aperture formed by the iris in the anterior segment of the eye. By dilation or contraction of the iris, the size of the pupil varies to regulate the quantity of light permitted to enter resulting in larger pupils in dim light and smaller pupils in bright light. The aqueous humour is a thin, watery fluid occupying the anterior chamber, the space between the cornea and the iris. It is continually produced by the ciliary body, the part of the eye that lies just behind the iris. This fluid nourishes the cornea and the lens and gives the front of the eye its form and shape. The lens, which is supported by suspensory ligaments, finely focuses light entering the eye. The focused image is projected through an essentially

transparent, gelatinous matrix called the vitreous humour, onto the retina, a thin film of tissue lining the back of the eye. The vitreous humour serves to create a cushioned support for the eye and also to provide a clear pathway for incoming light. The anterior portion of this body adheres to the lens whilst posteriorly, it is attached to the inner limiting membrane of the retina (Figure 2.2). Once projected onto the retina, the visual scene undergoes analysis and a coded series of electrical signals are sent to the brain via the optic nerve.

2.2.2 The retina

Covering $\sim 72\%$ of the inner surface of the eye [26], the human retina is typically only a couple of hundred microns thick. It comprises of several classes of cells which are layered in a planar fashion resulting in the retina being an approachable part of the visual system to study.

An unusual feature of the retina is that its input photoreceptor cells are positioned furthest away from incoming light. This could be explained as a secondary consequence of the infoldings of neural tissue from which the retina is derived. It does, however, also result in these cells being close to the retinal epithelium and choriocapillaris, which supply them with oxygen and nutrition.

Another characteristic of the retina is the macula, a region in the central retina comprising of increased density of cell types. It is small and highly sensitive and is responsible for detailed central vision. At the centre of the macula exists a pit, extending approximately 1.5 mm, termed the fovea. Here, anterior neurons are displaced laterally to expose the input photore-

ceptor cells directly to incoming radiation. The path of light will once again act as a guide on this occasion through the retina and Figure 2.2 provides a detailed schematic of the various layers of which the retina is comprised for reference. Preceeding this, an insight into how the cells in the retina connect is given.
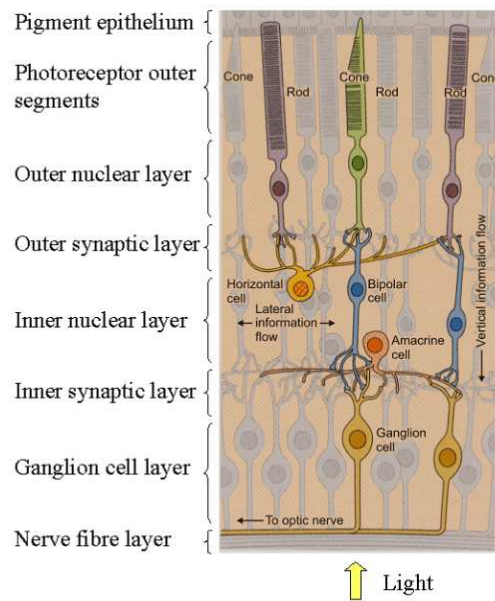
Figure 2.2: A cross sectional view of human retinal tissue showing its various cell layers [27].

Retinal wiring

In order to understand the functioning of any neural system, it is important to understand how the individual neurons connect. Light and electron microscopy [28] have provided a significant quantity of detail on the morphology of, and connections formed by retinal cells. It was found that these cells have "processes" named axons and dendrites which allow the neurons to communicate with each other. Axons are long nerve fibers projecting from a neuron

and are responsible for the conduction of electrical impulses away from the neuron cell body. Dendrites are the branched projections of a neuron that relay electrical stimulation received from other neural cells to the cell body, or soma, of the neuron from which the dendrites project. Electrical stimulation is transmitted onto dendrites by upstream neurons via synapses which are located at various points throughout the dendritic arbor. Dendrites play a critical role in integrating these synaptic inputs and in determining the extent to which action potentials are produced by the neuron.

Chemical synapses [29] [30] are specialised junctions between cells (see Figure 2.3). In the retina there are two types of synapses. Conventional chemical synapses exist between horizontal and amacrine cells and are characterised by a cluster of synaptic vesicles (containing neurotransmitter) near the membrane of the presynaptic terminal.
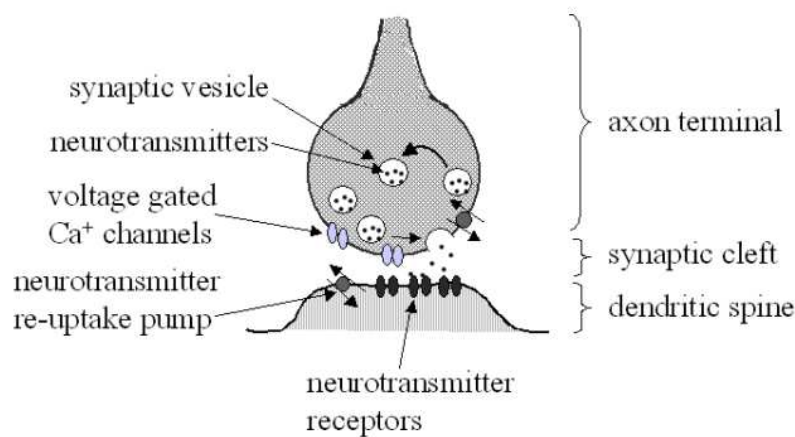
Figure 2.3: Schematic showing the mechanism of a chemical synapse.

The second type is called a ribbon synapse and forms chemical connections between photoreceptor and bipolar cells. These are characterised by an

electron-dense ribbon [31] which lies at right angles to the presynaptic membrane. Surrounding this ribbon is an accurately positioned arrangement of synaptic vesicles. The release of neurotransmitter is triggered by the arrival of an action potential. This nerve impulse produces an influx of calcium ions through voltage-dependent, calcium-selective ion channels. Calcium ions then trigger a biochemical cascade which results in vesicles fusing with the presynaptic-membrane and releasing their contents to the synaptic cleft. The membrane added by this fusion is later retrieved by endocytosis (the uptake of material into a cell by formation of a vesicle) and recycled for the formation of fresh vesicles. Receptors on the opposite side of the synaptic gap bind neurotransmitter molecules and respond by opening nearby ion channels in the post-synaptic cell membrane, causing ions to rush in or out and changing the local transmembrane potential of the cell. The resulting change in voltage is called a postsynaptic potential. In general, the result is excitatory, in the case of depolarising currents, or inhibitory in the case of hyperpolarizing currents. The type of ion channel conducting the post-synaptic current defines whether a synapse is excitatory or inhibitory, and in turn is a function of the type of receptors and neurotransmitter employed at the synapse.

Other connections exist less commonly in the retina, such as basal and gap junctions but these are not described here [21].

Photoreceptors

On being focused by the lens, light travels through the layers of the retina for detection by input photoreceptor cells, of which there are around 100 million in the human eye. These are light sensitive central nervous system cells containing visual pigment molecules, which are responsive to different light

properties. Two broad classes of photoreceptors exist. Rods provide the ability to recognise varying light intensities in low light conditions. With the exception of their absence in the centre of the fovea, they are distributed fairly evenly across the retina.
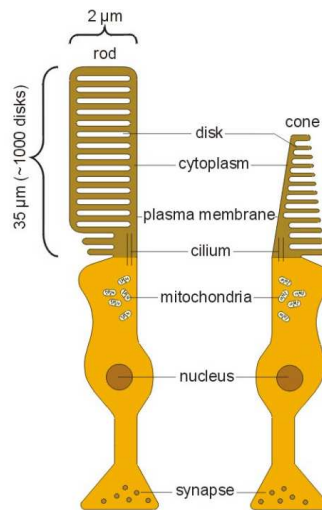
Figure 2.4: Diagram showing scaled structure and components of photoreceptor rods and cones [27].

Cones, the second class of photoreceptor, are less sensitive to light intensity and only function in bright light conditions. Unlike rods, they subserve the perception of colour and depth and due to a faster response time allow better visual acuity. Cones are distributed across the whole retina although a far higher concentration is present in the foveal region and are found exclusively in the very centre of the fovea giving rise to a rod free zone. This is the area of the retina responsible for detailed vision. Figure 2.4 is a diagram of a photoreceptor rod and cone and illustrates their structure and components.

To relay the visual image as neural signals, photoreceptors perform pho-

totransduction, a property exclusive to photoreceptors and a particular class of ganglion cells. It is a very complex biological and chemical process and will only be described briefly. Further information can be found in [20] and [32]. Whilst in a dark state, a steady current of positive ions flows through cation channels in the photoreceptor membrane. The transduction mechanism is initiated when incident photons cause photoreceptor visual pigment, consisting of a cis-retinal and opsin complex, to be isomerized resulting in their activation. A cascade of enzymic reactions then ensue leading ultimately to the closure of the cation membrane channels and hyperpolarization of the cell potential. This change in potential signals to the intermediate cells that photons have been detected.

Horizontal cells

Intermediate processing in the retina, which is not entirely understood [20], enables better visual acuity than would be achievable if the incoming light was transferred directly between input photoreceptor cells and output ganglion cells. The honing of the image begins at the first synaptic level of the retina, the outer synaptic layer. Here, horizontal cells, named from their morphology, receive input from rods and cones. There are two classes of these cells in the human retina, some of which provide lateral inhibition, a means by which edge definition of photoreceptor stimulation is promoted. One class of cell has a short axon ($\sim 400\mu$m) and the other is an axonless cell. In some species (not mammals), the horizontal cell axons synapse to both the photoreceptor rods and cones as well as the bipolar cells, where the second layer of intermediate processing takes place.

Bipolar cells

The bipolar cells relay information between the photoreceptor and horizontal cell layers to the ganglion cell layer and in the process perform additional processing. Their nuclei are present in the inner nuclear layer and, as the name bipolar suggests, they have both dendrites and axons. In the outer synaptic layer, whilst also contacting horizontal cells, bipolar cells synapse with either rod or cone photoreceptors (never both) and this defines two major classes: rod bipolar and cone bipolar cells. The second set of processes contact output retinal ganglion cells which form the inner synaptic layer. Each class of bipolar can also be categorised into ON and OFF cells which react differently to stimuli from photoreceptors. For example, the detection of light by a photoreceptor is followed by a decrease in its release of the enzyme glutamate. This change causes ON bipolars to depolarise (potential difference across the cell membrane will increase). The OFF bipolar cells, on the other hand, respond to an increase in glutamate release, caused by the absence of light, by hyperpolarising (potential difference across the cell membrane will decrease).
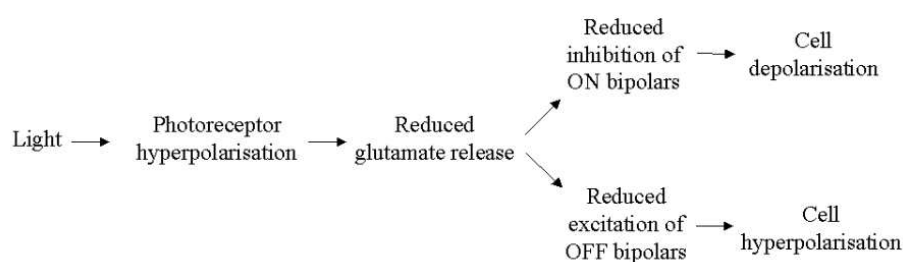
Figure 2.5: Summary of ON and OFF bipolar responses to light.

The interactions between bipolar cells and the horizontal cells result in mechanisms which, although not fully understood, are explained in brief. Whilst

ON bipolars depolarise to a stimulus that is in the centre of their receptive field, and hyperpolarise to a stimulus that is in the periphery of the receptive field, OFF bipolar cells show exactly the opposite behaviour. The receptive field (RF) of a cell is the surrounding area in which a stimulus will cause the cell to respond. This mutually inhibitory centre-surround relationship results in increased retinal image contrast by enhancing the edges of the object being observed.

Amacrine cells

The most diverse cells of the retina are the amacrine cells which are active in the inner synaptic layer. They exhibit many shapes, sizes and functions and the class contains at least 30 different types of cell. Cell bodies of amacrine cells are found in the inner nuclear layer, inner synaptic layer and in the ganglion cell layer. They receive from, and transmit to, both bipolar cells and other amacrine cells whilst they transmit also to ganglion cells. These cells are the basis of neural circuits responsible for the generation of directional selectivity and local edge detection response properties. Different classes of this cell are also responsible for mediating surround inhibition in either rod or cone pathways. Low light intensities are mediated through amacrine cells whilst high intensities are mediated through both horizontal and amacrine cells. In fact, around 80% of amacrine cells are known to be inhibitory.

Ganglion cells

The final layer of cells comprising the retina are output neurons named ganglion cells, which number around 1 million. Ganglion cells receive visual information generated by bipolar cells in the form of slow potentials and transform them into voltage spikes (action potentials). These electrical sig-

nals are then transmitted via the optic nerve to particular regions of the brain. The axons of ganglion cells form the optic nerve and extend to the brain visual centres, principally the lateral geniculate nucleus and superior colliculus. In a human, the optic nerve is composed of more than a million ganglion cell axons. Based on differences in morphology and behaviour, there exist at least five main classes of ganglion cell in primate retina. It is found that different classes can respond to different stimuli including direction, colour and contrast. The mechanisms for ganglion cell signalling are discussed in more detail here since these are the signals detected by the fabricated microelectrode arrays.

Two of the main classes of ganglion cells are midget and parasol. Diagrams of these are shown in Figure 2.6. Their names are representative of the physical properties of the cells.

Midget cells: In the human retina, 60% of the million ganglion cells are midget cells. The size of these neurons increases with eccentricity meaning that there are fewer and smaller cells in the peripheral regions of the retina. The ganglion cells in the peripheral retina are 40% midget ganglion cells whilst in regions closer to the centre of the fovea this can increase to as much as 95%. They are so named because of their small cell bodies and dendritic axons. As a consequence, each receives input from only one midget bipolar cell. Midget cells primarily respond to changes in colour and in contrast. In the fovea, midget cells are responsible for fine spatial discriminations since each foveal cone is served by two midget ganglion cells. Midget ganglion cells exist as either ON- or OFF- cells, where ON and OFF describe whether the cell responds to the onset or offset of light respectively. In fact, the

level of the cell's dendrites dictates their response type i.e. if the dendrites terminate in the inner synaptic layer a (ISLa) they exhibit OFF responses and if they terminate in the ISLb, they have an ON response. They have centre-surround receptive fields, where the center may be either ON or OFF to one of the cones while the surround is the opposite to another cone. More information on midget ganglion cells can be found at [20], [21] and [33].

Midget: Parasol:

10 μm
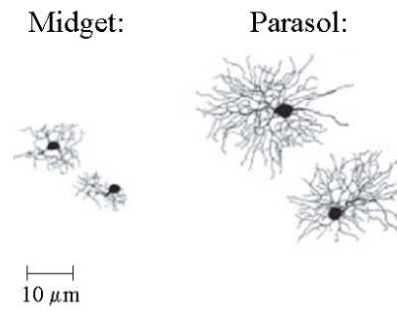
Figure 2.6: Diagrams showing the morphology of midget and parasol ganglion cells [35].

Parasol cells: A further 8-10% of the population of human retinal ganglion cells are parasol cells whose dendritic field size alters with position on the retina. The name relates to the physical appearance of the cells, which have large dendritic fields and cell bodies (see Figure 2.6). This structure allows them to receive from many more bipolar cells and collect from many more cones than midget ganglion cells. They respond to low-contrast stimuli, but are not very sensitive to changes in colour [30]. Parasol ganglion cells have relatively large receptive fields (cf. midget ganglion cell receptive field). Similar to midget ganglion cells they have centre-surround receptive fields. More information on parasol ganglion cells can be found at [20], [21] and [34].

Whilst at their resting potential ($\sim$-70 mV), a ganglion cell's inside charge is negative relative to the outside charge. The resting potential of a cell is largely determined by the ion concentrations on both sides of the cell membrane. Typically, there is a high concentration of potassium (K^+) ions intracellularly and high concentrations of sodium (Na^+) and chlorine (Cl^-) ions extracellularly. There is an excess of positive ions (Na^+) outside the cell hence a negative resting potential. Therefore an electrochemical gradient exists. At rest, the cell membrane is most permeable to K^+, less to Cl^- and least to Na^+. However, a voltage stimulus results in changes in the membrane permeability and allows ion movement against the concentration gradient and this changes the cell potential. Action potentials are generated when the membrane potential is decreased by $\sim$15 mV: from -70 to -55 mV. At this threshold, a large and rapid change in membrane permeability to Na^+ is initiated. This change allows enough positive Na^+ ions into the cell to shift the membrane potential to +50 mV. The action potential typically has a duration of $\sim$1 ms. K^+ ion channels then open and allowing K^+ ions to leave the cell. The inside of the cell becomes more negative, and the membrane potential is restored to -70 mV. The whole process occurs in 1-2 ms, shortly after which (refractory period) a new action potential can be generated in the axon [20], [21]. Figure 2.7 shows the form of a typical action potential produced by a ganglion cell.

A vast quantity of knowledge on the morphology and function of cells in the retina is known. Neurobiologists have learned and understand the complex chemical mechanisms used by the millions of neurons in the retina to carry and transmit information to the brain. However, key facts still remain

a mystery, creating a void in the understanding of retinal processing. In particular, questions remain on the mechanism by which action potentials are produced by retinal ganglion cells. Whilst hypotheses exist which state the importance of factors such as action potential firing rate or the synchrony of individual action potentials between nearby ganglion cells, there is no definite explanation.
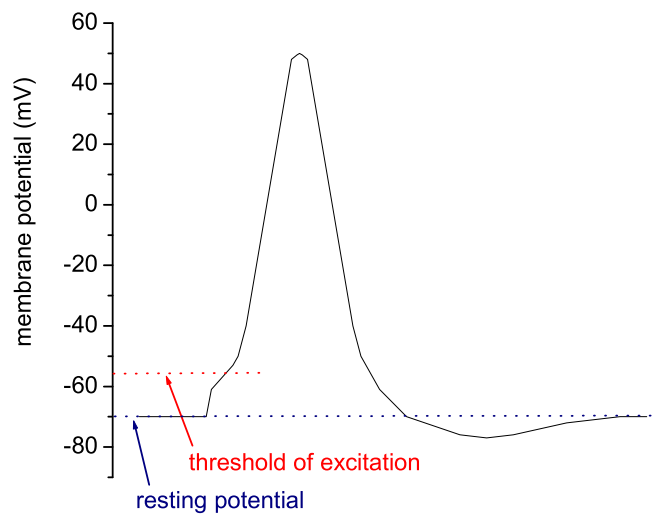
Figure 2.7: Typical form of an intracellular action potential (∼1 ms duration) produced by a retinal ganglion cell. Ganglion cell resting potential is -70 mV and threshold voltage for cell excitation is -55 mV.

2.3 Experimental overview

In this project, light is used to stimulate the retina by projecting a dynamic optical image onto the input retinal photoreceptor cells. The responses of the output ganglion cells are recorded simultaneously from hundreds of closely spaced electrodes on a microelectrode array. By analysing the patterns of

electrical activity, generated by the retinal ganglion cells in response to this moving light stimulus, a greater understanding of how the retina processes and encodes visual images is gained.

Measuring cell responses across larger areas of retinal tissue has many benefits over traditional individual cell studies. It enables the behaviour of populations of each cell type to be studied simultaneously. To do this, large area arrays of high-density microelectrodes are required to record extracellular ganglion cell responses. A custom designed system was made, into which these microelectrode devices are placed. Figure 2.8 is a schematic of the system which is setup to allow experiments to be performed.
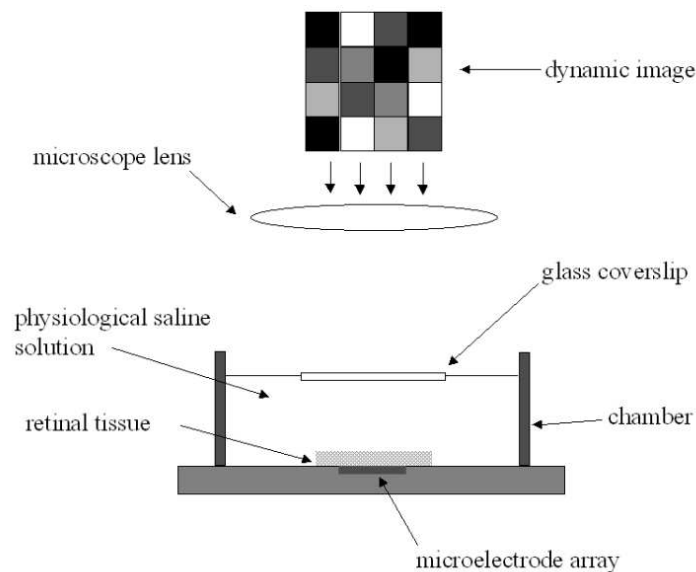
Figure 2.8: A schematic showing the setup for retinal experiments where the retina is placed ganglion cell side down on the electrode array.

The device has a cylindrical chamber sealed to its surface, encompassing the microelectrodes. Retina tissue is placed in to this chamber over the array

of electrodes and immersed in a physiological saline solution as outlined in Section 2.5. The electrodes are connected, via wire bonds (or elastomeric connections), to readout ASIC (application specific integrated circuit) technology as described in Section 2.4.
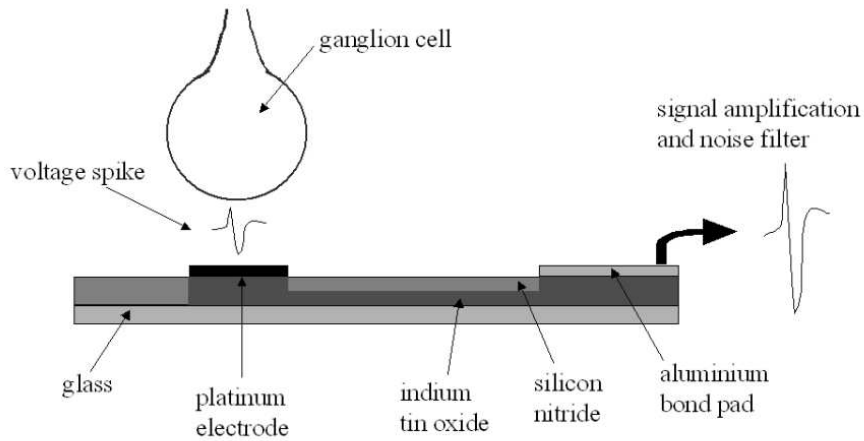
Figure 2.9: A schematic showing a close-up of the connection between an electrode and a ganglion cell.

With the system having a readout rate of 20 kHz, each microelectrode on the array records local ganglion cell potentials, simultaneously, every 50 μs. A trigger pulse is sent to the readout system when the light stimulus is initiated. Figure 2.9 shows a schematic of the readout chain from a single ganglion cell. This readout rate results in massive quantities of data ($\sim$ 1.2 - 4.8 TB per one-day experiment for the 512-channel setup), for storage and subsequent analysis. This quantity of data dictates the need for automated analysis and this is described in Section 2.6.

2.4 The readout system

At the beginning of the retinal readout project, arrays of 61 electrodes were designed and fabricated on glass/ITO wafers [37] and a system capable of acquiring data from this number of channels was required. To serve this purpose, a low noise 32-channel integrated circuit was designed to record extracellular neuronal signals [38], produced by the ganglion cells. In order to study a larger area of the retina, the array size increased to 512 electrodes [39] and 519 electrodes [40] and to compliment this advancement in array output, the readout system was upgraded to process 64-channels [41]. The electronic readout systems developed for recording of neuronal signals are shown in Figure 2.11.

To explain the difference in large area electrode array numbers a brief summary follows and reference can be made to Figure 2.10:

512-electrode array - Fabricated at Stanford Nanofabrication Facility (SNF) using photolithography. It has 5 μm diameter electrodes with inter-electrode spacings of 60 μm. The electrodes are arranged in a hexagonal close-packed geometry, but with a rectangular area coverage.

519-electrode array - Fabricated in Glasgow using a high resolution Leica electron beam writer in the James Watt Nanofabrication Centre (JWNC), a hexagonal close packed structure is employed. More advanced fabrication technology allows smaller feature sizes. This permits hexagonal area coverage more suited to the radial distribution of ganglion cells in the retina. The higher density 30 μm spacing 5 μm diameter electrodes is designed to improve the efficiency of cell detection. The hexagonal geometry leads to the

unconventional number of 519 electrodes.

Regardless of the number of electrodes (512 or 519), only 512 channels are read out as a consequence of the 64-channel data acquisition system.
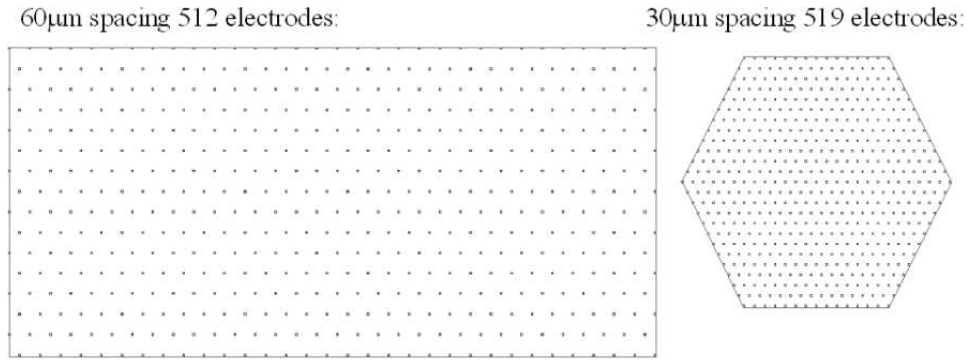
Figure 2.10: Electrode array plots for both the 512-electrode array with 60 μm inter-electrode spacing and the state-of-the-art 519-electrode array with 30 μm inter-electrode spacing.

2.4.1 Readout circuitry

Since the main focus in this work has been the successful fabrication and performance of the 30 μm spacing 519-electrode array, the 64-channel readout set-up is described in this section. As a consequence of there being 519 electrodes, they are read out in 8 sets of 64 channels. Two varieties of chip are employed in the system and these are named the Plat64 and Neuro64 chips. Their functions are described in the following two sections and a more detailed description is given at [41].
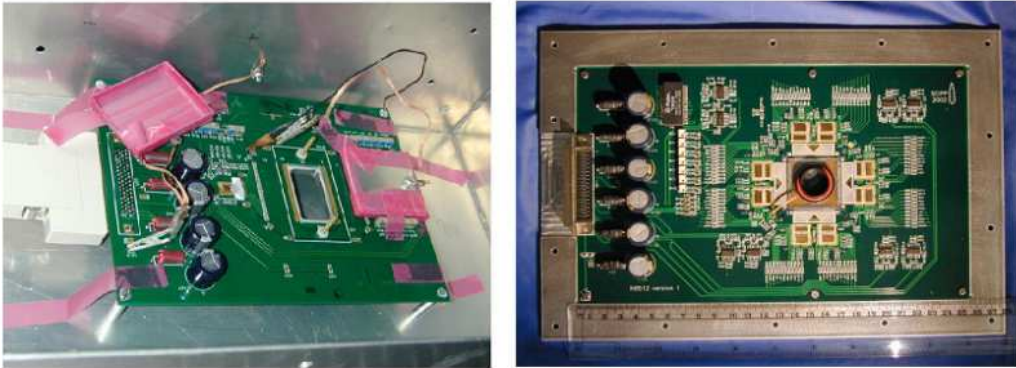
Figure 2.11: A photograph showing the bench top electronic readout systems used for recording neuronal signals simultaneously from 64 (left) and 512 (right) electrodes [36].

Plat64 chip

The Plat64 chip serves two functions. Primarily, to create a low impedance interface between electrodes and the retina, electrodes are electroplated with a porous material called platinum black. To form these, a constant current is applied to each electrode through a platinum based electrolytic solution. To this end, the Plat64 chip is utilised. It is able to supply a DC current to the electrodes (each channel features a programmable current source) which provides the ability to platinise. The Plat64 chip is also used to AC couple the electrodes (to their corresponding Neurochip channel) using 150 pF decoupling capacitors. AC coupling is necessary to avoid propagation of the differential offsets on electrodes through the entire signal path. By altering the control software for the Plat64 chip, stimulation capabilities were realised and this provided pilot data for the design of a new stimulation chip. The circuit diagrams for both Plat64 and Neuro64 chips are shown in Figure 2.12.
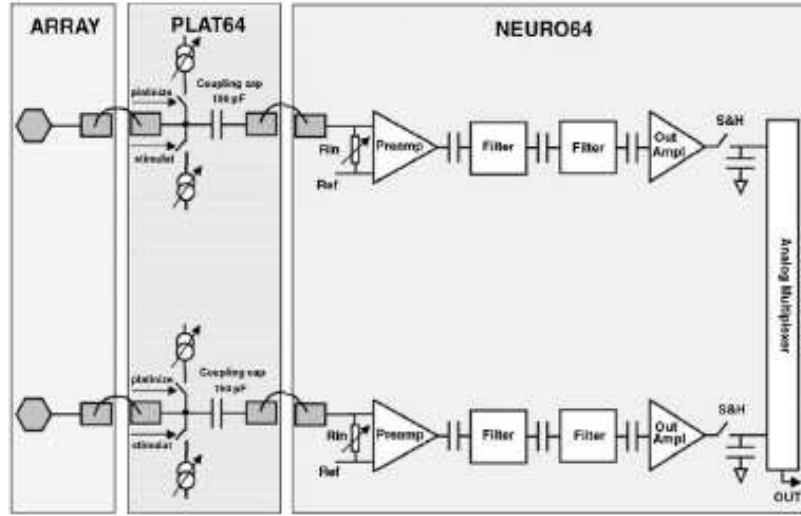
Figure 2.12: Circuit diagrams of the Plat64 chip and the Neuro64 chip connected to electrode array [41].

Neuro64 chip

During recording experiments, trains of retinal spikes travel through the Neuro64 chip which samples at 20 kHz. This chip is designed to amplify, filter and multiplex the signals. Since typical retinal pulses have amplitudes of only tens to hundreds of μV, the Neuro64 chip features 64 identical channels of amplifiers and filters. A low noise (5 μV RMS) preamplifier precedes a band-pass filter with a passband between 50 and 2000 Hz (this is the typical spectral density of spikes produced by retinal tissue studied here). It follows that the Nyquist frequency, which is the minimum sampling frequency required of a continuous signal to ensure no loss of information, is 4000 Hz and hence the spike data is over-sampled at 20 kHz. Having removed unnecessary noise, the signals are further amplified before being multiplexed to a single data channel by a 64:1 analog multiplexer. This is a space and cost effective method of transferring the data for storage.

Data acquisition

A data acquisition (DAQ) PC is used for the acquisition and recording of data. It uses 2 ADC (analog to digital converter) cards. Each of the eight multiplexed analog signals are digitised by one of four 12-bit ADC channels at a rate of 1.28 MHz. The DAQ computer records data at a rate of 15 MB/s.

2.5 *In-vitro* experiments

At the Salk Institute for Biological Studies, San Diego, under the lead of Prof. E.J. Chichilnisky, *in-vitro* retinal recording experiments are performed. *"In-vitro"*, which translates as "within glass", means the experiment is performed outside of the living organism. That is to say, the retina is removed from the eye and placed into a controlled environment. This compares with *"in-vivo"* experiments, "within the living", which are carried out in a whole, living organism. To guarantee the successful execution of *in-vitro* retinal experiments, a very precise biological procedure is followed and this is described in this section.

2.5.1 Sample preparation

A variety of species of retinal tissue have been investigated in past experiments, including mouse, guinea pig and monkey retina. With the exception of tissue extraction, the procedure is independent of the source of the retina. Whilst terminally anaesthetised, the eye of the subject animal is enucleated [44]. The posterior region of the eye, containing the retina is separated from the anterior portion of the eye including the vitreous humour. The retina, still supported by the eye cup is immersed in a buffered saline solution in darkness prior to dissection. A few millimetre diameter sections of retina

are cut from the region of the retina appropriate for the experiment (for example, position with respect to fovea). At this point the tissue is ready for experimental use.

2.5.2 Experimental procedure

The slice of live retinal tissue is placed ganglion cell side down, ensuring it covers the electrodes. The chamber is then permeated with Ames' solution. This solution has a dual purpose. As well as creating an electrical connection between the ganglion cells and the microelectrodes it mimics the physiological conditions inside the eye and encourages the tissue to stay alive. It is a precise mixture of vitamins, sugars, inorganic salts and amino acids chosen carefully to resemble closely *in-vivo* conditions [45]. The solution is closely monitored guaranteeing precise physiological parameters, pH = 7.4 and temperature = 35 - 36 °C, are maintained. Provided these conditions are supplied, the retinal tissue can be kept alive for up to 12 hours. The health of the tissue is validated by monitoring cell activity in response to a light stimulus across the electrode array area.

An externally connected platinum wire is fixed to the chamber and inserted into the saline solution, serving as a reference electrode. When the photoreceptors are stimulated by a dynamic image projected from a computer screen, the chemical processes occur, as described in Section 2.2, which result in the ganglion cells generating action potentials. Since the retina has been detached from the optic nerve, these voltage spikes generate local currents in the saline solution which in turn provoke voltage drops across the electrode interfaces, with respect to the platinum wire. Using an array of microelectrodes with large-area coverage allows simultaneous recording from hundreds

of neurons. The technique by which the spatial and temporal responses of each neuron is calculated is explained in the next section. Also, as a consequence of their large area, these microelectrode arrays allow large amounts of data to be taken per preparation, therefore; fewer experiments are required to be performed.

2.6   Data analysis

The final section in this chapter deals with the analysis of data produced during the described biological experiments. Trains of voltage spikes must be sorted to allow each cell's receptive field to be mapped. The receptive field of a neuron is the area in which, if a stimulus is applied the neuron will respond. The mapping of receptive fields will form, ideally, a complete mosaic pattern representing total coverage of the visual field. To achieve this, the first stage in the analysis of data recorded from retinal tissue is to identify and classify the different types of ganglion cells which are producing action potentials.

2.6.1   Neuron identification

Since a one to one ratio of electrodes to cells does not exist, deciphering the output data is not a trivial procedure. A spike generated by a neuron is not limited to detection by a single electrode and is generally detected on several electrodes. However, a reasonable attempt to identify particular neurons is possible since they typically generate action potentials with a characteristic shape. Neuron classification was originally performed manually relying on comparisons of spike features such as width and amplitude but with a high number of electrodes this technique becomes very time consuming. Since

these experiments typically produce around 1 Tbyte of data over a period of 48 hours it is important to have an efficient automatic method of spike sorting. There are several automatic techniques in use now which allow a more thorough analysis [48]. In the study of the data produced from experiments involving devices fabricated during this thesis, a technique called principal component analysis is employed.

Principal component analysis

Principal component analysis (PCA) is a statistical technique used to identify patterns in data [49]. It expresses the data so as to highlight features with the highest level of variance. It is particularly useful for analysing data with many variables (high dimension), hence its application here to spike sorting. Briefly, the method involves transforming the original data set to an alternative co-ordinate system. The first co-ordinate represents a feature of the data with the greatest variation (the principal component), the second co-ordinate represents the feature of second greatest variation etc. It simplifies the datasets by reducing its number of dimensions whilst retaining the characteristics of the dataset which contribute most to its variance. In this work, the features of greatest variation include spike rate, amplitude, width and polarity.

Mathematically, the fundamental procedure is to find the covariance matrix of the original data, i.e. the voltage waveform, by displaying in a 2-dimensional array the covariances between elements of a vector. The eigenvalues and eigenvectors are then found for this matrix. Note: A scalar λ is an eigenvalue of a matrix A if there exists a non-zero vector x such that: Ax = λx and in this case, x is called an eigenvector (corresponding to λ).

The eigenvectors of the covariance matrix are ordered in terms of highest to lowest eigenvalues. This gives the components in order of significance. Considering only the components of the highest significance, results in lost information although this is minimal if only small eigenvalues are ignored. A matrix, called the feature vector, is formed using the selected eigenvectors as columns. This matrix is transposed and multiplied with the transposed, mean adjusted original data to give it in the form of data columns and dimension rows. This final data captures the characteristics of largest variation. The remaining eigenvectors are ignored. To represent a particular data point the principal components are scaled and added together. This technique provides a method of classifying neurons by the physical properties of their action potentials. In this work, the characteristics of highest variation include amplitude, rate and width.

Once individual neurons are identified the next stage of analysis is to map accurately their receptive fields.

2.6.2 Spike triggered average

To obtain an estimate of the shape and size of a neuron's receptive field a spike triggered average (STA) must be found for each neuron. During the biological studies, one experiment involves light stimulation of the retinal photoreceptors with a dynamic image designed to represent "white noise" [46]. While white noise is a sound with equal intensity at all frequencies within a broad band, it is used here to mean a series of images made up of coloured pixels of varying intensity with time. A small section of an example of a white noise stimulus is shown in Figure 2.13.

The intensity of each pixel is chosen around a mean value [47]. This sequence
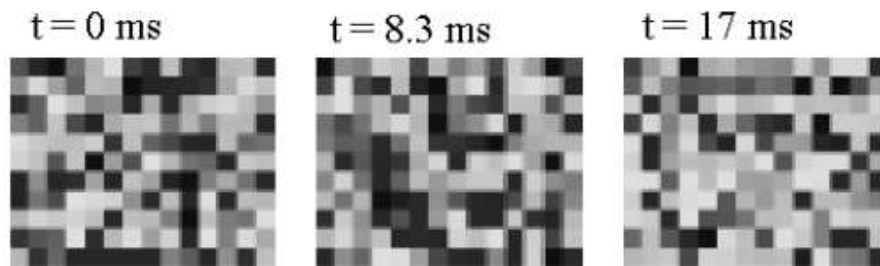
Figure 2.13: An example of white noise stimulus where t is the time preceeding observation of an action potential [36].

of coloured checker board images is projected onto the retinal photoreceptors. Subsequently, when a neuron generates a spike, the random sequence of images preceding the occurrence of the spike can be repeated by knowing the seed from which the random data were generated. For every spike from an identified neuron, the pixel intensities on the checker board images responsible are averaged and this produces the STA. In the averaged image, the region which is related to the generation of a spike will contrast against the unrelated surrounding area which averages out to the mean value.

The area responsible could appear either lighter or darker than the mean value and its area represents the cell's receptive field. As a consequence, the receptive field can be mapped as a 2D Gaussian distribution [39]. This method gives information on colour, space and time properties which stimulate particular neurons to fire action potentials. A generator signal is calculated by applying the STA as a linear filter to the stimulus image. In other words, it is calculated by linearly pooling contrast modulations over space and time. By measuring the mean spike rate as a function of the generator signal, the spike rate can also be calculated from the STA, altogether pro-

viding a substantial quantity of information on the properties of individual neurons.
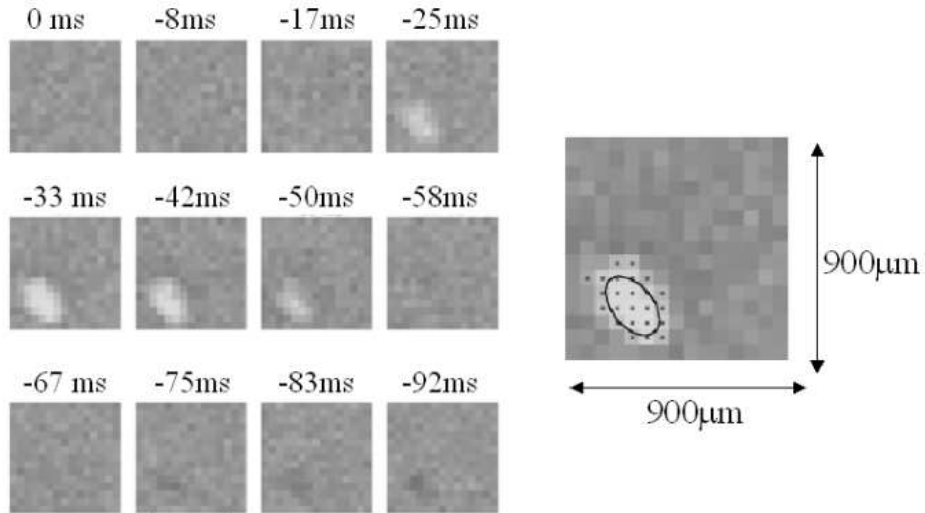
Figure 2.14: A diagram showing how a neuron receptive field is calculated using a spike triggered average [36].

Chapter 3

Fabrication

3.1 Introduction

This chapter focuses on the techniques needed to realise the high density microelectrode arrays which form an integral part of the system described in the previous chapter. The first half of this chapter summarises the semiconductor fabrication procedures used. Utilising these techniques, specific processes were developed, over the course of this PhD, for the production of microelectrode arrays and these are detailed in the second half of the chapter.

The substrates onto which devices are fabricated are four inch diameter glass wafers, sputter coated with 150 nm of indium tin oxide (ITO), purchased from Thin Film Devices [50]. These typically have a sheet resistance of 17 ± 3 Ω/square and an optical transmission value of 85 to 90 % at a wavelength of 550 nm. ITO is a highly conducting and durable material that adheres extremely well to the 1.1 mm thick glass substrate on which it is supported.

The work detailed in this thesis has relied heavily on the use of standard photo-, electron beam, lift-off and etch lithographic techniques to pattern the ITO into appropriate devices. In particular, arrays with 61 electrodes are fabricated using both photo- and etch lithography whilst a process was developed for the larger, more dense arrays such as those with 519 electrodes, which use a combination of all of the four techniques mentioned above. These procedures are described throughout this chapter with reference to "The Science and Engineering of Microelectronic Fabrication" by S. A. Campbell [51] and "Semiconductor Devices, Physics and Technology" by S.M. Sze [52]. All the fabrication work was carried out in the James Watt Nanofabrication Centre, University of Glasgow, and the Stanford Nanofabrication Facility, Stanford University, where cleanliness classes of 10, 100 and 1000 (10, 100 and 1000 particles greater than 0.5 μm per cubic foot respectively) are maintained.

3.2 Photolithography

Photolithography or optical lithography is the process of transferring geometric shapes from a mask to the surface of a wafer using light (Fig. 3.1). The steps involved in the basic photolithographic process are wafer cleaning; photoresist application; soft baking; mask alignment; exposure; development and hard baking.

3.2.1 Wafer processing

Wafer cleaning and photoresist spinning

In the first step, the sample is traditionally cleaned using various solvents. It is placed in a beaker of acetone and agitated in an ultrasonic bath for
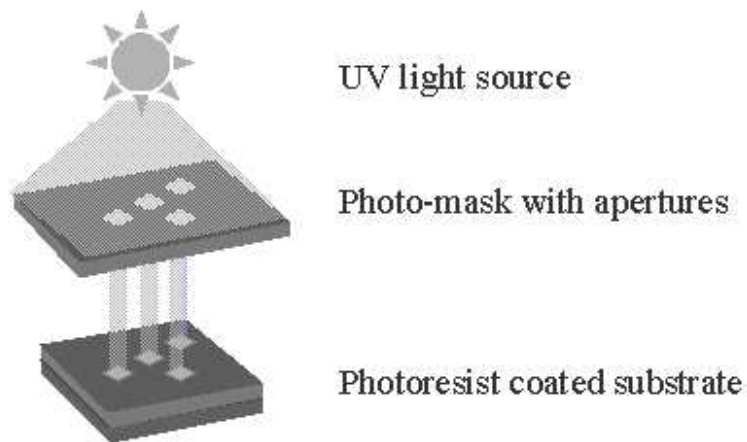
Figure 3.1: A diagram showing the mechanism of photolithographic pattern transfer.

5 minutes to dissolve and dislodge any particulate matter. Once removed, it is rinsed with isopropanol (IPA), dried using a high pressure nitrogen gun and, to ensure all moisture is evaporated, baked for 5 minutes at 90 °C. Photoresist, a radiation sensitive compound, is applied to the surface of the wafer by the standard method of high-speed centrifugal rotation. This technique, known as "spin coating", produces a thin uniform layer of photoresist on the wafer surface.

Photoresist mechanism for photolithography

Photoresist consists of three components: a base material (resin), a photo active compound (PAC) and a solvent. The solvent controls the mechanical properties of the resist. It makes it a liquid and determines its viscosity, the latter being important for thickness and hence resolution. The PAC makes photoresist highly soluble in developer after exposure to UV light. There are two polarities of photoresist: positive and negative. Positive resists

are exposed to ultraviolet light wherever the underlying material is to be removed. Exposure to UV light changes the chemistry of the resist causing it to become more soluble in a developing solution. Negative resists behave in the opposite manner. Exposure to UV light causes the negative resist to polymerise making it resistant to the developing solution. The processes outlined in this thesis require only positive resists.

Soft baking

Once the resist is spun onto the wafer it is soft baked or cured. This is the step during which almost all of the solvents are removed from the photoresist coating. The coating of photoresist becomes photosensitive during soft baking and the baking time chosen is critical to the procedure. The photosensitivity is degraded if over baked, as either the developer solubility is reduced or a portion of the sensitiser is destroyed. When under baked, light is prevented from reaching the sensitizer. Positive resists are incompletely exposed if considerable solvent remains in the coating. The developer in both exposed and unexposed areas readily attacks under baked resist causing less resistance to subsequent etching processes.

Contact printing

A crucial step in the lithography process is mask alignment. A mask is a glass plate with a patterned metal film on one side. When used in conjunction with positive resist, the mask contains an exact copy of the pattern that has to remain on the wafer. Using a sophisticated machine capable of micron resolution, the mask and resist coated wafer are aligned to allow the pattern to be accurately transferred onto the wafer surface. Once the mask and wafer are in the correct position, the photoresist is exposed through the pattern on

the mask with a high intensity ultraviolet light (365 nm in our case). The exposure method used here is called contact printing. In contact printing, the resist-coated wafer is brought into physical contact with the metal coated side of the glass mask. The wafer is held on a vacuum chuck, and the whole assembly rises until the wafer and mask contact each other. The photoresist is exposed with UV light, for a time dependent on resist thickness, while the wafer is in contact position with the mask. The contact between the mask and the resist enables very high resolution patterns to be formed. In fact, a resolution of around 1 μm per 0.5 μm of photoresist is achievable.

Development and hard baking

One of the last steps in the photolithographic process is development. A resist coated and exposed sample is immersed in an aqueous developing solution. For positive resists, the resist solubility in developer is finite even at zero-exposure energy. The solubility is proportional to exposure time and at some threshold, it becomes completely soluble. The developed sample is post-baked to harden the photoresist making it more resistant to etchants and also to improve adhesion of the photoresist to the wafer surface.

3.3   Electron beam lithography

For the fabrication of the high-density electrode arrays with 519 electrodes, the process described in Section 3.2 had to be adjusted to enable feature sizes of around 1 μm to be formed. In the new process, direct-write electron beam lithography replaces photolithography. This is a complicated technology which uses a focused beam of electrons to generate patterns directly on to a semiconductor surface. Although, the use of electrons enables more flex-

ible, higher resolution patterning, it is a more time consuming method than optical lithography (Section 3.2). There are several steps involved in the procedure: wafer cleaning; metal deposition; resist application; soft baking; electron beam write and development. These, along with the operation of the beam writer, are described in this section.

3.3.1   Electron beam writer operation

Before operation a CAD package, such as L-Edit or WaveMaker (WAM), is used to design the pattern to be written. Using specialised software, the pattern file is processed and translated into a format suitable for the e-beam lithography tool. The completed file, which includes parameters such as the electron beam spot size, dose, beam energy as well as write position and time, is submitted to the control room where it can be accessed by the beam writer.

Machine operation

A schematic of an electron beam lithography system is shown in Figure 3.2. A thermionic electron beam gun with a lanthanum hexaboride filament is chosen for its high current density and brightness. By heating the cathode, a stream of electrons is generated. This stream is focused into a narrow beam using a combination of condenser lenses, blanking plates and apertures. The beam moves with respect to the wafer to expose blocks of resist successively. For patterns greater than this area, the blocks must be stitched together flawlessly. An error in either the beam deflection or the table movement causes a misalignment of successive writing fields resulting in a mis-matched pattern. To reduce the likelihood of stitching errors, it is essential that the substrate is flat. The beam writer forms a height map by use of laser

reflections off the substrate surface.
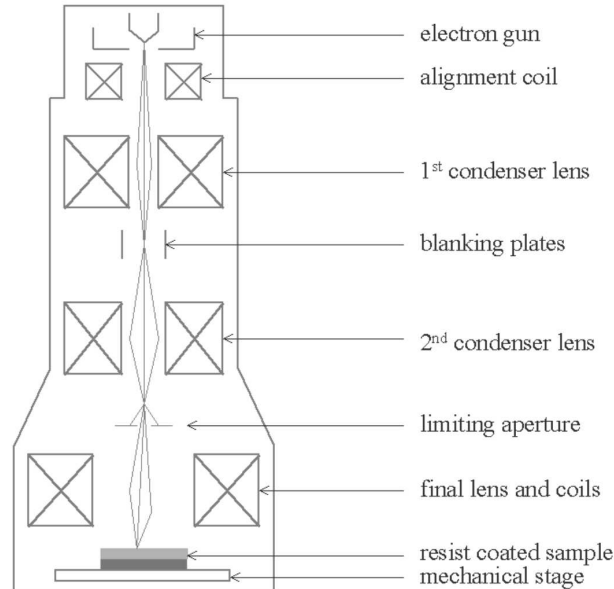
Figure 3.2: A schematic showing the basic components of an electron beam write system.

Compared to optical lithography, electron beam lithography is a much more flexible process since the pattern is written directly onto the sample dictating that mask plates are not required to be manufactured, a time consuming and expensive task. Also, electrons are subjected to acceleration voltages of around 10 - 100 kV in an electron beam writer causing them to have a much lower wavelength than a typical UV source. It follows then from Rayleigh's criteria that smaller feature sizes are achievable using electron beam lithography:

$$W_{min} = k\lambda/NA$$

where W_{min} is the resolution (minimum feature size), k is a constant re-

lated to resist sensitivity and λ is the source wavelength [53]. NA is the numerical aperture of the exposure unit and is defined by:

$$NA = \text{nsin}(\theta/2)$$

where n is the refractive index and θ is half the maximum angle of the cone of light produced. On the other hand, electron beam lithography is less time efficient than optical lithography. The difference is that the entire pattern is exposed simultaneously (parallel exposure) in optical lithography. The electron beam writer scans across the wafer (serial exposure) and can employ two scanning methodologies. In vector scanning, the beam travels over the required regions only, whilst raster scanning covers the whole wafer, switching on the beam of electrons where necessary. Both of these methods are far more time consuming than optical lithography. This makes them unsuitable for mass production.

3.3.2   Wafer processing

Resist application, exposure and development

The standard cleaning procedure (see Section 3.2.1) is followed, preparing the sample for subsequent processing. Prior to resist spinning, it is important to coat the substrate with a thin layer of hexamethyldisilazane (HMDS) primer. This solution bonds to oxides which form naturally on the wafer surface. Without the use of HMDS, the oxides would bond to water vapour available in the air causing the subsequent coating of resist to attach to moisture on the surface of the sample as opposed to the sample itself. Also, since molecules in the primer are attracted to the resist, increased adhesion

is achieved. If the sample is coated excessively the photosensitivity of the resist may be reduced. The sample is then baked to ensure all moisture is removed. A resist, sensitive to electrons, is then spun on to the wafer and soft baked following the appropriate recipe for the resist being used. The soft bake serves the same purpose as described for photolithography, in Section 3.2.1.

At this stage the sample is ready to have the required pattern transferred to the resist surface. The wafer is loaded into the electron beam machine and kept under vacuum. Primarily, this prevents electrons being scattered by dust particles during machine operation but it also inhibits resist deterioration. The resist is exposed as described in Section 3.3.1. Once exposed, a liquid chemical development process is followed to remove the exposed resist from the sample.

3.4   Etch Lithography

Once all the appropriate photo- or electron beam lithography steps are completed, the substrate holds the resist pattern temporarily on its surface. It is necessary then to transfer this pattern permanently onto the semiconductor layer underneath. This is achieved by etching away the exposed and unwanted material. Etchants work by attacking a material either chemically, physically or by a combination of both, but are normally categorised as either a wet or a dry etch. These forms of etching are expanded upon in the following sections.

3.4.1 Wet etching

Wet etching is a process which relies solely on liquid chemicals to remove unwanted material. In general, the film to be etched will not dissolve directly in the solution and a chemical reaction is required to occur first. The whole operation can be divided into three actions all of which must occur for the etching process to be successful: movement of the reactive species in the etchant to the sample, chemical reaction with the exposed layer and movement of the reaction products away from the sample. Although wet etching can be a highly selective process, it is an isotropic etch with limited control. As seen from Figure 3.3, etch isotropy creates a serious problem where small feature sizes are required (approximately ≤ 5 μm). The isotropic etch widens the etch profile since it undercuts the resist. The highly selective property provided by a wet etch, however, make it ideal for low resolution removals where an anisotropic etch is not essential.
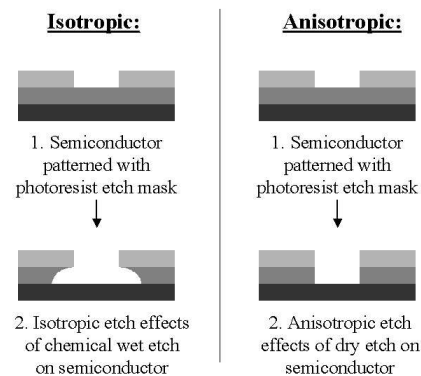
Figure 3.3: The effects of etching a substrate isotropically (left) and anisotropically (right). The properties of each etch make them suitable for different tasks.

3.4.2 Dry etching

Since the lack of anisotropy of a wet etch renders it a poor candidate for the fabrication of high resolution devices, the alternative approach of dry etching is needed. Dry etch, which is a means of material removal via bombardment with particles or ions, can be organised into a spectrum from physical to chemical processes. Ion milling is a purely mechanical process capable of highly directional (anisotropic) etches (Figure 3.3) but with poor selectivity. At the other end of the scale is plasma etching, a chemical process which occurs due to chemically reactive species in the plasma reacting with, and subsequently removing, the exposed film.

Reactive ion etching

Reactive ion etching (RIE) is a highly selective technology which is capable of anisotropic removal of material. Unlike chemical plasma etching and ion milling, RIE uses a combination of chemical and mechanical etching. Two variations of machine can be used to perform an RIE: parallel plate reactors and hexode batch systems. For the purposes of this work, only parallel plate reactors were used and hence will be described. The reader is referred to "The science and technology of microelectronic fabrication" by S.A. Campbell [51] for more information on hexode batch systems. Carefully selected gases are introduced to the parallel plate reactor through inlets at the top of the chamber and an RF (radio frequency) source is applied (Figure 3.4). The RF power creates an oscillating electric field which ionises the gas molecules, by removing electrons, and initiates a plasma. The sample to be etched is placed on the neutral electrode and is exposed to the flux of ions from the plasma. The powered electrode is attached to the chamber wall causing a large potential difference to exist between the plasma and the neu-

tral electrode thereby increasing ion bombardment energy. It is important to maintain a low enough pressure to ensure the plasma remains in contact with the chamber walls otherwise the ion energy would decrease and the parallel plate system would fail to operate effectively.
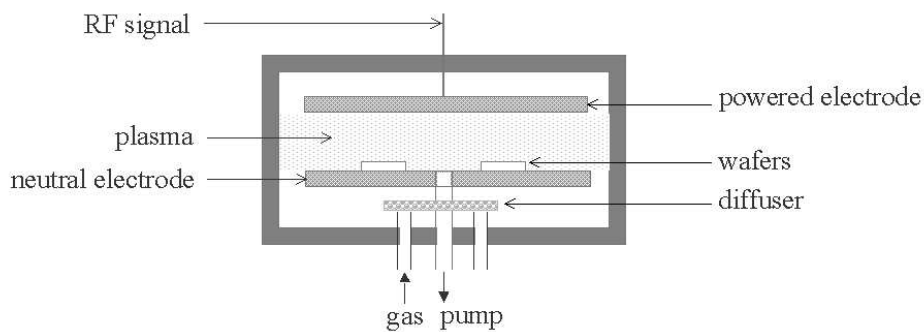
Figure 3.4: A schematic showing the components of a basic parallel plate reactive ion etch system.

The ions react chemically with the materials on the surface of the samples forming compounds or molecules which leave the surface either as a result of ion bombardment or high vapour pressure, but can also etch some material due to their high kinetic energy. The mostly vertical delivery of reactive ions toward the substrate results in very anisotropic etch profiles. There are several parameters which affect the quality of the etch. These include chamber pressure, gas flow, and RF power. By changing the balance of these conditions, the directionality of the etch can be adjusted since the physical aspect is anisotropic and the chemical is isotropic.

3.5 Thin film depositions

Thin film depositions are commonly used in many fields. Their use in optics includes depositing reflective and anti-reflective layers. In electronics, they are used for the deposition of insulators, conductors and semiconductors to form integrated circuits. Here, there are several fabrication steps that involve the deposition of thin films of material. Similar to etching, methods of deposition can be categorised as either physical or chemical. The method required depends on the material being deposited and its purpose.

3.5.1 Plasma enhanced chemical vapour deposition

Chemical vapour deposition (CVD) is a method of depositing thin films via the decomposition of gases. The gaseous compounds of the material to be deposited are introduced into a chamber where the substrate to be coated is resting on a hot susceptor ($\sim$6-8 x 10^2 ^oC). As the gases reach the substrate, a thermal reaction occurs which causes them to decompose. It is an extremely complicated but versatile chemistry allowing the deposition of a wide range of compounds and elements such as nitrides, oxides, carbon and silicon.

Variations on the system described above are atmospheric pressure, low pressure and plasma enhanced chemical vapour deposition (APCVD, LPCVD and PECVD), however, only the latter is of interest here. PECVD systems accommodate a lower substrate temperature ($\sim$300 ^oC) by providing an R-F plasma as an alternative energy source. This technology encourages ion bombardment of the substrate promoting the diffusion of species along the wafer surface. This results in very uniform depositions. A schematic of a high density PECVD system is shown in Figure 3.5.
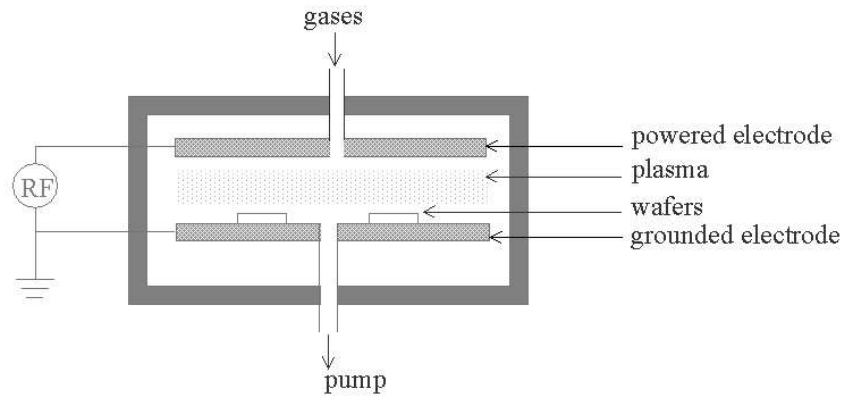
Figure 3.5: A schematic showing the components of a basic plasma enhanced chemical vapour deposition (PECVD) system.

3.5.2 Physical deposition

The most common way to deposit layers of metal is using a physical technique such as evaporation or sputtering. In this project, both methods were used and are described in the following paragraphs.

Evaporating metal

A schematic of an electron gun evaporating system is shown in Figure 3.6. The sample to be coated is loaded into a high vacuum chamber. A crucible containing a high purity metal wire is heated using a beam of electrons.

The electrons are refracted by a strong magnetic field to an angle which causes them to strike the metal as opposed to the crucible causing only the target to heat. This minimises the risk of the target being contaminated by the crucible as happens with alternative crucible heating systems. As the metal heats, it releases vapour which strikes the surface of the substrate accumulating there as a film. Shutters operate above the crucible to obstruct

(a) Basic evaporator diagram

(b) Components of electron gun
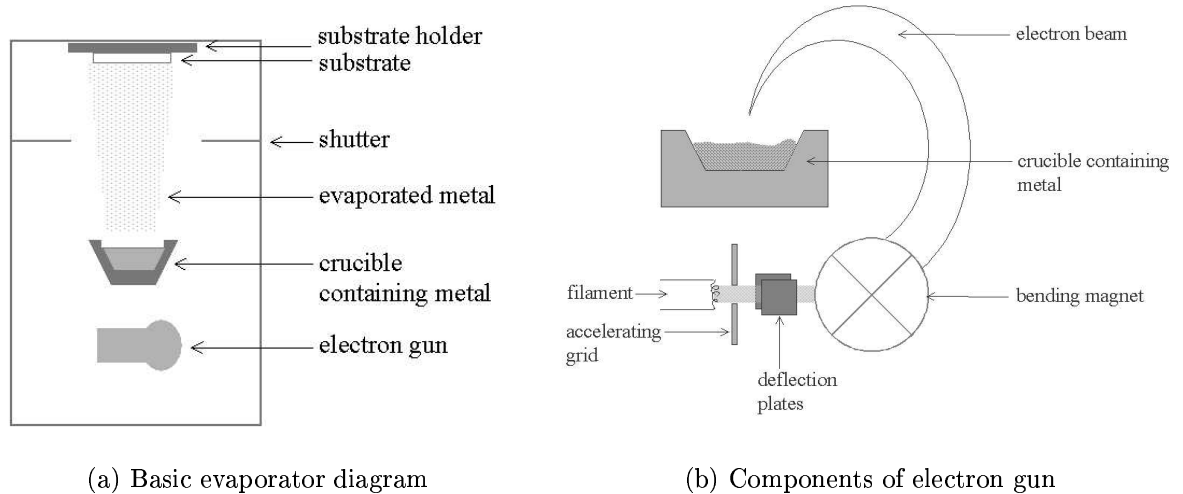
Figure 3.6: Schematics showing the components of a basic electron gun evaporator and mechanism of the electron gun in this system.

vapour prior to deposition commencing. A problem associated with metal evaporation is poor step coverage (ability to cover surface topology), however, this is not a deterrent provided the layer is formed on a flat surface.

Sputtering metal

Sputtering is the most popular method of depositing thin films of metal as it exhibits good step coverage. Figure 3.7 shows a schematic of a sputtering system.

It is a very similar technology to the RIE system as described in Section 3.4.2. When sputtering, however, the metal target is bombarded with ions as opposed to the sample in an etching system. Initially, an inert gas, such as argon, is introduced to the chamber at a low pressure. A large voltage is applied between the metal target and the sample, igniting a plasma. This

causes ions from the plasma to be accelerated toward the target (negative electrode). The impact of these ions on the metal, causes momentum transfer from the in-coming particle to the target and results in the release of metal atoms as a vapour. The vapour drifts toward the sample where a film is subsequently deposited on its surface.
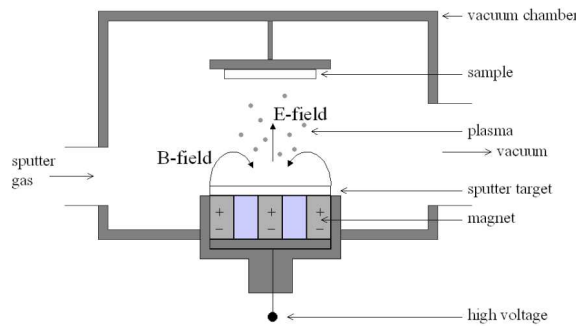
Figure 3.7: A schematic showing the components and mechanism of a basic magnetron sputtering system used to deposit metal layers.

3.6   Lift-off

Lift-off is the process used to allow a pattern of metal to be formed on a surface and is a cleaner and less aggressive alternative to etching. The steps (A,B...) illustrated in Figure 3.8 and 3.9 are referred to throughout the following sections describing the lift-off process.

3.6.1   Sample preparation

The basic process entails a pattern of resist being formed on the substrate surface (A,B) following the procedure described in Section 3.2.1, and ensuring

that apertures in the resist layer are positioned where metal is required to remain. Three main methods exist to lift-off metal selectively and these are described.

Chlorobenzene soak

This method involves soaking the resist coated sample in chlorobenzene for 15 minutes prior to development (C). It is crucial here that both the sample and soak dish are completely dry as any water negates the effect of the soak. Chlorobenzene has a hardening effect on the top surface of the photoresist causing it to develop at a lower rate than the underlying resist (D). This creates an overhang of resist. Metal is evaporated or sputtered on top of the layer of resist (E). The afore-mentioned overhang guarantees a break in the metal where the resist profile starts and ends and hence leads to improved lift-off. The hardening effect of the chlorobenzene soak requires that the resist is developed for a longer duration.

Lift-off resist (LOR)

This method involves building a bilayer of resists. Primarily, a lift-off resist (LOR) is spun onto the substrate surface and soft baked (see Figure 3.9 - A). Onto this surface a layer of photoresist is spun and also soft baked (B). As before, the photoresist is exposed to UV light through a patterned photomask (C). Agitation in a developing solution removes the UV exposed photoresist. The LOR subsequently exposed to the developing solution is dissolved isotropically creating an overhang of photoresist (D) and, therefore, a good lift-off profile. Metal is deposited (E) onto the surface of the wafer (metal thickness $\leq$ LOR thickness). Soaking the sample in acetone removes the bilayer of resists and unwanted metal (F). The metal contact remains on

A) Photoresist spun
onto wafer & soft baked

D) Develop sample to
create lift-off profile

B) UV exposure of
pattern through photo-
mask

E) Layer of metal
deposited onto sample

C) 15 min soak in
chlorobenzene hardens
top layer of resist

F) Immersed in acetone
to remove resist
leaving metal contact
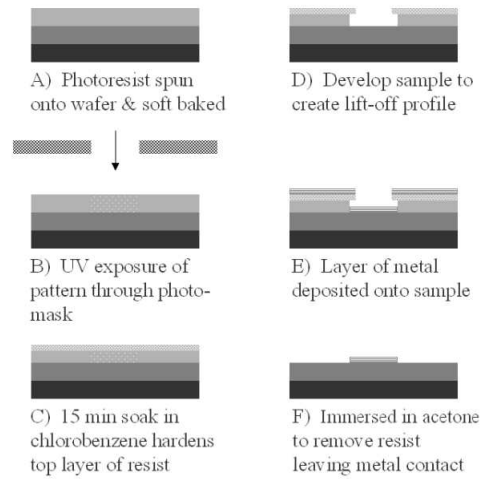
Figure 3.8: Process diagram showing the steps involved in the metal lift-off procedure which uses a chlorobenzene soak to create a good lift-off profile.

the wafer.

Over exposure

This method very simply involves increasing the resist exposure time. The principal is that the underlying layers of resist will be less exposed than the top layers and will create an undercut during regular development. There is no rule to calculate the over exposure time and it is, in fact, trial and error. Since over exposure of photoresist typically increases feature sizes, this technique is only suitable for low resolution patterns where exact size, as patterned on the photomask, is not crucial.

3.6.2   Metal removal

Photoresist is extremely soluble in acetone, so immersing in this solution results in the metal layer "lifting-off" the sample where it interfaces to the

A) Lift-off resist (LOR) spun onto wafer & soft baked

D) Develop resist. LOR develops isotropically creating lift-off profile

B) Photoresist (PR) spun onto wafer & soft baked

E) Layer of metal deposited onto sample

C) UV exposure of PR through patterned mask

F) Immersed in acetone to remove resist leaving metal contact
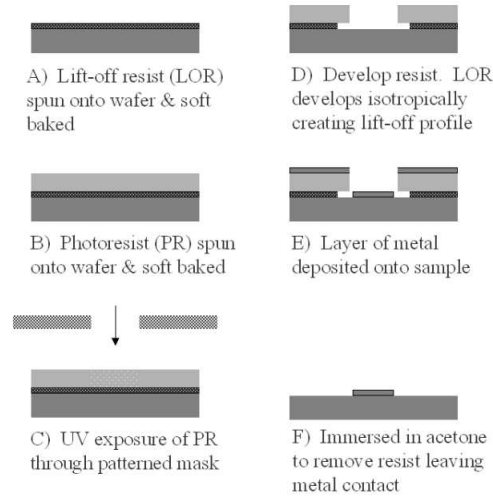
Figure 3.9: Process diagram showing the steps involved in the metal lift-off procedure which uses a lift-off resist/photoresist bilayer to create a good lift-off profile.

resist (F). The metal directly in contact with the sample remains in place as intended. The time for this to happen can vary from minutes to days depending on the quality and adhesion of the resist mask and metal layer.

3.7 Electrode array fabrication

Different combinations of the above processes are employed depending on the substrate material and device pattern. This section describes the processes developed by the author for the fabrication of arrays with varying numbers and densities of electrodes. They are fabricated on glass substrates coated in 150 nm of indium tin oxide (ITO).

3.7.1   61-electrode arrays

Array design

Initially, each 61-electrode array (of dimensions: 24 x 40 mm) was fabricated individually on to a 4 x 4 cm glass (1.1 mm)/ITO (300 nm) plate. In the interests of efficiency and ITO quality, however, manufacture of these devices was moved to 4 inch diameter glass (1.1 mm)/ITO (150 nm) wafers, providing the ability to fabricate four devices simultaneously. This required the design of new photo-masks for both ITO and passivation patterning. The GDS file for the mask used to pattern the ITO is shown in Figure 3.10. It shows the ITO and passivation mask pattern for a single array. The WaveMaker layout package was used for the design of all masks. At the centre of each device, the 61 electrodes are hexagonally close packed for highest density coverage. On each wafer, three arrays have electrodes spaced by 60 μm whilst the fourth has the increased density of 30 μm spaced electrodes (coverage area = 0.17 mm^2 and 0.04 mm^2 respectively) with the electrically exposed area of each electrode being 5 μm in diameter. These dimensions are specifically chosen to correlate well with typical ganglion cell sizes and densities. Since the electrodes are wired out through the array, their hexagonal close-packed structure places restrictions on the density of electrodes achievable.

The 60 μm spaced electrode arrays, have a minimum ITO trace width of 10 μm whilst the 30 μm spaced arrays approach the limits of photolithography with 4 μm minimum ITO trace width. The wires are routed to 64 bond pads (3 disconnected channels due to hexagonal structure), dimensions: 0.62 x 3 mm, with 1.27 mm pitch. This facilitates easy connection to readout electronics through z-axis connectors.
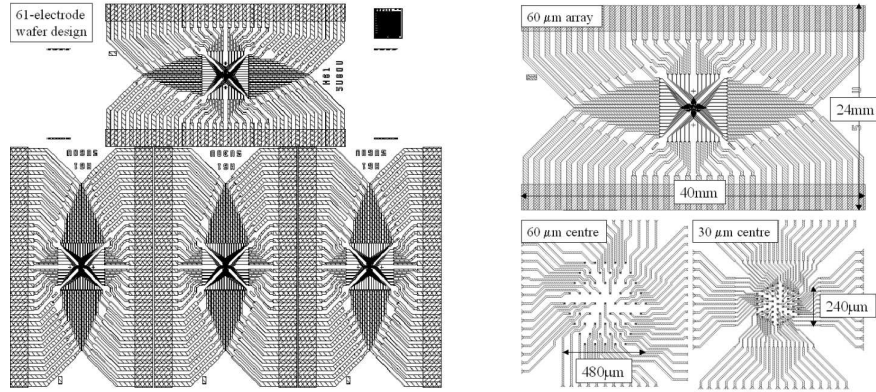
(a) Wafer mask pattern for four 61-electrode arrays

(b) Array mask pattern for 61-electrode arrays

Figure 3.10: Design files showing the wafer layout of the 61-electrode arrays and the hexagonal close-packed array of 61-electrodes on each device.

Fabrication process

A summary of the fabrication process for 61-electrode arrays is illustrated in Figure 3.11. Before processing begins, the wafer, onto which a pattern is to be written, is simply prepared by removing any particles using a high pressure flow of nitrogen since the wafers come pre-cleaned from the supplier. Photolithography is the technique used for the first step in the fabrication of the 61-electrode arrays, where the pattern of wires and electrode sites (with a minimum feature size of 4 μm) is replicated on the ITO surface. Positive Shipley 1818 photoresist (giving a resist layer of 1.8 μm when spun onto wafer at 4000 rpm for 30 s) was used for the fabrication of these arrays, as it offers better controllability for small features than a negative resist would. A 30 minute soft bake at 90 °C is required. Contact printing is performed by a Süss MicroTec MA6 and the S1818 is exposed for approximately 6 sec-

1. Glass / ITO wafer

2. Resist spun on ITO

3. Resist pattern UV exposed through photo-mask

4. Sample developed to remove exposed resist

5. Exposed ITO removed by CH_4/H_2 RIE

6. Remaining resist removed in acetone

7. ITO pattern insulated with PECVD Si_3N_4

8. Photolithography used to create resist mask

9. Si_3N_4 removed by SF_6 RIE and resist removed

Figure 3.11: Schematic of the fabrication steps involved in the manufacture of indium tin oxide 61-electrode arrays.

onds. For development, the wafers are agitated in a ratio of 1:1 microposit developer:RO (reverse osmosis) water for 75 seconds and then rinsed in RO water for 5 minutes prior to a 5 minute, 120 °C post bake.

To translate the resist pattern of electrodes and wires on to the substrate, the exposed ITO must be removed. The combination of methane and hydrogen is chosen as a reactive ion etchant. In this process, the oxygen in the ITO reacts with adsorbed CH_3 and similar radicals forming gaseous CO_x and H_2. The indium and tin are believed to combine with the carbon and are removed as organometallic compounds [54], [55]. The gases and parameters chosen for critical etches used throughout this thesis are shown in Table 3.1.

The CH_4/H_2 plasma, used to etch ITO, reacts with the resist mask forming a polymer layer which can be extremely difficult to remove. The wrong

Etch	Etchant	p (mTorr)	F (sccm)	P (W)	R (nm/min)
Ti	$SiCl_4$	9	18	250	$\sim$15
ITO	CH_4/H_2	11	5/25	100	$\sim$10
Si_3N_4	SF_6	open	10	120	$\sim$20

Table 3.1: Parameters for etching of titanium, ITO and Si_3N_4 where p, F, P and R are the pressure, flow, power and etch rate respectively.

combination and order of clean processes can, in fact, result in permanent fixture of the polymer to the substrate. It was found that cleaning the wafer in solvents (acetone and isopropanol) in an ultrasonic bath, followed by a high power oxygen plasma clean was successful in removing this material.

A PECVD system (STS PECVD, property of Stanford Nanofabrication Facility) was used for the deposition of 2 μm thick, high quality, low-stress films of silicon nitride, at low substrate temperatures (350 °C), onto the clean glass/ITO pattern. This deposition was performed on both 61- and 519-electrode arrays to electrically isolate the ITO electrodes and wires from the biological solution and tissue. A high quality layer is essential as any pinholes or cracks in the passivation render the electrode useless. 2 μm is considered to be a relatively thick insulation layer, but is necessary to withstand the rigours of biological experiments and to reduce capacitive coupling between the wires and the retinal tissue/electrolyte placed above. For these reasons, this insulation is chosen over other methods [56].

Silane and nitrogen gas are the precursors, which react to form Si_3N_4 on the substrate surface in the reaction chamber. The chamber is operated at

350 °C (much lower than temperatures $\geq$ 600 °C required for other CVD systems). The stress of the film, which to withstand biological experiments must be kept low, is precisely controlled by a programmable dual frequency function available on the STS PECVD. The deposition rate was found to be around 7 nm/min and four 4" wafers can be processed simultaneously.
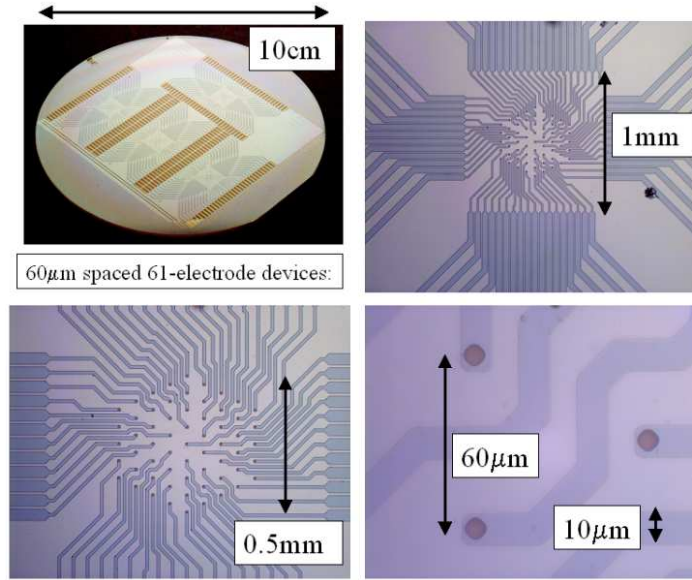
Figure 3.12: Images of arrays of 61-electrodes successfully fabricated using the process described. The layout of 4 devices on a 4 inch wafer are shown (top left). Various magnifications of the hexagonally close-packed array of electrodes (top right and bottom left) and individual 5 μm diameter electrodes spaced by 60 μm are also shown.

The final step is to etch holes (vias) in the passivation layer to allow an electrical connection to be made at the electrodes and bond pads. Using photolithographic techniques, AZ4562 positive tone photoresist is spun onto the Si_3N_4. This photoresist is particularly viscous and spin parameters are chosen to obtain a 3.5 μm layer. Since this resist will act as an etch mask for

a 2 μm depth of Si$_3$N$_4$, it is essential that it forms a durable mask. The thick mask created using AZ4562 makes it ideal for this purpose. Vias are formed over the bond pads and electrodes using standard photolithography techniques as described in Section 3.2. A reactive ion sulphur hexafluoride (SF$_6$) plasma (Table 3.1) is employed to selectively etch the Si$_3$N$_4$ exposing the underlying ITO and creating electrically conducting bond pads and electrodes. Images of 61-electrode arrays are shown at various stages of fabrication in Figure 3.12.

3.7.2   519-electrode arrays

Array design

To cover a larger area of retinal tissue, enabling a more effective study of the connectivity of cells, an array with 519 electrodes was designed. As with 61-electrode arrays, this device was also originally fabricated onto 4 x 4 cm glass/ITO plates and for time and cost efficiency as well as ITO quality, the process was moved to 4 inch diameter wafers onto which four devices are patterned. The design file for the wafer pattern and individual array patterns are shown in Figure 3.13.

Each device is 32 x 32 mm, separated by a cutting margin of 250 μm. Hexagonally close-packed in the central section of the device are 519, 5 μm diameter, electrodes with either 60 or 30 μm spacing. The 60 μm spaced array has a minimum feature size of 2 μm wide ITO traces and the array of electrodes covers an area of 1.7 mm^2. The state-of-the-art 30 μm spacing 519-electrode device reaches the limits of electron beam and etch lithography on ITO. Each array has a minimum feature size of 1 μm traces in the very central region

and covers an area of 0.45 mm^2. The wires route out to 520 bond pads (of dimensions: 0.11 x 1.8 mm and pitch: 0.2 mm) since the geometry of this device requires that there is only one disconnected channel.

(a) Wafer e-beam pattern for four 519-electrode arrays

(b) Array mask pattern for 519-electrode array
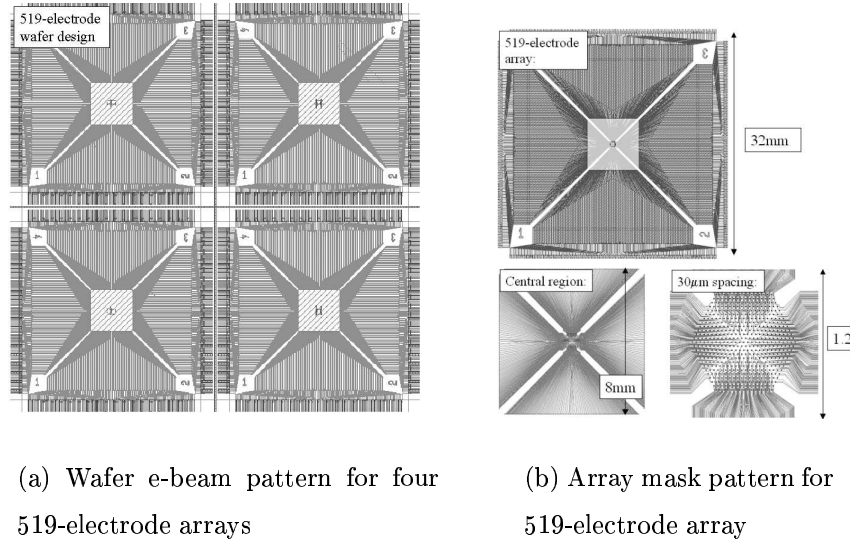
Figure 3.13: Design files showing layout of 519-electrode arrays on wafer and the hexagonal close-packed array of electrodes on each device.

Fabrication process

For the fabrication of these devices, the wafer is firstly cleaned using high-pressure nitrogen before depositing metal onto the ITO surface. This layer forms a reflective surface, allowing an accurate height map to be formed by the electron beam-writer, reducing the likelihood of stitching errors between successive writing fields. It also has the added benefit of forming an effective etch mask during subsequent processing. Due to its tendency to adhere well to almost any material, including ITO, 100 nm of titanium is evaporated onto the surface of ITO/glass wafers. This metal is also chosen as it can

be easily dry etched, a necessary quality of material used in the fabrication of these devices. An illustration of the fabrication process of 519-electrode arrays is shown in Figure 3.14.

Due to the higher density of wires and electrodes, electron beam lithography is used to generate the 519-electrode pattern on to the ITO surface. The tool used is a EBPG5-HR100 beam writer. As with 61-electrode devices, four devices are patterned onto a four inch diameter glass/ITO wafer which is pre-cleaned by the wafer suppliers. 150 nm of titanium is evaporated on to the wafer using a Plassys electron gun evaporator. HMDS primer is then spun at 3000 rpm for approximately 5 s and baked at 80 °C for 15 mins. For the purpose of the fabrication of 519-electrode arrays, a positive deep UV (DUV) resist is used, 58 % Shipley UVIII. This is a type of resist which is in fact sensitive to both UV light and electrons and is chosen as it is exposed at low doses resulting in large area patterns being written in reasonable periods of time. Added advantages are its feature size capabilities and good dry etch resistance. It is spun onto the wafer surface at 3000 rpm for 60 s and soft baked on a hotplate, set to 130 °C for 1 minute.

With a minimum feature size of 1 μm, a beam spot size of 112 nm is selected for the central section of the design and the outer section is written using a 300 nm spot. Altering the spot diameter according to the feature sizes decreases the job write time, which is around 4.5 hours for this pattern. A dose of 30 μC/cm^2 is used and this is corrected to account for electron scattering proximity effect. The beam writer is operated at 50 kV. Once written, the pattern is developed. This involves an initial bake on a hotplate at 130 °C to harden the unexposed resist. The exposed pattern becomes

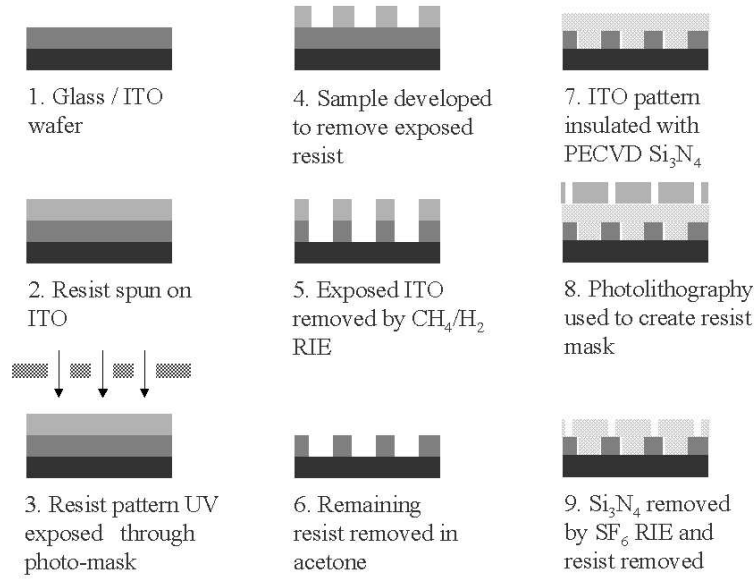visible during this bake. Following this, the exposed resist is removed by immersing the sample in neat CD26 developer for 1 min.
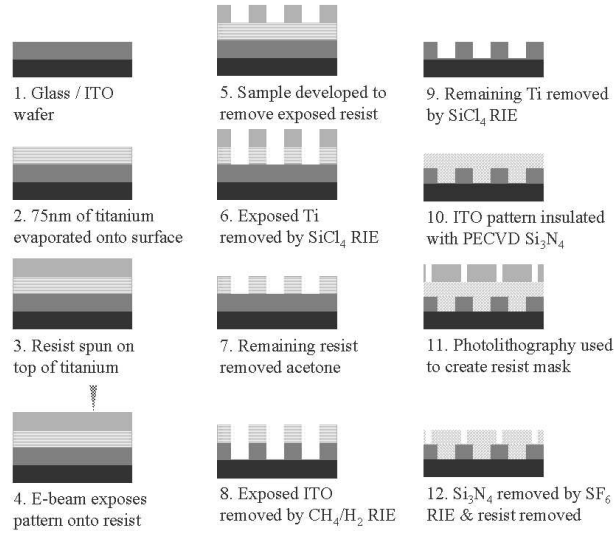
Figure 3.14: Schematic of the fabrication steps involved in the manufacture of indium tin oxide 519-electrode arrays

Transferring the device pattern onto the ITO surface involves removing the reflective titanium layer to expose the ITO. A silicon tetrachloride reactive ion etch achieves this. UVIII acts as an excellent etch mask at this stage but must be cleaned off once the etch is completed. Using the remaining titanium as a mask, the exposed ITO is then removed using a CH_4/H_2 RIE (see Table 3.1). To render the array transparent, a necessary requirement of these devices, the remaining titanium is removed using a $SiCl_4$ RIE as before. Care must be taken here to etch only the Ti as $SiCl_4$ also reacts with ITO. An alternative would be to wet etch the Ti in a 5:1:1 ratio of RO water : hydrogen peroxide (H_2O_2) : ammonia solution (NH_3) which is

very selective and does not react with the ITO. The gases and parameters for these etches are shown in Table 3.1. The same procedure is followed as described in Section 3.7.1 to passivate the electrode arrays and etch the passivation to create electrical contact points.
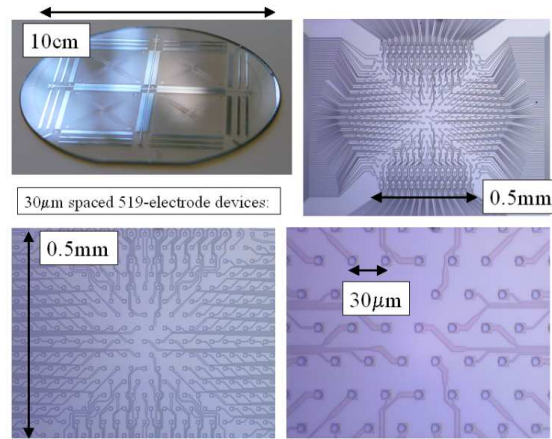
Figure 3.15: Images of successfully fabricated state-of-the-art arrays of 519 electrodes. The layout of 4 devices on a 4 inch wafer is shown (top left). Various magnifications of the hexagonally close packed array of electrodes are shown (top right and bottom left) as well as a close up of individual electrodes spaced by 30 μm with 1 μm wide connecting wires (bottom right).

Since the array is wire bonded to a readout system (see Section 2.4) to perform biological experiments, a 1 μm layer of aluminium is sputtered onto the bond pads of 519-electrode arrays and selectively removed by lift-off. This aluminium layer provides a low resistance (2.7 $\mu\Omega$/cm) connection which adheres well to both the wire bonds and clean ITO surfaces. Images of fabricated 519-electrode arrays are shown in Figure 3.15

3.7.3 Low stress passivation

Literature states that silicon nitride should measure between 50 and 150 MPa whilst regular silicon nitride can measure between 300 and 600 MPa [57]. To ensure that low stress silicon nitride was being deposited onto the electrode arrays, stress tests were performed on blank silicon wafers. These depositions were also used to calculate the deposition rate. The two most popular silicon nitride deposition recipes were used to deposit 200 nm thick films onto blank silicon wafers using the STS plasma enhanced CVD system at SNF. Each run contained two 4" wafers (A and B). The recipes used are shown in Table 3.2. The parameter altered is the High RF time.

	Recipe 1	Recipe 2
Silane gas flow (sccm)	2000	2000
Ammonia gas flow (sccm)	150	150
Chamber pressure (mTorr)	650	650
Temperature (^{o}C)	350	350
Low RF time	2	2
High RF time	5	4

Table 3.2: Recipe parameters for the deposition of 2 μm thick layers of low stress silicon nitride using a PECVD system at SNF.

To measure the stress induced on a substrate by the deposited Si_3N_4 film, a Frontier SMSi 3800 Stress system (SNF) was used. It uses a non-contact, optical procedure. Deflection of a scanning laser beam allows the curvature of the wafer to be determined before and after film deposition. If the height of the substrate is expressed as a continuous function of distance along the substrate surface then the radius of curvature is expressed as:

$$R(x) = (1+y'^2)^{3/2}/y''$$

where:

y' is dy/dx and

y'' is d^2y/dx^2

The following equation uses the pre- and post-deposition wafer curvature to calculate the stress in the film:

$$s = (1/6)[E/(1-v)][h^2/6t\Delta R]$$

where:

s is the film stress (Pa)

E/(1-v) is the substrate biaxial elastic modulus (1.805E11 Pa for 100 Si)

h is the substrate thickness (m)

R is the substrate radius of curvature (m) and

t is the film thickness (m)

Figure 3.16 shows the calculated values for each of the four wafers. The conclusion from this was to deposit Si_3N_4 using recipe 2, whose values were within the correct range for a low stress film. The Nanometrics Nanospec system (SNF) was used to measure the thickness of the film. It uses non-contact, spectro-reflectometry (measurement of the intensity of reflective light as a function of incident wavelength) to determine the thickness of transparent films on substrates that are reflective in the visible range. A duration of 28 minutes was found to deposit 200 nm (averaged over the surface of a 4" silicon wafer) hence a deposition time of 280 minutes was used to deposit 2 μm of low stress Si_3N_4 onto the glass/ITO wafers.
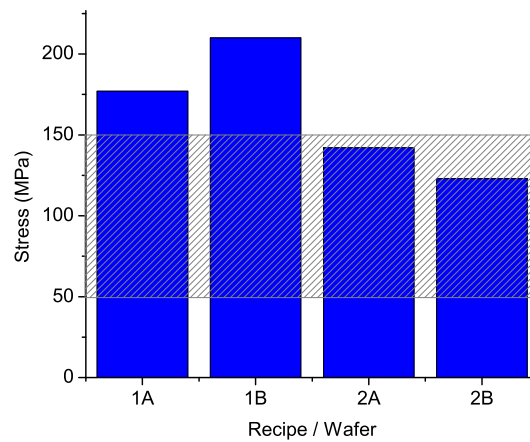
Figure 3.16: Bar graph showing the measured stress on silicon wafers deposited with 200 nm of silicon nitride. The shaded region represents expected values for low stress silicon nitride.

3.8 Wafer dicing

The final procedure in wafer processing is to separate the devices by dicing. This is challenging and requires process development as there are many variables which depend on sample material, thickness etc. These parameters greatly affect the quality of the cut. The technology used to dice the wafers is an in-house Disco DAD321 automatic dicing saw.

Before dicing, there are several variables which must be taken into consideration such as substrate thickness, material and cut width and these properties define the necessary parameters (see Table 3.3). In this case, the substrate is 1.1 mm thick glass coated in a comparatively fragile, 2 μm layer of silicon nitride and the cut widths (defined by the array positions) are 100 or 250 μm. The ideal parameters arrived at for the dicing of these devices are listed in Table 3.3. The consequences of choosing the wrong parameters are shown in

Blade speed	30000
Blade type	diamond
Blade width	100/230 μm
Blade outer diameter	52 mm
Feed speed	1 mm/sec

Table 3.3: Blade and cutting parameters for dicing 61- and 519-electrode wafers on 1.25 mm thick glass/ITO substrates.

Figure 3.17.
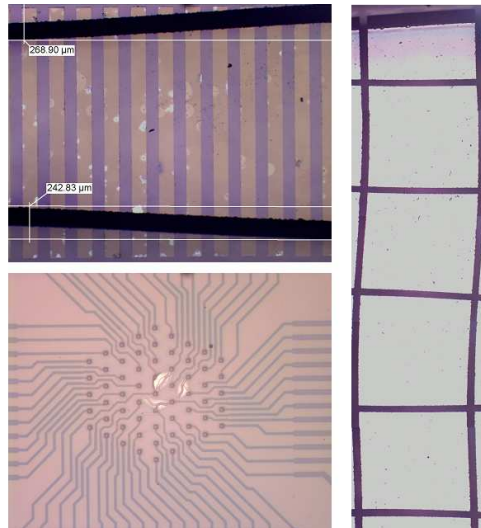
Figure 3.17: Images showing consequences of poorly chosen dicing parameters: stress on nitride causing cracks (bottom left), blade movement during dicing (top left and right).

Chapter 4

Recording microelectrode arrays

4.1 Introduction

To record simultaneously individual neuronal responses over a large area, arrays of 61 and 519 electrodes with inter-electrode spacings of 60 and 30 μm were designed and fabricated as previously described. In this chapter, details of the procedures followed for the final preparation and characterisation of these arrays for use as biological recording devices are given. Evidence of their successful use in experiments is also presented in the form of retinal spike recordings, electrophysiological images and the visual field represented as map of cell receptive fields.

4.2 Platinisation

The recording sites, determined by the size of hole etched in the passivation layer, are only 5 μm in diameter creating a highly resistive contact through

saline solution to retinal cells. To lower the resistance, a material called platinum black is electroplated over the electrodes. Often used as an interface in biological experiments, platinum black is desirable as it is both biocompatible (platinum is a noble metal) and has a low resistivity. The latter property is a consequence of its porous, granular structure, which effectively increases the surface area of the electrode, significantly reducing the impedance at the cell-electrode interface. Platinising the electrodes serves not only to lower their impedance (impedance of ITO, $Z_{ITO} > 20$ MΩ at 1 kHz) but is also a very effective method of highlighting broken channels, which when numbering greater than $\sim$5% can result in the device being unsuitable. This number of broken channels, however, is low and typically only around 1 - 2% channels are broken on a single array. Figure 4.1 shows several arrays badly affected by broken channels arising from different defects.
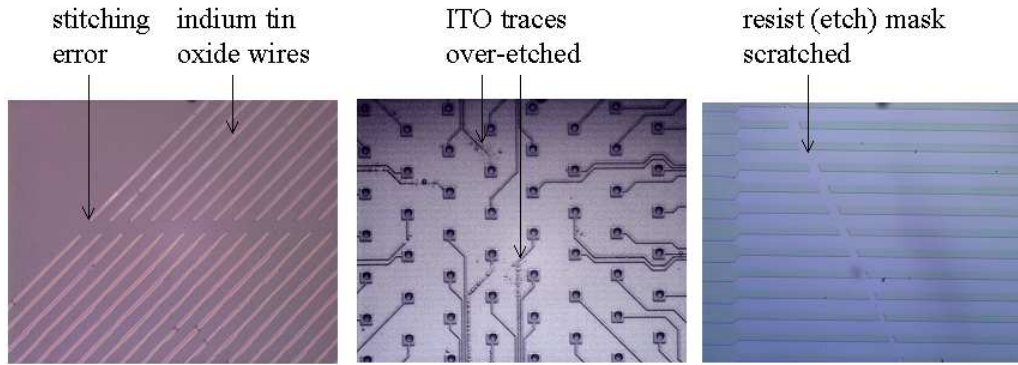
Figure 4.1: Broken channels caused by stitching errors during the e-beam lithography step (left), poor titanium etch mask (middle) and scratched photoresist (right).

4.2.1   Method

Electrodes are immersed in a solution of 1 % platinic chloride, 0.08 % lead acetate and 98.92 % R.O. water. A length of platinum wire acting as an anode is inserted into the solution and the electrodes act as the cathode, attracting Pt^+ ions. A probe contacting the bondpads completes the circuit and a current density of 4 nA/μm^2 is applied individually to each electrode for approximately 10 s. An image of the system and a schematic of the array set up is shown in Figure 4.2. Ideally, the platinised electrode should have a diameter no greater than the hole in the passivation layer and an average impedance (at 1 kHz) of around 200 kΩ. Figure 4.3 is an SEM image of an electrode pre- and post-platinisation.

(a) Photo of the system used   (b) Schematic of set-up at electrode
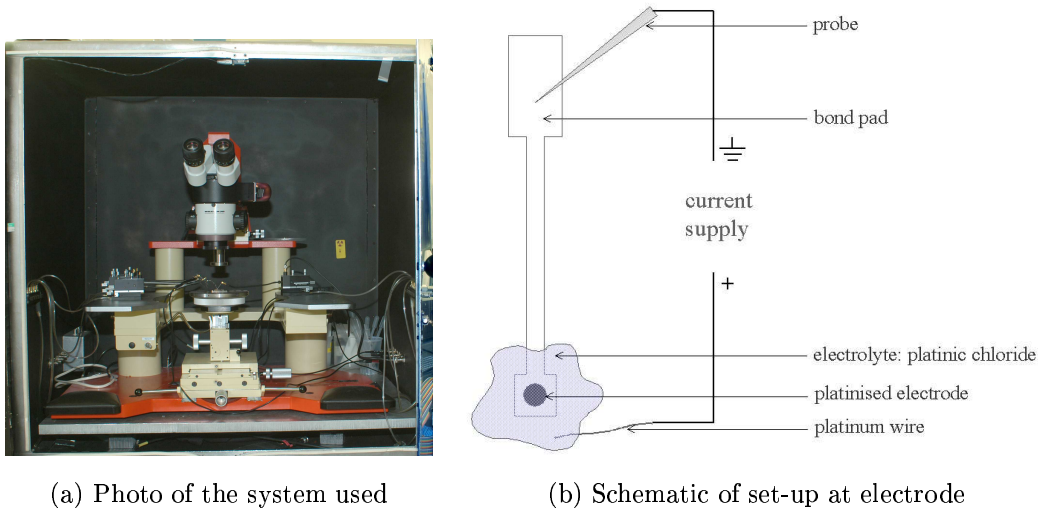
Figure 4.2: System used for the platinisation of ITO electrodes.

Figure 4.3: SEM images of an unplatinised electrode (left) and a well platinised electrode (right), each 5 μm in diameter.

4.3 Device characterisation

Before use, it is important that the electrode arrays are carefully examined. This includes inspection optically, physically and electrically.

4.3.1 Passivation

To maintain biocompatibility and electrode isolation, the silicon nitride passivation layer must be intact. Any holes or cracks in the layer disqualify it for use. Not only must the passivation layer undergo a meticulous optical inspection for any defects, but it is also destructively tested. This involves subjecting the silicon nitride to a high pressure clean with acetone and cotton swabs ensuring it is durable enough to withstand the rigours of biological testing. Cracks in the passivation layer are most likely to appear between electrode vias as this is the region of highest stress. Examples of defects found in the silicon nitride layer are shown in Figure 4.4.

Figure 4.4: Pictures showing typical defects found in the silicon nitride passivation layer. Cracks (or holes), alone, are a failure mechanism on these devices.

4.3.2 Inter-channel resistance

The devices are characterised electrically to ensure good quality ITO traces and a good electrical connection between the electrodes and bond pads. There are several measurements which must be made, the first of which is to measure the inter-channel resistance between every electrode. These measurements are performed using the semi-automated Cascade Microtech S300 12" probestation along with the Keithley 4200 semiconductor characterisation system. The system is shown in Figure 4.5.

To allow low noise measurements, the system is well shielded utilising double shielded triaxial connections to the level of the probe and single shielded coax to the probe tip as well as meter pre-amplifiers. Probes are placed on neighbouring bond pads and a current-voltage measurement is performed allowing the resistance to be calculated. Typical values for well isolated channels are measured to be greater than 200 GΩ and shorted channels have inter-channel resistance values of $\leq 10^2$ kΩ although this varies depending on the nature of

the short. Approximately 10 % shorted channels is the maximum acceptable on any device and it has been shown to be possible, on both 61- and 519-electrode devices, to achieve no shorts, although this is a challenge on larger area, higher density arrays such as the 30 μm spacing 519-electrode device.
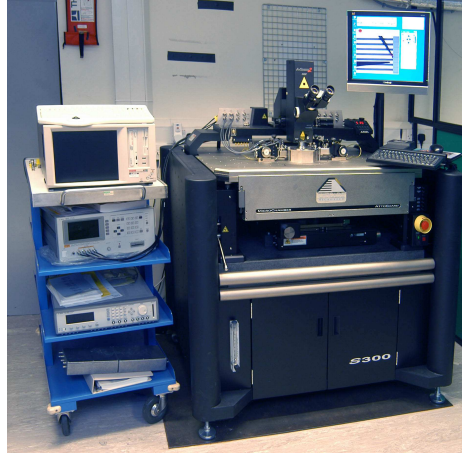
Figure 4.5: Image of Microtech 12" probestation and Keithley characterisation system used for the measurement of inter-channel resistance.

In the early stages of fabrication, defects in the resist mask hinder its development causing shorted channels. Further in to the process, shorts are commonly caused by debris (e.g. dust particles) effectively forming an etch mask over the ITO or titanium. Figure 4.6 shows examples of shorted channels.

4.3.3   Inter-channel capacitance

Using the Cascade Microtech probestation in conjunction with an Agilent 4284A precision LCR meter (20 Hz - 1 MHz), inter-channel capacitance is measured. Any two channels effectively act as a parallel plate capacitor: ITO wires form plates with the passivating silicon nitride as the dielectric.
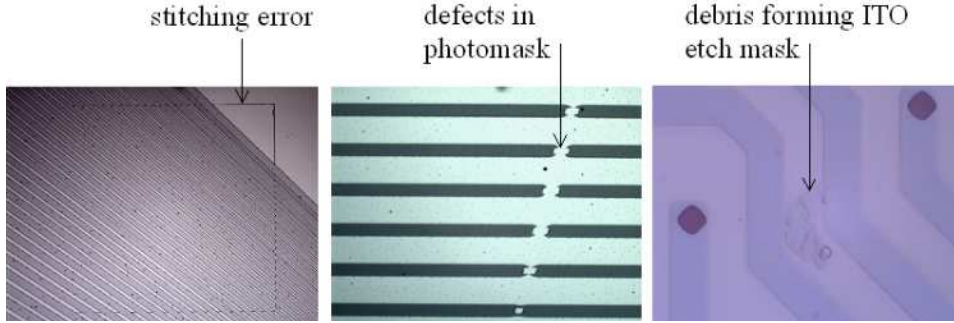
Figure 4.6: Pictures showing shorted channels caused by stitching errors in e-beam lithography, mask defects in photolithography and debris on the wafer during etch lithography.

These measurements, therefore, are necessary to examine the isolation of adjacent channels, an important quality of these devices as the electrodes are required to record independently for an accurate analysis of resulting data. Neighbouring bondpads were probed and the capacitance was measured at various different positions. Figure 4.7(a) shows how the inter-channel capacitance changes along a side of various arrays and Figure 4.7(b) shows the electrode numbering system for both 61- and 519-electrode arrays.

The trends shown in Figure 4.7(a) are explained by the geometric layout of the arrays and also the capacitance being inversely proportional to the channel separation. Referring back to the design of the arrays (as detailed in Chapter 3), the outer bondpads (positions 1 and 5) require longer ITO traces and also there is symmetry about the centre bondpad. For each array, however, the inter-channel capacitance is measured in the range of 0.2 - 2 pF showing good isolation of the ITO traces.

The capacitive coupling between successive neighbours was also measured. As is shown in Figure 4.8 the values show a 1/r dependence for every next nearest neighbour, as expected.
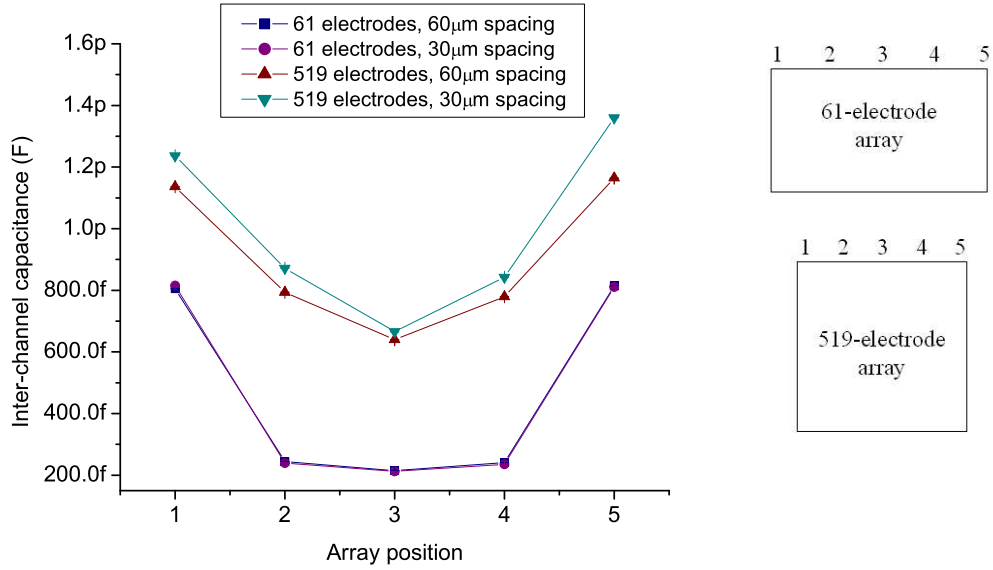
(a) Inter-channel capacitance as a function of array position where positions 1 - 5 are equivalent to left - right along one side of an array.

(b) Electrode numbering system.

Figure 4.7: Inter-channel capacitance measurements as a function of array position on both 61- and 519-electrode arrays.

4.3.4 Electrochemical impedance spectroscopy

Platinised electrode impedance, Z, is another important electrical characteristic which must be measured. ITO electrodes are platinised as a means to reducing the resistivity of the cell-electrode interface. Measuring this impedance gives the necessary quality control.
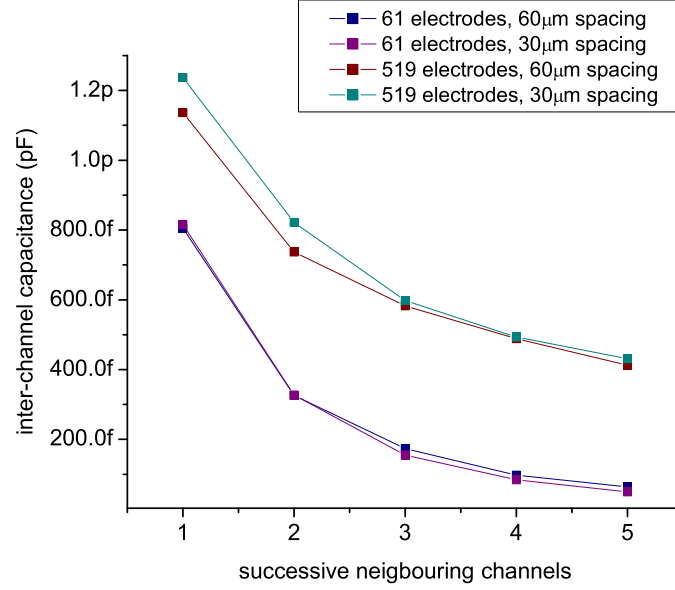
Figure 4.8: Inter-channel capacitance measurements for successive neighbouring channels on both densities of 61- and 519-electrode arrays where 1 = electrode number 1. Nearest neighbours are represented by 2, 3, 4 and 5.

The impedance of each electrode is measured individually. The electrodes are immersed in 0.9 M saline solution (resembling eye conditions). Into the solution a platinum wire is inserted to apply an A.C. sinusoidal voltage stimulus of 100 mV peak to peak. The bondpad of interest is probed and subsequently the impedance is measured over a range of frequencies (100 Hz-100 kHz). Since access to the array is required for the platinum wire these measurements cannot be performed using the Cascade Microtech probestation as it is fully shielded. Instead, a manual Karl Suss PM5 probestation is used in conjunction with an HP4274A multi frequency LCR meter.

Whilst the impedance of each electrode is measured over a range of frequen-

cies, the region of interest is around 1 kHz since retinal action potentials, detected by the electrodes, typically have a duration of around 1 ms. Values for well platinised electrodes are expected to lie between 100 kΩ and 500 kΩ.

I_d (nA/μm^2)	Time (s)
2	10, 15, 20, 25
4	10, 15, 20, 25
7	10, 15, 20, 25
10	10, 15, 20, 25

Table 4.1: Current densities (I_d) and times investigated to find optimum parameters for platinum black electrode formation.

Optimum parameters

Experiments were undertaken to investigate the effect of altering the platinisation current density and time on the physical and electrical properties of electrodes. To find the optimum platinisation parameters for 5 μm diameter ITO electrodes a variety of parameters were used to platinise 5 μm diameter electrodes and the results are displayed in Table 4.1. The impedance versus frequency curves are shown in Figure 4.9 for each current density averaged over the different platinisation times.

Although electrodes platinised at 10 nA/μm^2 have the lowest impedance value, Figure 4.10 shows that these electrodes are much larger than 5 μm in diameter as they have formed mostly around the perimeter of the silicon nitride via whilst the centre is poorly platinised. In fact, this is also the case for electrodes platinised at 7 nA/μm^2. This electrode structure results

in decreased spatial localisation and only the outer ring makes contact with retinal cells which is not ideal. When a current density of $2 \, nA/\mu m^2$ is used, the impedance is significantly higher and not suitable for measuring retinal action potentials. Figures 4.10 and 4.9 show that both the electrical and physical properties of platinum black electrodes formed at $4 \, nA/\mu m^2$ are ideal for the proposed experiments with retinal tissue.
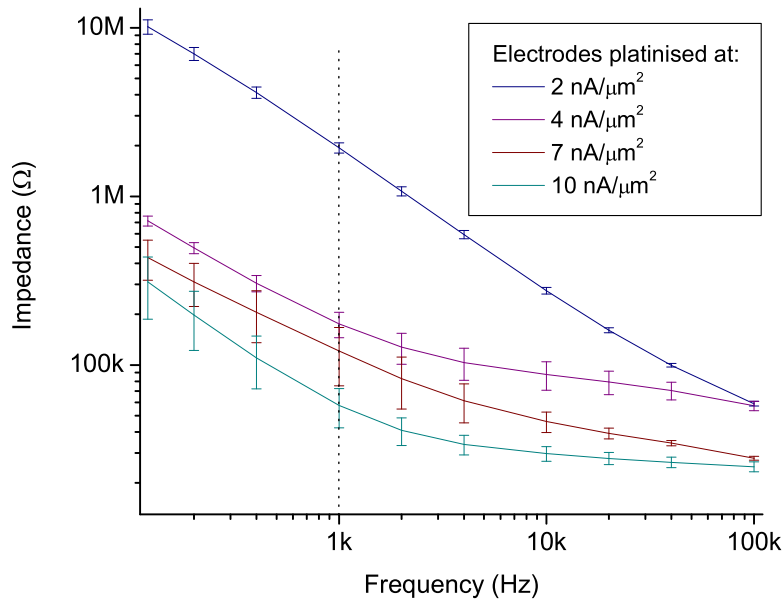
Figure 4.9: Impedance versus frequency for electrodes platinised at current densities varying between 2 and $10 \, nA/\mu m^2$. The vertical dotted line highlights the impedance values at 1 kHz, the frequency of interest in these experiments.

Electrochemistry is a very fragile chemistry and any variations in environment, particularly surface or solution contamination, can greatly alter the conditions required for success. It can be stated, however, that $4 \, nA/\mu m^2$ is a reasonable starting point to attempt platinising from. Again, due to the nature of electrochemistry, it is impossible to calculate a precise optimum
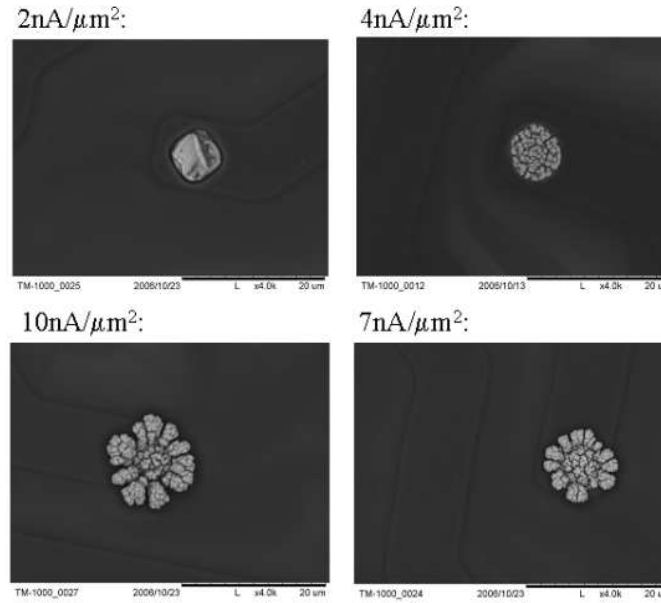
Figure 4.10: SEM images of electrodes platinised for 10 seconds at various current densities.

time for platinisation. A more reliable method of judging the quality of the electrode during the formation of the platinum black is to monitor the voltage with time since a repeatable trend was found to be observed. A gradual increase in voltage is typically followed by a swift reduction which, slowing down, plateaus in the region of 0.6 - 0.7 V for these devices. To examine consistency, each electrode on a 60 μm spacing 61-electrode array was platinised at 4 nA/μm^2 for 15 s. A labview program was used to readout the voltage during each platinisation and the traces are shown in Figure 4.11. The impedance values were plotted against frequency for each electrode and these are shown in Figure 4.12.

Examining Figure 4.11, there is a trend with each subsequent platinisation. Consider $V_{n,t}$ where V is the voltage measured, n is the order of electrode

platinised (independent of array position) and t is the time (in seconds) during platinisation. Then for these tests it can be seen that $V_{n+1,0} < V_{n,0}$ and similarly, $V_{n+1,15} > V_{n,15}$. This effect is reflected in Figure 4.12, where $Z_{n+1} > Z_n$ for electrode impedance Z.
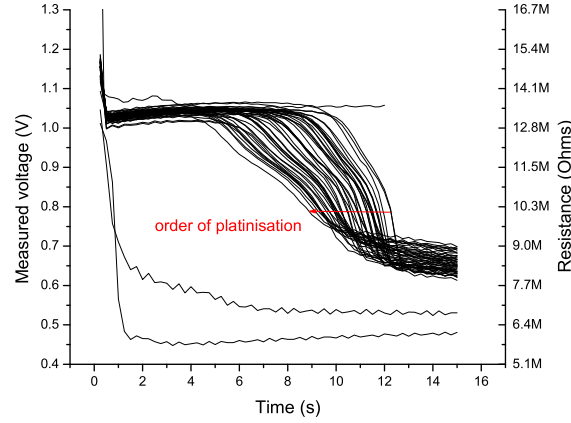
Figure 4.11: Measured voltage versus time when 4 nA/μm^2 is applied to an electrode for electrode platinisation. The electrode requires $\sim$1 V to initiate the electroplating process. As the platinum deposits, the required voltage reduces. Since the purpose of the electroplating process is to reduce the resistance of the electrode a 2nd y-axis is shown to quantify this. The red arrow shows the order in which subsequent electrodes were platinised.

A test was performed to ascertain the cause of this effect. The impedance of an unplatinised ITO electrode was measured. Neighbouring electrodes were platinised and the ITO electrode impedance was subsequently re-measured. From Figure 4.13, it was deduced that coupling occurs between neighbouring electrodes through the platinic chloride electrolyte causing a mild platinising effect. Provided the electrode impedances remain in the region of 100 kΩ to 500 kΩ, this effect is not detrimental to the quality of the device for use in experiments.

Figure 4.12: Impedance versus frequency averaged over electrodes well platinised (4 nA/μm^2 for 15 s).
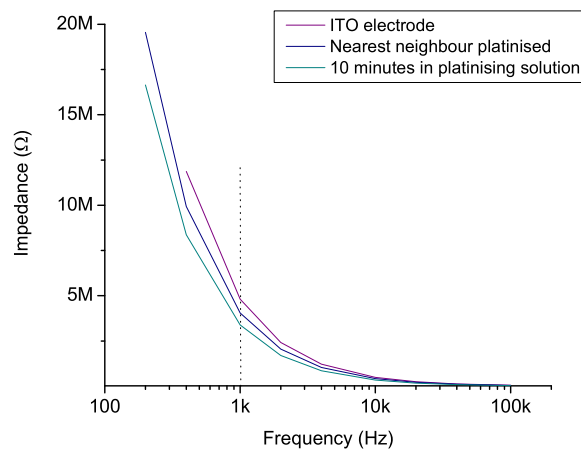
Figure 4.13: Impedance versus frequency of ITO electrode before and after contact with platinic chloride solution and platinisation of neighbouring electrode.

4.4 Array performance results

Having qualified for use in a biological experiment, an electrode array is fixed into the appropriate readout board. In the 61 electrode system, the

104

readout electronics and the electrode array are connected using elastomer (zebra) connectors which are silicone rubber strips made up of sequentially spaced conductive and non-conductive material. However, to accommodate the 200 μm pitch used in the 512 electrode system, wire bonding is employed. Platinising the electrodes manually, as described in Section 4.2.1, is good practise as a test of well etched electrode vias and continuous ITO traces. Since wire bonds securely attach the array to the 512 channel readout system, the electrodes are re-platinised using the Plat64 chip. The most challenging aspect of the work presented here was the fabrication of the novel, state-of-the-art 30 μm spaced 519-electrode array. Biological results from this array are shown here and compared to the previous 512-electrode arrays with a lower density of electrodes.

4.4.1 System noise

With a platinised electrode array immersed in saline solution and fixed in the system, the equivalent input rms noise is measured to be $\sim$7 μV which is the same as the 60 μm spacing 512-electrode array system noise. The typical signal amplitude range of interest is 50 - 800 μV. In Figure 4.14 the readout of noise for each electrode on the 30 μm spacing 519-electrode array is shown. Well platinised, un-shorted channels measure in the region of 7 μV. Poorly platinised electrodes (resulting from shorted channels), however, measure between 20 and 30 μV and disconnected channels, of which there are four, are the zero points. These are easily identifiable in Figure 4.14. This is the final test before beginning tissue experiments using this array.
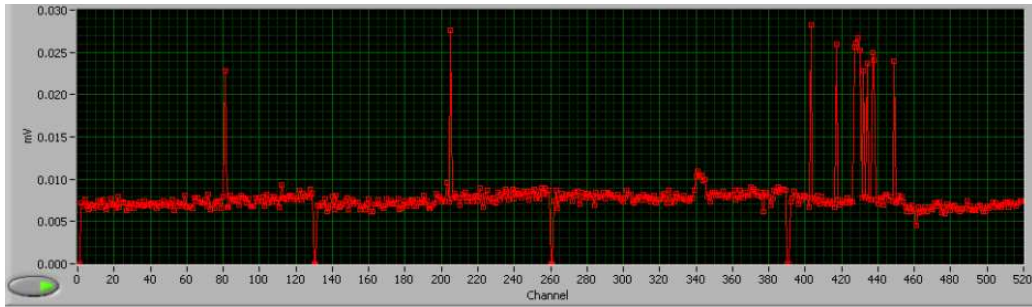
Figure 4.14: Noise level read out for each channel of 30 μm spacing 519-electrode system.

4.4.2 Biological measurements

The successful fabrication of the 30 μm spacing 519-electrode array allowed its use in pilot macaque monkey studies at the Salk Institute for Biological Studies, San Diego, under the supervision of E.J. Chichilnisky. The experimental procedure is described in Section 2.5. This section will show evidence from these experiments of the arrays capability not only to record mammalian retinal pulses but to record these signals simultaneously from hundreds of electrodes. A comparison is also made between results obtained from this state-of-the-art device and from previous lower density arrays of electrodes showing the improvement and advantage offered by decreasing the electrode density from 60 μm to 30 μm. The biological data shown in this section result from retina stimulated by a white noise light stimulus as described in Section 2.6.2.

Recording action potentials

As evidence of the 30 μm spacing 519-electrode array's ability to record consistently retinal pulses from mammalian retina over an extended period

of time, Figure 4.15 shows raw data collected from a single electrode. This data is in the form of action potentials (see Section 2.2.2) produced by an ON-small midget ganglion cell from macaque monkey retina in response to a white noise light stimulus. Figure 4.15(a) shows action potentials over a period of 1 s and Figure 4.15(b) is a close-up of one of these spikes (30 ms duration). In these plots 1 ADC count is equivalent to 1.1 mV of output (after ×1500 amplification from readout circuitry). These are extracellular action potentials and so have reverse polarity to the intracellular action potentials shown in Figure 2.7. From these recordings it can be seen that well defined action potentials can be recorded by this device and read out.

(a) Retinal ganglion cell action potentials recorded over 1 s (20,000 samples at 20 kHz).

(b) Biphasic retinal ganglion cell action potential recorded over 30 ms (600 samples at 20 kHz).
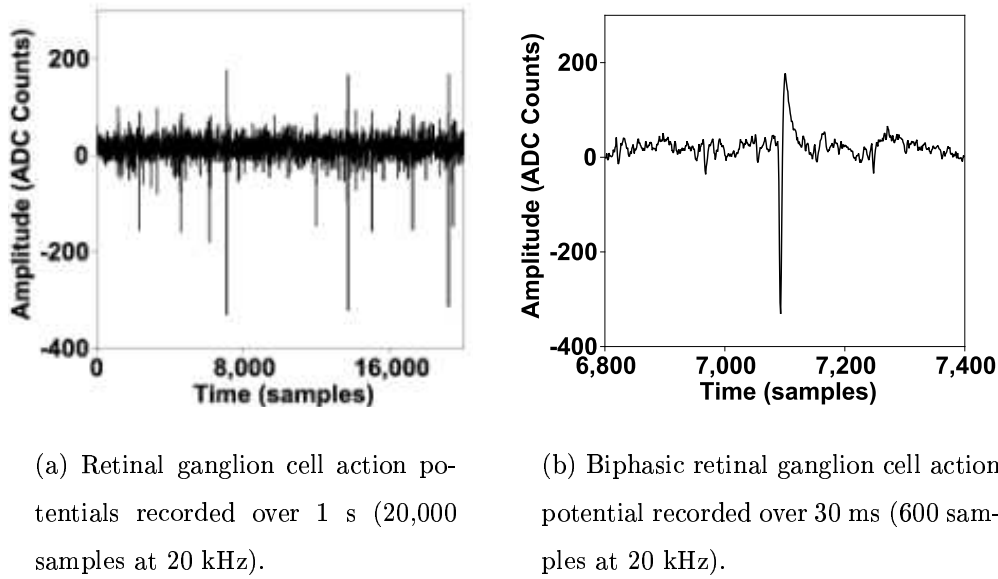
Figure 4.15: Action potential recorded using 30 μm spacing 519-electrode array and shown over two time durations.

Multiple electrode recordings

The advantage of this system over traditional methods, however, is that it allows the study of the behaviour of populations of neurons. Proving the arrays capability to do this, Figure 4.16 shows simultaneous recordings from several electrodes on the 30 μm spacing 519-electrode array.

An action potential produced by a neuron is typically recorded over many electrodes and whilst a complex 5-dimensional principal components analysis technique is used to correlate recorded signals with individual neurons, Figure 4.17 shows recordings from the same period of time over 19 neighbouring electrodes. The action potentials shown are not proven to be from the same neuron, however, they are another effective example of the arrays ability to record from multiple electrodes.

Electrophysiological imaging

Following the neuron identification procedure described in Section 2.6.1, the analysed data can be displayed in the format of an "electrophysiological image" (EI). This involves imaging each identified neuron in terms of the average analogue waveform generated on each electrode as the neuron spikes. For each neuron, the average electrode signal is represented by a circle at the electrode location, with a diameter given by the maximum (negative) signal amplitude. The EI of a midget ganglion cell produced by a 60 μm spacing 512-array is shown in Figure 4.18 and is interpreted as follows: the large circles give the approximate locations of the soma (cell body) on the array, and the line emanating from the cell body region is an image of the corresponding axon.
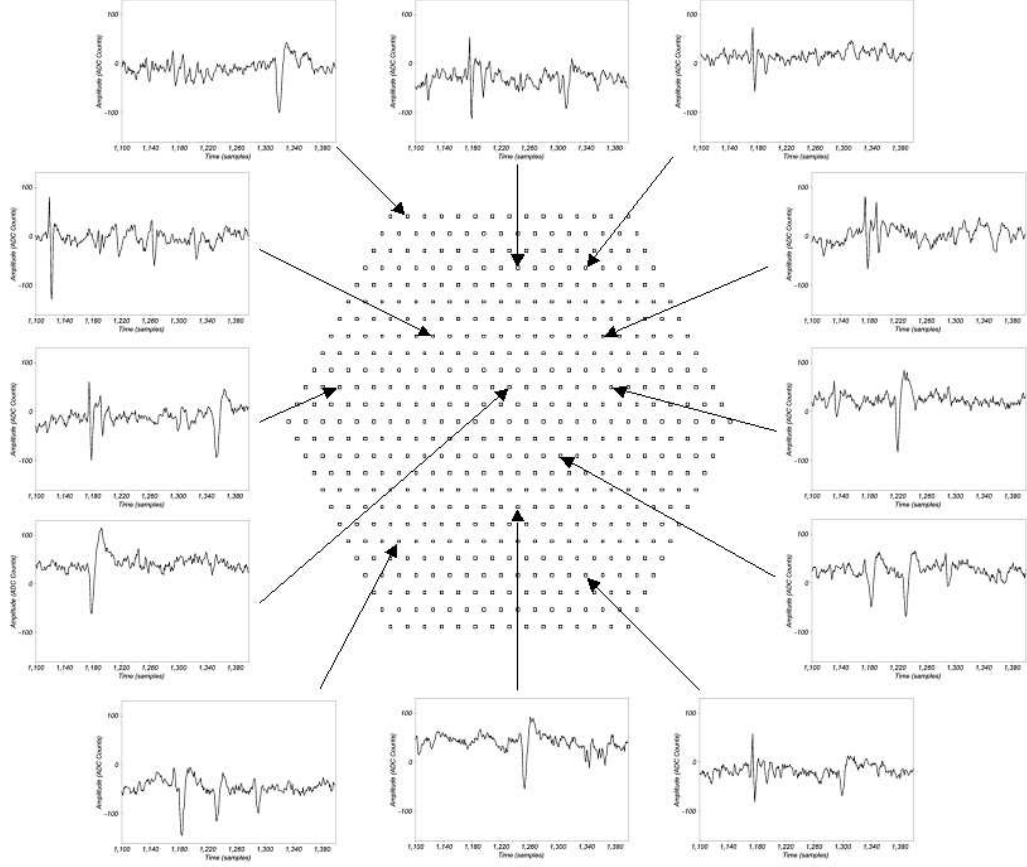
Figure 4.16: Examples of action potentials recorded simultaneously, over a duration of 15 ms (x-axis), from various electrodes on the 30 μm spacing 519-electrode array. Each dot represents an electrode on the array. On each recording plot, the y-axis is spike amplitude measured in mV (ranging from -150 to 150 mV after $\times$1500 amplification from readout circuitry).

To determine the improved performance of the higher density device, the development of which has been described throughout this thesis, an EI of a midget ganglion cell produced by the 30 μm spacing 519-electrode array is shown in Figure 4.19.
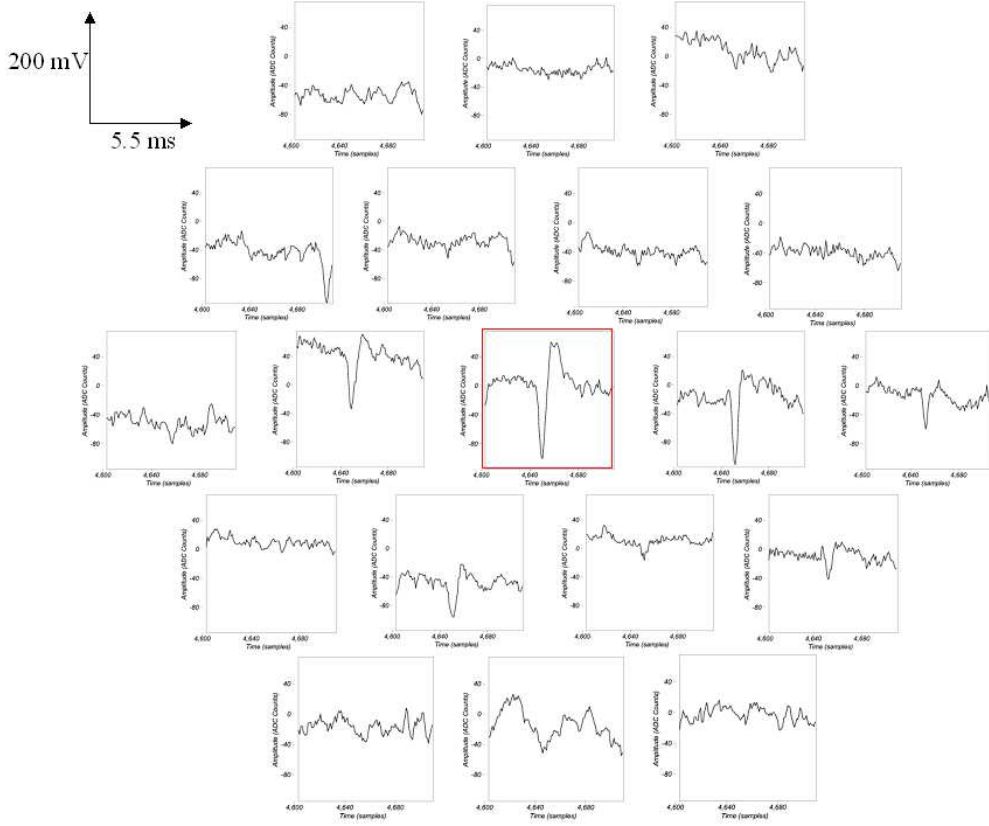
Figure 4.17: Recordings from 19 neighbouring electrodes, over the same time period, showing capability of 30 μm spacing 519-electrode array to record from multiple electrodes simultaneously. The x-axis is time samples (equivalent to 5.5 ms) and the y-axis is spike amplitude in mV (ranging from -120 to 80 mV after $\times$1500 amplification from readout circuitry).

The difference between the EI's from both devices is as expected. The higher density of electrodes on the 519-electrode device results in a larger number of electrodes recording action potentials from a neuron. Referring to Figure 4.19, typical action potentials generated from each region of the cell are highlighted. The soma generates a bipolar signal (a). Signals from dendrites (b) are typically bipolar of opposite polarity and the axonal signals (shown
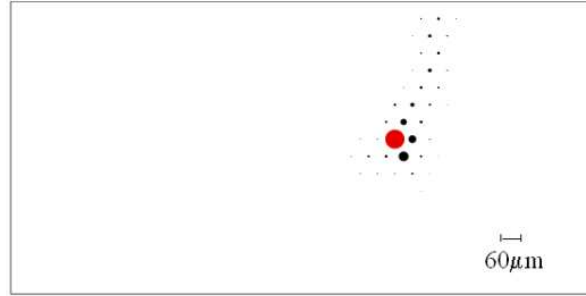
Figure 4.18: Electrophysiological image of a midget ganglion cell as recorded from a 60 μm spacing 512-electrode array. The bounded area represents the array coverage area and the red dot represents the electrode closest to the soma.

at 2 positions on the axon) (c)(d) are triphasic. The ability to produce these images contributes greatly to the identification and classification of neurons [39]. The vertical scales are in mV as recorded by an ADC card. The amplifier gain was ×1500, so 15 mV recorded signal corresponds to ∼10 μV signal on the electrode.

Cell mosaics

The response properties of identified neurons are measured by correlating the visual images focused on the retina with the spiking activity of the neuron. Using the white noise stimulus, the light sensitive region (the receptive field, RF) associated with each neuron is measured and the plotted as a 2-D Gaussian. "Mosaics" of receptive fields of classes of neurons can be plotted where classes are determined by the size of the neurons' RFs (large or small) and the neurons' response properties (ON or OFF). Typically, the mosaic for OFF-small midget ganglion cells is particularly incomplete due to inefficient detection of this class of neuron by the 60 μm spacing 512-electrode array.
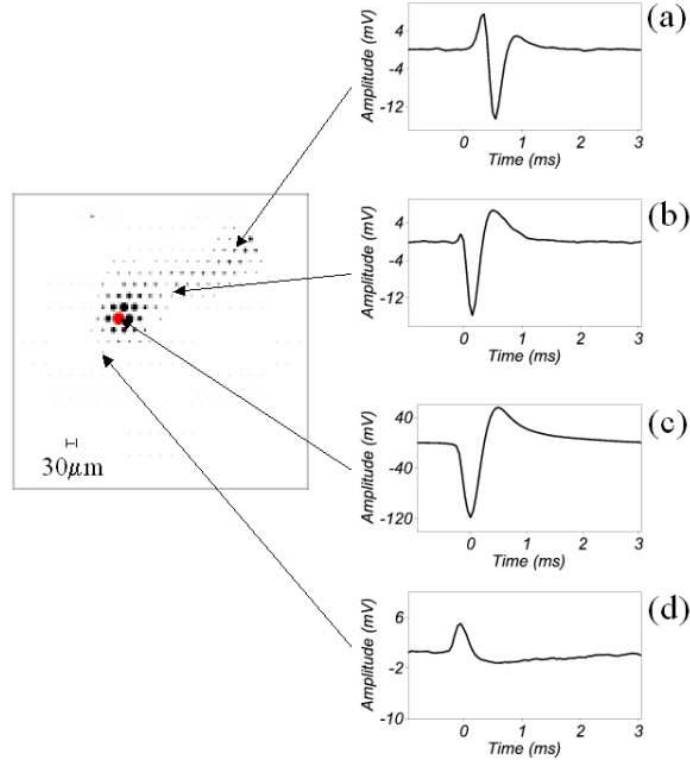
Figure 4.19: Electrophysiological image of a midget ganglion cell as recorded from the 30 μm spacing 519-electrode array. Typical action potentials from different regions of the cell are shown. The bounded area represents the approximate array coverage area. The vertical scales are in mV as recorded by an ADC card (after $\times 1500$ amplification from readout circuitry).

This inspired the development of a higher density array of electrodes in order to improve detection of this class of cell. A comparison of the OFF-small midget ganglion cell mosaics from the 60 μm and 30 μm spacing electrode arrays are shown in Figure 4.20.

Several large gaps can be seen on the 60 μm electrode spacing mosaic raising the question of whether it is a consequence of inefficient cell detection by the
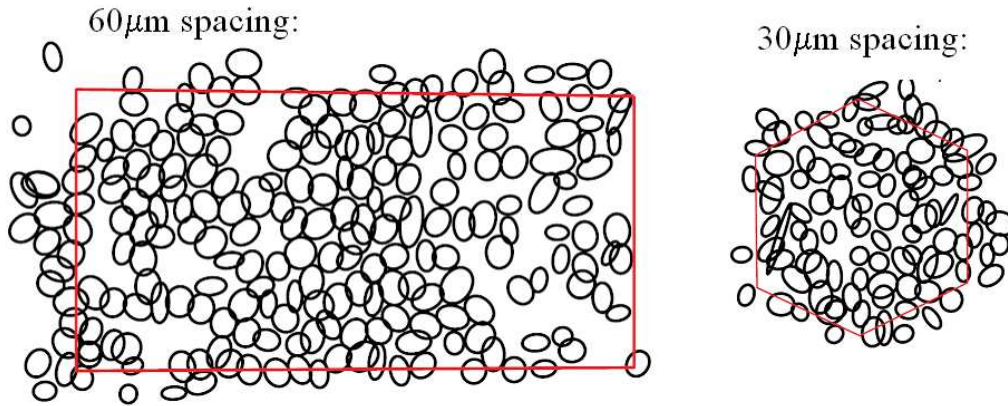
Figure 4.20: Mosaics for OFF-small midget ganglion cell classes from both 60μm and 30μm spacing electrode arrays. Largest gaps in 30 μm mosaic are a consequence of disconnected channels.

electrode array or a physiological effect. The 30 μm spacing 519-electrode array provides better detection, over a relative area, of OFF-small midget ganglion cells. The mosaic is from preliminary experiments using this array and since many factors can result in inefficient cell detection, including biological issues such as unhealthy tissue, further experimentation will hopefully improve cell detection further. Most importantly, the pilot data is extremely promising and a device is now in place for future experiments. From the results displayed earlier in this section the array is shown to behave well as a neuronal signal recording device and has already achieved success in its use to improve detection of OFF-small midget ganglion cells.

Chapter 5

Stimulating microelectrode arrays

5.1   Introduction

In recent years there has been an increased interest in the electrical stimulation of neurons via microelectrodes. The trend has been to use smaller area microelectrodes in order to focus the stimulation and excite individual cells. However, a challenge presented by this technology is forming a small electrode which is capable of repeatedly delivering current densities substantial enough to stimulate cells without the cell-electrode system exhibiting any deterioration [58] [59]. Electrodes with this capability allow the function of networks of neurons such as the retina to be probed further by measuring cells' responses to controlled electrical stimuli. Their usefulness also extends to the field of neural prosthetics as a biological implant would be required to deliver large currents through small conducting sites [60] and for long periods of time.

A popular material chosen for stimulating microelectrodes is iridium oxide because it has a porous structure and can assume several oxidation states [64] [65]. As a consequence, it has a high charge capacity and has also been shown to be resistant to dissolution and corrosion during biological stimulation [66] [67]. It is a particularly attractive material for the stimulation of neural tissues [68] [69] since it can dissipate charge through reversible faradaic reactions [70] [71] resulting in the formation of no new substances and hence no harmful reactants are released into the neural tissue. There are several methods of depositing this material including activation, electrodeposition, thermal deposition and sputter deposition (AIROF, EIROF, TIROF and SIROF respectively) and these have been investigated by several research groups. A summary of some deposition techniques can be found at reference [72]. For information on SIROFs and TIROFs, the reader is directed also to [73] [74] as they are not discussed any further in this thesis.

In this chapter, platinum black, AIROFs (activated iridium oxide films) and EIROFs (electrodeposited iridium oxide films) are investigated as materials capable of creating very small (5 μm diameter, 20 μm^2 area), low impedance, high charge capacity, durable and biocompatible electrodes for electrical stimulation of neural tissues. These particular iridium oxide deposition techniques were chosen as they are most easily adapted to suit the devices involved. With AIROF and EIROF techniques currents can be applied to individual electrodes to form the conducting oxide. Thermal and sputtered IRO films are not suitable for these devices since they cannot be deposited on selected areas. The deposition technique requires the whole device to be treated unlike AIROFs and EIROFs which rely on applying a current to the site to be oxidised.

These proposed electrodes can be compared with those manufactured by other groups for biological uses. Amongst the current state-of-the-art stimulating electrodes in terms of size are those offered through research at John Hopkins University, Baltimore. Iridium oxide electrodes with geometrical surface areas between 400 and 1600 μm^2 are manufactured [59] for neural prosthesis applications. Similar sized electrodes are also manufactured by groups at the EIC Laboratories, Massachusetts and Illinois Institute of Technology, Illinois [61] and are fabricated at the Huntington Medical Research Institute. Cone shaped activated iridium oxide electrodes with a geometrical surface area of 877$\pm$100 μm^2 are formed at the end of a wire shaft. The charge storage capacity of these activated iridium oxide electrodes is 23 mC/cm^2. Similar technologies include circular electrodeposited iridium oxide electrodes, 127 μm in diameter ($\sim$12667 μm^2 geometrical surface area), also manufactured at the EIC Laboratories, Massachusetts [62], and these have a charge storage capacity of 25-50 mC/cm^2. Another example of this technology, on a larger scale again, are electrodeposited iridium oxide electrodes produced at the University of North Carolina [63] and the EIROF is formed on the tip of a platinum wire (2 mm length, 1 mm diameter, 7.85 mm^2 area).

5.2 Electrical characterisation

Stimulating electrodes are electrically characterised in the same fashion as recording electrodes. It is necessary to measure the electrical impedance, inter-channel capacitance and inter-channel resistance, the methods of which were described in Section 4.3. However, for stimulating electrodes, it is also

important to quantify the charge capable of being delivered by each electrode and thereby its suitability for cell stimulation. The electrode charge capacity measurement theory and technique are described in this section.

5.2.1 Charge capacity

To measure each electrode's charge capacity, a method called cyclic voltammetry is employed [78] [79], a well established and important electrochemical technique. It involves measuring the current response of an electrode when excited by a potential waveform. The electrode being studied is immersed in an electrolytic solution (saline) and a triangular potential waveform is applied. A platinum wire (reference electrode) is inserted into this solution completing the circuit. The potentials at which reversal takes place are called switching potentials and are carefully chosen to protect the electrolytic solvent from undergoing a reduction-oxidation (redox) reaction. In this experiment, the solvent is water which has a potential window of approximately 2 V hence the choice here of -0.6 V and +0.7 V switching potentials (scan rate = 50 mV/s). It is recommended that the switching potentials remain at least 100 mV within the water window. The resulting cyclic voltammogram (a plot of current versus potential) traces the transfer of electrons during the redox reaction and has an area equal to the charge able to be delivered through the electrode, the electrode's charge capacity.

An example potential waveform and the ideal current response to this stimulus are represented in Figure 5.1. At the initial potential, a tiny anodic current is observed which immediately decreases to zero as the scan is continued. This initial negative current arises from the oxidation of the water in the electrolyte to give oxygen. As the scan continues, a cathodic current de-

velops due to the reduction of the electrolyte. A rapid increase in the current occurs as the concentration of reduced electrolytic ions becomes smaller. The current at the peak is made up of two components. One is the initial current surge required to adjust the surface concentration of the reactant to its equilibrium concentration. The second is the normal diffusion-controlled current. The first current then decays rapidly as the diffusion layer is extended farther away from the electrode surface.

(a)   (b)
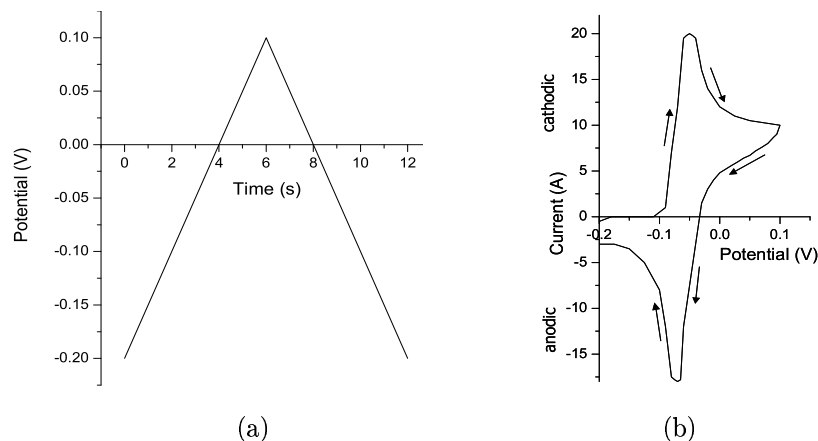
Figure 5.1: (a) Example of triangular waveform used to excite current response of electrode (b) Cyclic voltammogram showing ideal current response to triangular voltage stimulus. The scales on these figures are examples only.

When the scan direction reverses, the current continues to be cathodic until the electrolyte ceases to reduce. As a result of the re-oxidation of the electrolyte the current becomes anodic. This anodic current peaks and then decreases as the accumulated reduced electrolyte ions are used up by the anodic reaction. In brief, oxidation of the working electrode occurs at cathodic currents and reduction occurs at anodic currents [78], [79].

5.3 Platinum black

Initially, platinum black electrodes were investigated as a potential candidate for direct cell stimulation. This material performed very successfully as a low impedance interface to retinal tissue through saline solution and allowed the recording of retinal action potentials. The method of platinum black deposition, as well as evidence of its successful use as a recording electrode, is detailed in the previous chapter.

5.3.1 Platinum results

In Chapter 4, the optimum parameters for platinum black electrode formation were investigated. Using various current densities, well isolated 5 μm diameter platinum black electrodes were formed and electrically characterised.
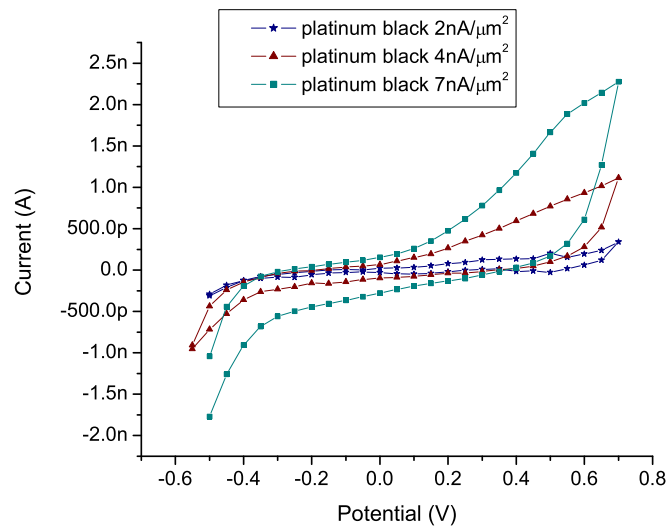
Figure 5.2: Cyclic voltammograms - Plots of the current responses of various platinum black electrodes to a triangular potential waveform.

Using the method described in the previous section, the charge capacity of

each electrode was then measured. Figure 5.2 shows the current responses of various electrodes to a triangular voltage cycle with switching potentials of -0.6 V and +0.7 V. Since the charge capacity is proportional to the area enclosed by the cyclic voltammogram, it can clearly be seen that an electrode's charge capacity increases with electrode area as would be expected. A complete account of the electrode characteristics are shown in Table 5.1.

I_d (nA/μm^2)	Z (kΩ)	Q_{cap} (mC/cm^2)
2	1940$\pm$133	0.083$\pm$0.0095
4	175$\pm$30	0.263$\pm$0.0035
7	121$\pm$45	0.591$\pm$0.025

Table 5.1: Impedance (Z) and charge capacity (Q_{cap}) values for electrodes platinised for 10 seconds at varying current densities (I_d). Values are averaged over three electrodes at each current density.

Referring to [80], it is recommended that mammalian retinal tissues (rat and monkey) require a charge density in the region of 0.2 mC/cm^2 to elicit a ganglion cell response. It is recommended that electrodes are capable of delivering charge at least an order of magnitude higher than the spiking threshold. Looking at Table 5.1 the charge capacity of platinum black electrodes make them unsuitable for direct electrical stimulation of retinal cells. Although platinum black electrodes formed at higher current densities (7 nA/μm^2) approach this recommended electrode charge capacity, their large and fragile structure is unsuitable. Platinum black electrodes formed at 4 nA/μm^2 are, in fact, used in electrical stimulation experiments at the Salk

Institute for Biological Studies, San Diego, however the electrodes are required to be re-platinised following each experiment. Therefore, they are not suitable for long-term stimulation studies. The alternative material studied here is iridium oxide [81].

5.4 Iridium oxide electrode deposition

5.4.1 Iridium electrode formation

Pure iridium

For these experiments, 60 μm spaced 61-electrode arrays were used with a 1 μm thick passivating Si_3N_4 layer. These arrays were fabricated using the procedure described in Section 3.7.1. The suitability of the arrays used was tested using procedures described in Section 4.3. These measurements included inter-channel capacitance and resistance measurements as well as electrical impedance spectroscopy and optical inspection. Both iridium oxide formation mechanisms require an initial layer of pure iridium, a noble metal showing resistance to oxidation and chemical attack, which is patterned using an acetone lift-off technique. Photolithography is firstly used to pattern S1818 photoresist with openings in the resist directly over the existing Si_3N_4 vias. A 15 minute chlorobenzene soak is employed to harden the top surface of the resist for a more effective lift-off (as described in Section 3.6). Onto this mask, a 100 nm layer of iridium is deposited using a Leybold peltier cooled magnetron sputter coater operated for 10 x 2 minutes at 75 mA. The excess iridium, surrounding the electrodes, is removed via lift-off in acetone to create pure iridium electrodes well contained within 5 μm diameter vias. In Figure 5.3, a 50x magnification of these electrodes is shown before and

after lift-off.

Figure 5.3: Images of 5 μm diameter iridium electrodes. Left: Before lift-off of excess iridium. Right: After lift-off only iridium electrodes remain.

Titanium/platinum/iridium electrodes

Although, the initial investigations of iridium oxide films were performed on 100 nm thick iridium electrodes, it is important for the electrodes to make contact with retinal tissue in biological experiments. To achieve this, the metal electrodes must fill the via in the passivating silicon nitride layer. This is accomplished by evaporating seed layers of 900 nm titanium followed by 100 nm platinum onto the photoresist mask. Titanium is an ideal initial layer as it adheres well to ITO and is inexpensive compared to platinum and iridium so can be used to form a thick film by evaporation. Platinum is used as the penultimate layer as it is noble and will not oxidise during the transition between deposition equipment. It also has a similar work function to iridium making it an ideal contact. A 100 nm thin film of iridium is finally sputter deposited onto the electrodes and lift-off is used to remove the unwanted metal (as above). Using a Veeko surface profiler, images of

both a pure iridium electrode and a Ti/Pt/Ir electrode were taken and are compared in Figure 5.4. A cross section of each electrode is also plotted and this shows the problem with the 100 nm iridium electrode. The iridium contact lies in the region of 0.8 μm below the surface of the silicon nitride insulating layer thereby preventing the electrode from making contact with neurons in retinal tissue. The Ti/Pt/Ir electrode seems much more promising for this purpose. The diagram on the top right shows that the Ti/Pt/Ir electrode stands around 500 nm proud of the surface of the silicon nitride. This will increase significantly the electrical connection between the electrode and neurons and defines the difference between a good and a poor stimulating electrode.
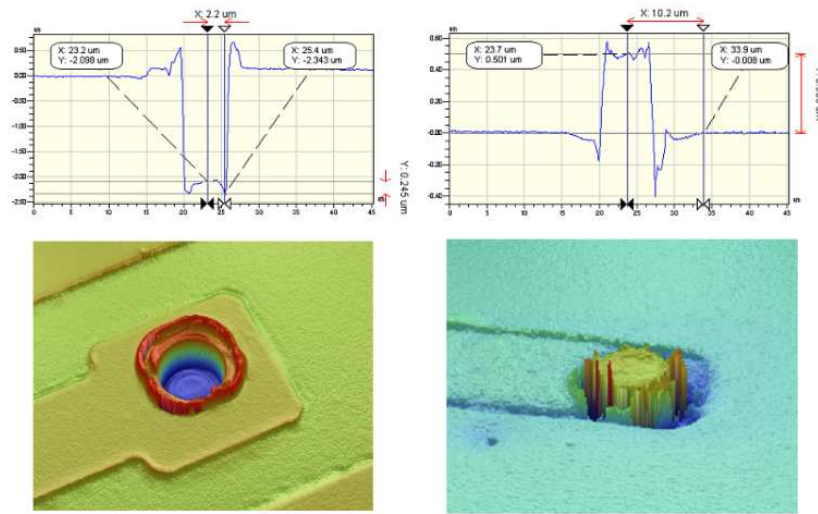
Figure 5.4: Surface profiles of pure iridium (100 nm layer) and Ti/Pt/Ir (1.1 μm layer) electrodes showing the unsuitability of thin electrodes for making contact with tissue.

5.4.2   Electrodeposited iridium oxide films

Using a procedure described by Yamanaka, iridium oxide electrodes were anodically electrodeposited. Whilst more in depth details of this procedure can be found at [75], the following sections describe the experimental work performed on 100 nm thick pure iridium electrodes, formed on ITO arrays of 61 and 519-electrodes.

Electrodepositing solution

The depositing solution was made from iridium tetrachloride, hydrogen peroxide, oxalic acid and potassium carbonate. The following recipe was used:

- Iridium chloride hydrate ($IrCl_4$,H_2O: 0.15 g) was dissolved in 100 ml of water using a magnetic stirrer for 30 minutes.
- 1 ml of aqueous hydrogen peroxide solution (H_2O_2: 30 wt.%) was added and the resulting solution was stirred for 10 minutes.
- Oxalic acid (($COOH)_2$,$2H_2O$: 0.5 g) was added and the resulting solution was stirred for 10 minutes. Anhydrous potassium carbonate was added very slowly to adjust the solution's pH to 10.2 (the solution saturated at this pH).
- The resulting solution was left to stabilise for 3 days.

Iridium tetrachloride is chosen to provide a source of iridium. Hydrogen peroxide allows the oxide to be deposited at lower current densities, although the mechanism here is unknown. Oxalic acid prevents precipitation in the solution. Potassium carbonate is used to increase the pH of the solution to make it alkaline and this is necessary since the oxides (or hydroxides) of iridium are not soluble in alkaline solutions. This leads to higher efficiency electrodeposition of iridium oxide from alkaline solutions containing iridium.

Electrodepositing mechanism

The electrodeposition of iridium oxide occurs as a result of the anodic oxidation of an Ir(IV) compound which is present in the depositing solution. This compound oxidises to produce an Ir(IV) oxide. The fact that an Ir(IV) oxide is obtained by the oxidation of an Ir(IV) compound can by interpreted by considering that iridium exists in the form of a complex compound in the depositing solution. For example, the reaction mechanism in which IrO_2 is formed by anodic oxidation of ligands in an Ir complex compound is:

$$(Ir(COO)_2(OH)_4)^{2-} = IrO_2 + 2CO_2 + 2H_2O + 2e^-$$
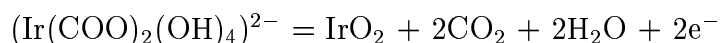
In this equation the oxalato ligand is oxidised to form CO_2, and IrO_2 is deposited. CO_2 evolution caused by oxidation of $(Ir(C_2O_4)_3)^{3-}$ with oxygen, is described in [72]. It is shown here that ligands in complex molecules of the depositing solution play an important role in the anodic electrodeposition of iridium oxides.

Electrodeposition technique

Electrochemistry is easily influenced by many factors and during the depositions it was important to vary only the current density and time to investigate optimum deposition parameters. To this end, the pH was monitored during depositions and the experiments were performed in a temperature controlled environment. Firstly a chamber is placed over the array of electrodes containing the electrodepositing solution, into which a platinum wire is placed. Deposition of iridium oxide then involves applying a constant current density for a period of time and there is no ideal recipe for this since every system varies. Here, electrodeposition was performed at various currents and times varying between 40 pA and 1 nA and 1 minute to 2.5 hours. The resulting

electrodes' impedances and charge capacities were measured.
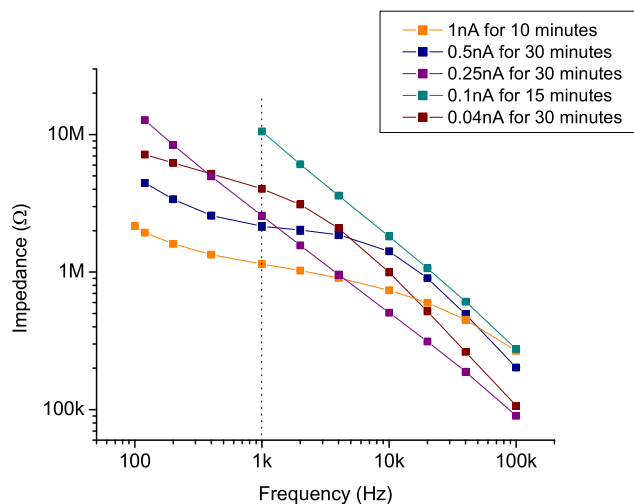
Figure 5.5: Impedance versus frequency for electrodes anodically electrode-posited with iridium oxide for various times. The vertical dotted line high-lights the impedance values at 1 kHz, the frequency of interest in these experiments.

Lowest impedance electrodes were found to be created by applying 1 nA to an ITO electrode through the electrodepositing iridium solution for 10 minutes. However, the impedance of these electrodes was still too high. The impedance measurements as a function of frequency are shown in Figure 5.5 for electrodes electrodeposited using various currents. The deposition time plotted is that which gave the lowest impedances. In many cases, longer depositions resulted in an increase in impedance or a plateau. Figure 5.6 shows the variation of the iridium oxide electrode impedance with time for 1 nA deposition. For these electrodes, the charge capacity was attempted to be measured but consistent measurements were unable to be taken. It was concluded for this form of iridium oxide that neither the impedance or the
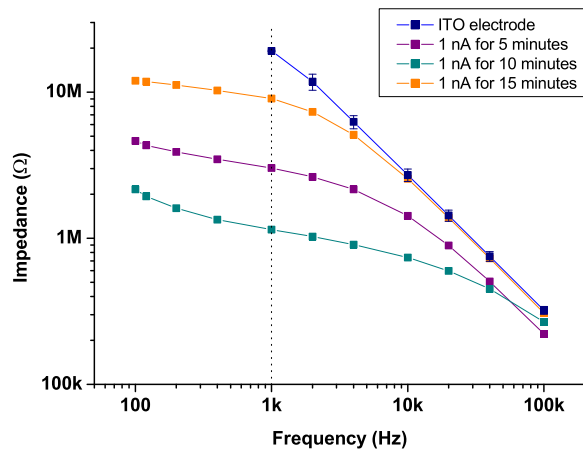
Figure 5.6: Impedance versus frequency for electrodes anodically electrode-posited with iridium oxide at 1 nA for various times.

charge capacity were suitable hence the need to investigate another method.

5.4.3   Activated iridium oxide films

The second method of depositing iridium oxide that was investigated was activation. Although it also employs electrochemical techniques for oxide formation, it differs from electrodeposition in that it chemically alters the existing iridium to form iridium oxide.

Experimental method

In initial tests, a procedure described by A. Blau [76] was followed to activate 100 nm thick, pure iridium electrodes. This process for oxidising iridium uses an electrochemical technique called cyclic voltammetry. Cyclic voltammetry is also employed to determine the electrodes' charge capacity and is described in more detail in Section 5.2.1. It requires an electrode cell to be setup. The

array of iridium electrodes (working) are covered in 1 M sulphuric acid into which a platinum wire and a silver chloride wire are inserted (counter and reference electrodes respectively). Across the working and counter electrodes, a triangular voltage profile is applied at a constant scan rate of 0.15 V/s between fixed anodic and cathodic switching potentials (-0.7 and 0.8 V). Precise control of the external applied potential is required, however this is difficult with a two-electrode system, due to the potential drop across the cell due to the solution resistance (potential drop (E) = current (i) x solution resistance (R)) and polarisation of the counter electrode required to complete the current-measuring circuit. Better potential control is achieved by using a third (reference) electrode, allowing the potential of the working electrode to be controlled relative to the reference electrode. In this case a silver chloride reference electrode is placed in the electrolyte. By this means iridium oxide films, whose thickness is controlled by the number of voltage cycles (100 to 10000), are obtained.

Activation mechanism

During the anodic potential sweep, an inner oxide (IrO_2) is formed from pure iridium. As the potential increases, the inner oxide changes to a hydrous outer layer ($Ir(OH)_3$). The fact that this layer is hydrated (water molecules are attached) limits formation to a monolayer.

The cathodic sweep causes reduction of the inner oxide back to iridium but does not go low enough to reduce the outer layer. The outer layer remains. Since the oxide is porous, the metal maintains contact with the electrolyte. Therefore, on the next potential sweep the process will repeat. In this way, a hydrous porous layer of iridium oxide is created. The potential limits are

chosen within the water window ensuring oxygen or hydrogen evolution do not occur. This mechanism is illustrated in Figure 5.7.
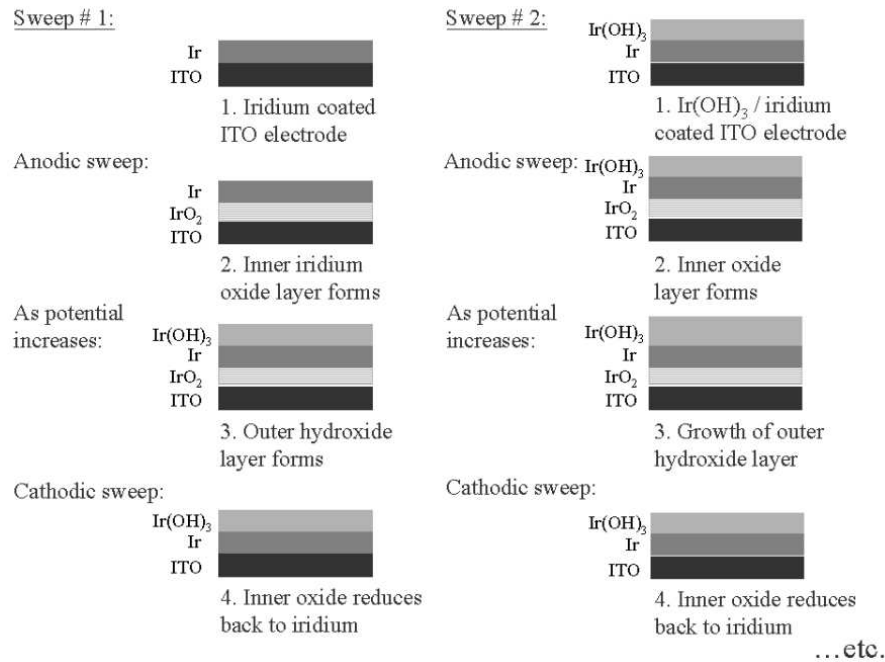
Figure 5.7: A schematic of the mechanism by which iridium is activated to form iridium oxide.

5.5 Electrode characteristics

To test their suitability for direct stimulation of cells, it is important to measure the electrodes' impedance and charge capacity. These test, respectively, their ability to record and deliver electrically to biological cells.

5.5.1 Electrochemical impedance spectroscopy

This procedure has already been described in Section 4.4.4 of the previous chapter. Figure 5.8 shows impedance measurements from various EIROF, AIROF and platinum black electrodes. From Figure 5.8 it is clearly shown that whilst platinum black electrodes, formed at 4 nA/μm^2, have the lowest impedance at 1 kHz, the iridium oxide films still have impedances at very acceptable levels for recording from cells.
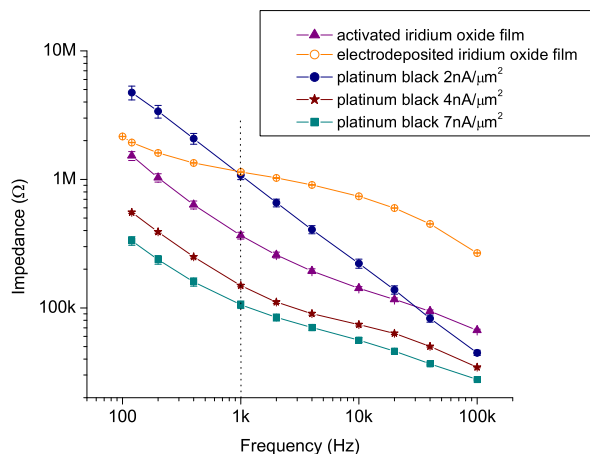
Figure 5.8: Impedance versus frequency comparison for EIROF, AIROF and platinum black electrodes. The frequency of interest is at 1 kHz.

5.5.2 Iridium charge capacity

The charge capacity of each electrode (EIROF, AIROF and platinum black) was calculated by finding the area of the current versus potential curve where current is scaled by a factor of 0.05 (potential scan rate). The above procedure was followed to obtain the cyclic voltammogram and in Fig. 5.9, the relevant plots are shown for each of the electrodes. It can be seen from Fig.

5.9 that activated iridium oxide films have a much higher charge capacity than EIROFs or any of the platinum black electrodes.
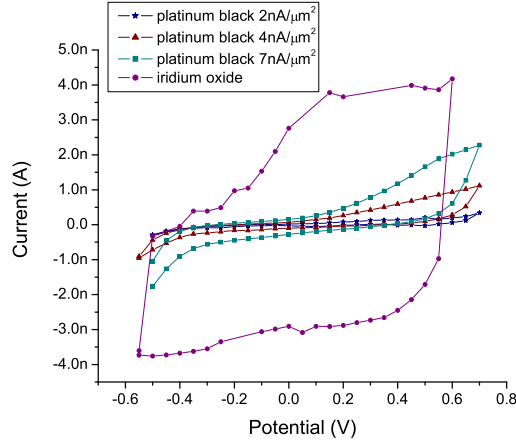
Figure 5.9: Cyclic voltammogram for AIROF and platinum black electrodes.

I_d (nA/μm^2)	Z (kΩ)	Q_{cap} (mC/cm^2)
2	1940$\pm$133	0.083$\pm$9.5
4	175$\pm$30	0.263$\pm$3.5
7	121$\pm$45	0.591$\pm$25
EIROF	1500	NA
AIROF	300	4.1

Table 5.2: Impedance (Z) and charge capacity (Q_{cap}) values for both platinum black and iridium oxide electrodes.

Table 5.2 assembles the electrical properties for each interface and by referring also to Fig. 4.10 it is shown clearly that for platinum black an increase in the electrode surface area results in increased charge capacity. They are still, however, an order of magnitude lower than the charge capacity of irid-

ium oxide which was calculated to be 4 mC/cm^2.

It can be seen from Fig. 4.10 and 5.3 that, unlike the platinum black electrodes, which are fragile and lack durability, the iridium oxide electrode geometry is well defined and has a robust and durable structure. These are electrode properties ideal for the stimulation of retinal cells.

Chapter 6

Further Work and Applications

6.1   Introduction

This chapter is divided into two main sections. Firstly, work will be described which has been carried out with a view to the future of the project. This includes the design, fabrication and characterisation of more advanced microelectrode arrays. These arrays either incorporate a larger number of electrodes or a higher density. Also, an existing circuit model was adapted to represent electrically the microelectrode arrays. From this model, characteristics of proposed future devices can be calculated determining their electrical feasibility. A section is also devoted to possible applications of this work. The likelihood of an eventual retinal prosthesis is strong, with a large number of research groups world-wide working toward this goal. It would be beneficial if such an implant could be programmed with knowledge of how the retina translates the visual scene into electrical signals understandable by the brain. This information could potentially be discovered using the state-of-the-art devices fabricated using technology described in this thesis. Initial studies into small area iridium oxide electrodes paves the way for an

array of microelectrodes to stimulate electrically across a large area of retinal tissue. This would be an exciting technology to realise as it would also allow the field of brain studies to be ventured into in unprecedented detail.

6.2 Further work

It is foreseeable that in the future, larger area and higher density electrode arrays may be required. This inspired the design of both a 60 μm spacing 1027-electrode array and a 15 μm spacing 519-electrode array. The devices were designed and fabricated. Characterisation of the 1027 array was performed and the proof of concept 15 μm spacing array was modelled (model described in the next section) to predict its electrical characteristics. The processes and results are described in this section.
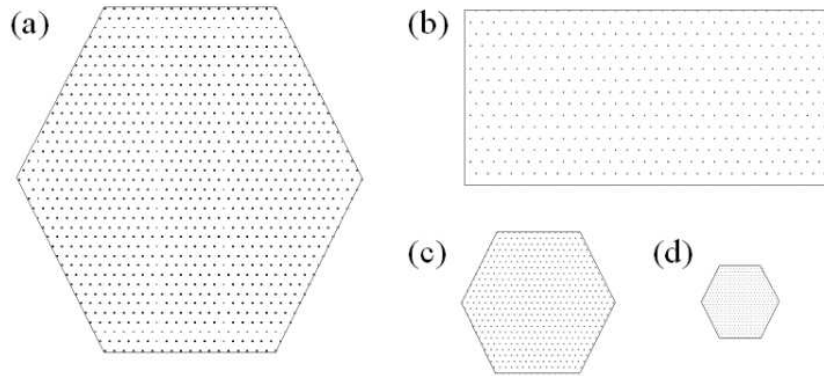
Figure 6.1: Diagram representing area covered by electrode arrays of various electrode number and density: (a) 1027 electrodes, 60 μm spacing (b) 512 electrodes, 60 μm spacing (c) 519 electrodes, 30 μm spacing and (d) 519 electrodes, 15 μm spacing.

6.2.1   1027 electrodes

An array of 1027 electrodes with inter-electrode spacings of 60 μm has a specific advantage over the previous 61- and 519-electrode arrays. Figure 6.1 shows the areas covered by various array sizes. The 1027 electrode array would allow an area of $\sim$7.1 mm^2 to be recorded from (4x larger than the most recent 60 μm spacing 512-electrode array), inevitably improving the study of cell connectivity. For comparison, this is compared to 8 mm^2 which is an example of a useful area of the retina for neural computation studies [39].
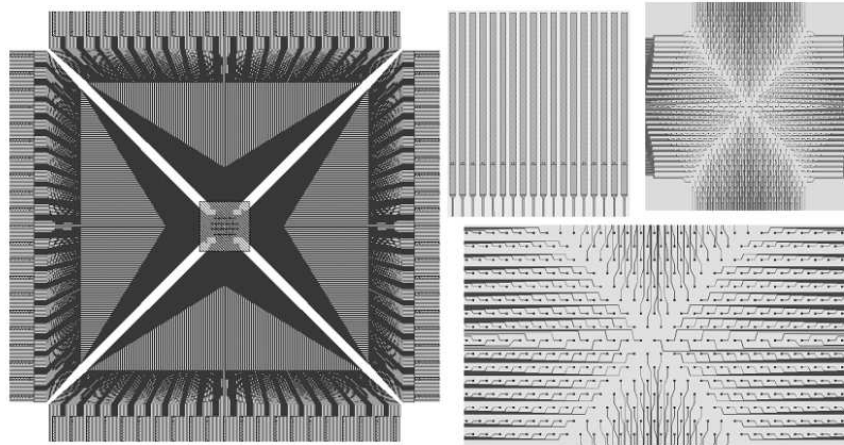
Figure 6.2: Design file of 60 μm spacing 1027 array design for submission to electron beam writer.

Figure 6.2 shows the layout design for the 60 μm spacing 1027-electrode array. The fabrication process for this new device is identical to that for the 519-electrode arrays (see Section 3.7.2, using solely electron beam lithography to transfer the pattern on to the ITO surface. The device, which is 3.2 x 3.2 cm in total, has 60 μm wide bond pads with 100 μm pitch. Images at various magnifications are shown of the 1027-electrode device in Figure 6.3.

The minimum feature sizes are 1 μm wires with 1 μm spacings. The ITO electrodes are 8 x 8 μm and are reduced to 5 μm once the passivating silicon nitride has been deposited and selectively etched.
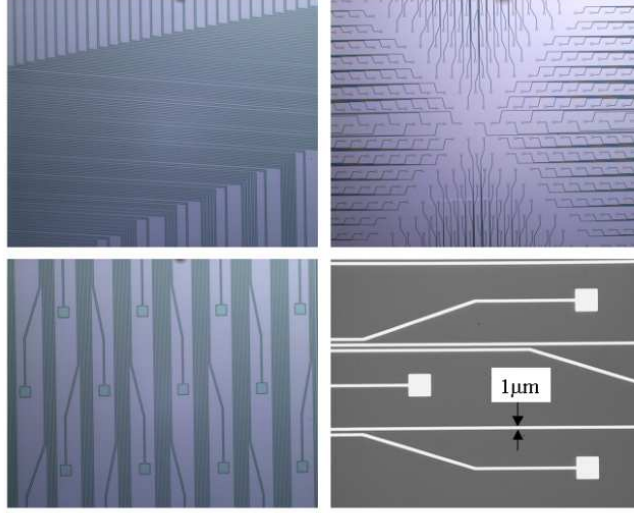
Figure 6.3: Images of the 60 μm spacing 1027 array fabricated on ITO/glass substrate using electron-beam lithography. Areas of highest resolution features are shown.

Once successfully fabricated, the device was electrically characterised following the procedures described in section 4.3. The inter-channel resistance was measured to be >200 GΩ showing good isolation of neighbouring channels, a crucial property. Figure 6.4 shows the inter-channel capacitance measurements for various positions along a side of the array and Figure 6.5 for capacitance between nearest neighbours. For comparison, the measurements for previous arrays are shown also. The five array positions referred to are spaced equally along one side of the device.

A final test was to platinise electrodes and measure the impedance. As hope-

d, the impedance of an electrode platinised for 10 seconds at 4 nA/μm^2 was found to be 270 kΩ at 1 kHz. Having completed all the above measurements, it was concluded that it is feasible to fabricate a working array of 60 μm spacing 1027-electrodes. The impedance versus frequency plot for an electrode is shown in Figure 6.6 alongside an image of the platinised electrode.
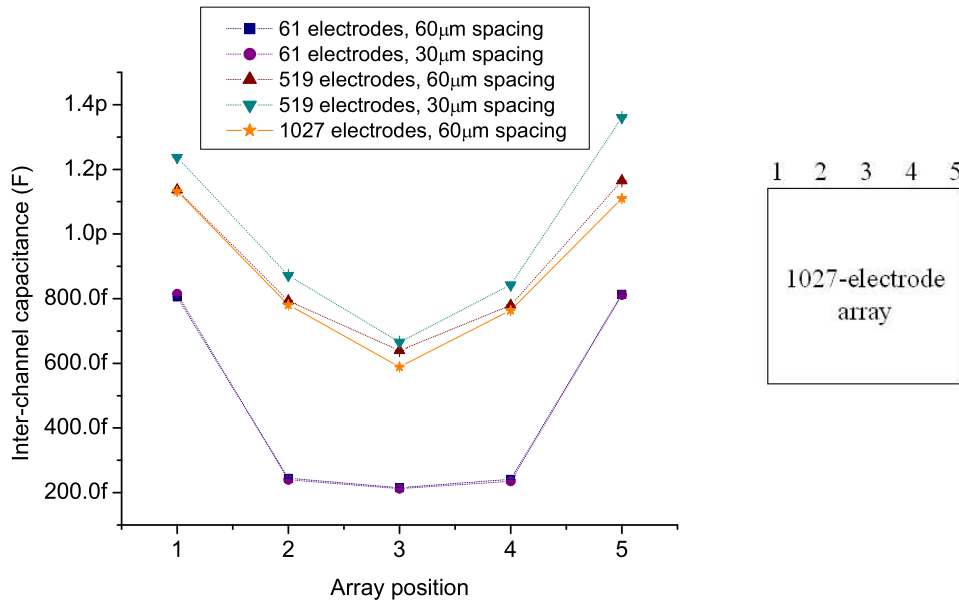
(a) Inter-channel capacitance measurements as a function of array position for 1027-electrode array where positions 1 - 5 are equivalent bond pad pairs spaced equally left - right along one side of an array.

(b) Electrode numbering system for 1027-electrode array.

Figure 6.4: Inter-channel capacitance measurements as a function of array position for 1027-electrode array.

Although the inter-channel capacitances for the 1027-electrode array are counter-intuitively lower than those of the 519-electrode arrays, it can be accounted for by differences in array fan-out. ITO wires leading from elec-
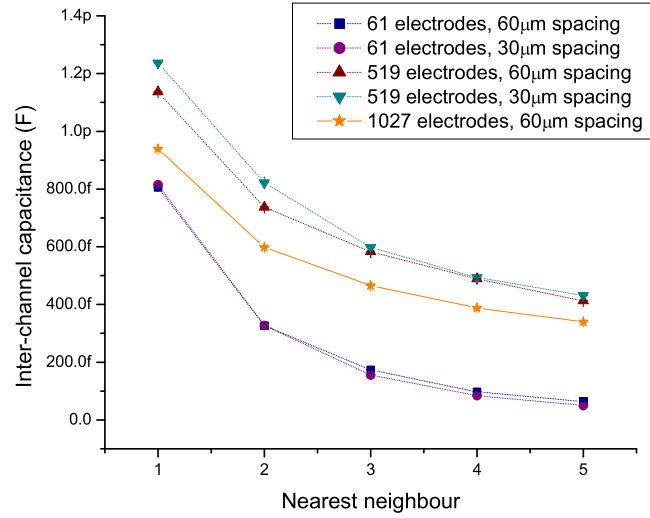
Figure 6.5: Inter-channel capacitance measurements as a function of nearest neighbours on the 1027-electrode array where 1 = electrode number 1. Nearest neighbours are represented by 2, 3, 4 and 5.

trodes on the 1027 array more immediately fan-out to wider spacings unlike the 519-electrode array where the wires are very closely spaced for a significantly longer length. This explanation is borne out in the results shown in Section 6.2.3. In conclusion, it can be said that the capacitance and impedance measurements taken from the 1027-electrode array compare very well with those from previous electrode arrays (61- and 519-electrodes) which perform well in biological experiments. These results are very promising for the use of an array of these dimensions in similar experiments.

6.2.2   15 μm spacing electrodes

An array of 519 electrodes with inter-electrode spacings of 15 μm was designed and fabricated. This will be a useful device for studying the foveal region of the retina where ganglion cells are packed much more closely to-
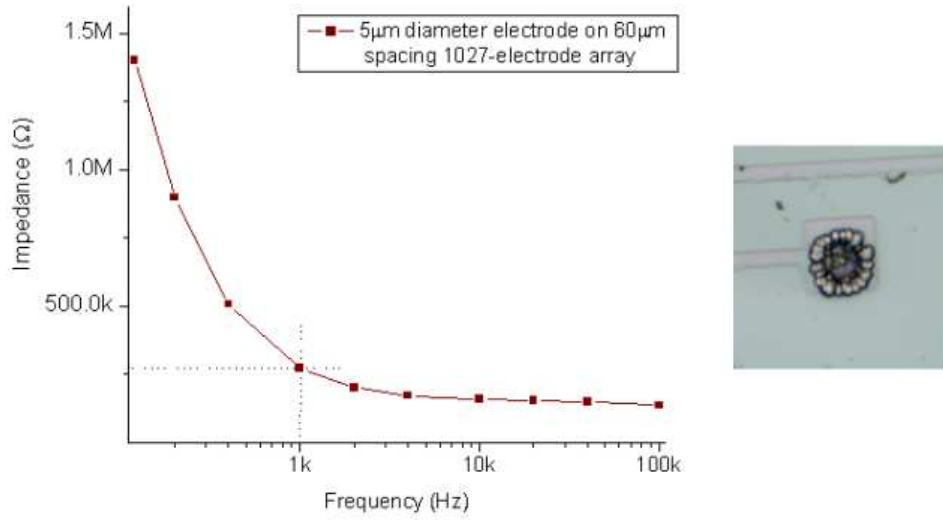
Figure 6.6: Left: Impedance versus frequency of electrode, on 1027-electrode array, platinised at 4 nA/μm^2 for 10 seconds. Right: Image of platinised electrode.

gether. This array challenges the existing semiconductor fabrication process in place as it requires a high density (500 nm spacing) of 500 nm wide tracks in the central region of the array. Initial studies have shown it is possible to pattern this feature size using the same electron beam lithography technique as for the previous 519 and 1027 electrode arrays. The inter-channel resistance of the device was measured to be greater than 200 GΩ proving that the wires are well isolated (not shorted). This eliminates the biggest potential concern with a device of these dimensions. Figure 6.7 shows images of the fabricated 15 μm spacing array.

Since this array was not passivated with silicon nitride and this layer allows electrodes to be platinised and is the dielectric for capacitive coupling measurements, electrode impedance and inter-channel capacitance values could

not be obtained. A promising consequence of the successful fabrication of this device, however, is that it has proven the ability to write a high density of 500 nm wires with 500 nm spacing.
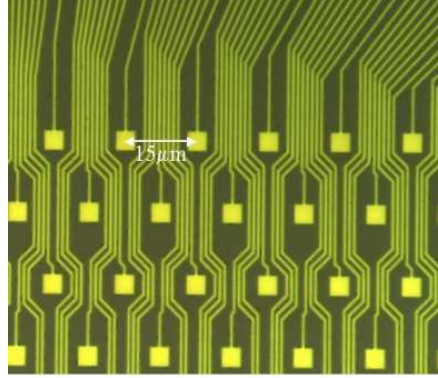
Figure 6.7: Images of the 15 μm spacing 519-electrode ITO array.

These are the feature sizes required for a 30 μm spacing 1027 electrode array. The door is therefore open to retinal studies on a larger and more in depth scale.

6.2.3 Test device

In order to investigate the limits of fabrication, a test array was fabricated using combinations of photolithography and electron beam lithography as described in Chapter 3. This test structure also allowed the investigation of the capacitive coupling between neighbouring channels and the effect that very narrow ITO tracks have on the recording capabilities of the electrodes. The test array design is shown in Figure 6.8. This study allowed the development of an equivalent circuit and offers insight into future higher density arrays. On the test device, ITO tracks with linewidths from 10 μm to 50 nm were fabricated over the lengths 40 - 5 mm. It was found that the limit of this

fabrication procedure was 400 nm wide ITO tracks. The capacitive coupling between channels with 1 μm separation was measured at 10 fF and increased to 85 fF when the separation was reduced to 800 nm.
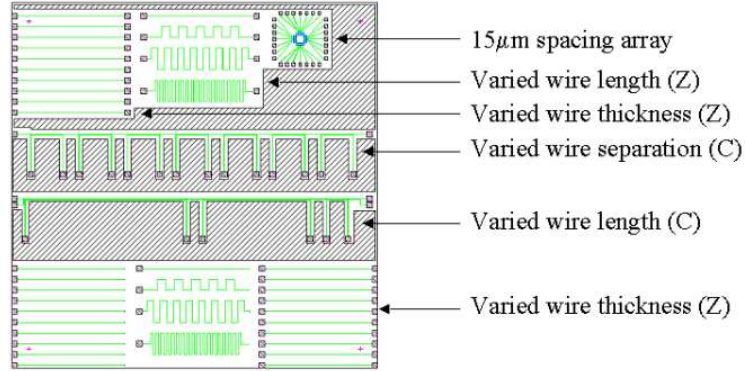
Figure 6.8: The design layout of the test array labelled with features for either measuring electrode impedance (Z) or inter-channel capacitance (C).
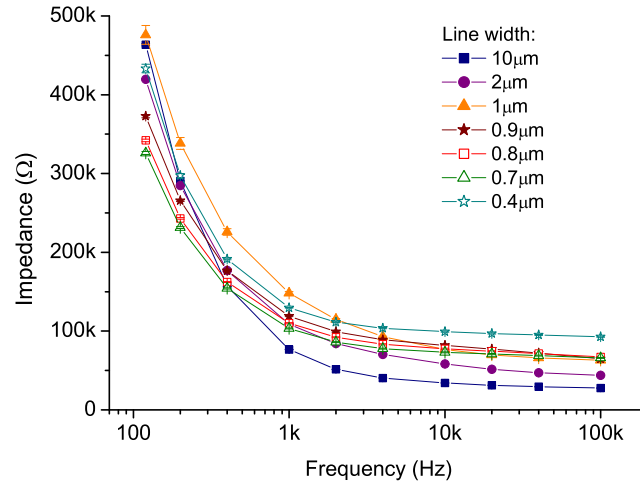
Figure 6.9: Comparison between impedances for line widths ranging from 400 nm up to 10 μm for tracks of length 5 mm

The impedance was found to be acceptable emphasizing the idea that, although the line width contributes to the overall impedance of the electrode-electrolyte interface it is not the dominant term. The factor which contributes most significantly to the impedance is in fact the quality of electrode platinisation. Figure 6.9 shows the impedance versus frequency plot for line widths ranging from 10 μm down to 400 nm, all of length 5 mm.

6.2.4 Equivalent circuit model

In conjunction with the tests described in the section above, a circuit model was formulated, based on early work by Chapman, Gouy and Helmholtz [82] and more recent work by Kovacs and Borkholder [83] [84], to represent the electrical characteristics of the electrode array. The equivalent circuit model is shown in Figure 6.10 and the relevant defining equations for the parameters shown are given in Table 6.1. These are theoretical values and are calculated from equations given.
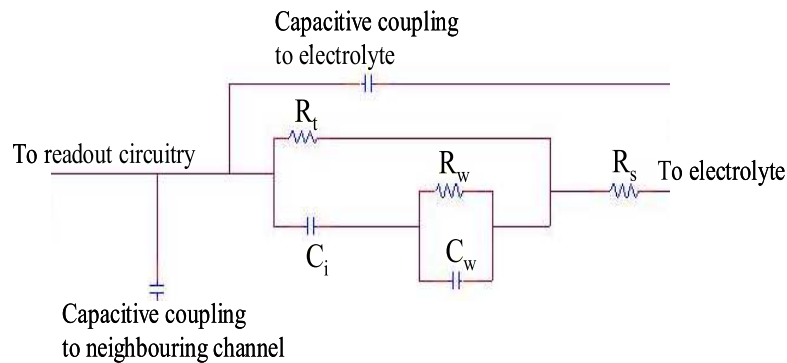
Figure 6.10: Equivalent circuit model for electrode/electrolyte interface

When a metal and electrolyte are in contact a complex space charge region is formed at the electrode interface. It can be described by the interfacial

capacitance, C_i, representing a layer of positive ions surrounding the negatively charged platinum black interface, and the charge transfer resistance, R_t, due to the DC current path across the electrode. Both these terms depend inversely on the surface area of the platinised electrode. Since the electrode/electrolyte interface does not behave exactly as a parallel plate capacitor, Helmholtz and Gouy-Chapman capacitances [83] are required in the definition of interfacial capacitance (see Table 6.1).

Parameter	Equation	Definitions
C_i	$\frac{1}{C_i} = \frac{1}{C_H} + \frac{1}{C_D}$	C_H = Helmholtz capacitance C_D = Gouy-Chapman capacitance
R_t	$R_t = \frac{\delta \eta_t}{\delta J}$	η_t = overpotential due to charge transfer J = exchange current density
R_s	$R_s = \frac{\rho}{4r}$	ρ = solution conductivity r = radius
R_w	$R_w = \frac{10^3 V_t}{z^2 q n^0 \sqrt{\pi f D}}$	V_t = thermal voltage, z = ion valence q = e$^-$ charge, n^0 = ions/litre in electrolyte f = frequency, D = diffusion coefficient
C_w	$C_w = \frac{1}{2\pi R_w}$	R_w = Warburg resistance

Table 6.1: Defining equations for parameters in circuit model used to simulate electrical characteristics of microelectrode array system.

The movement of charge into or out of an electrode requires a shift in its potential from its equilibrium value. This shift is referred to as the overpotential, η. A contributor to this term is the overpotential, η_t due to charge transfer. This term is important when calculating the charge transfer resistance. When in contact with an electrolyte under zero-bias conditions, an

electrode engages in chemical reactions which result in the accumulation of excess electrons at the surface of the metal. The value of J_0, the exchange current density, is a property of the electrode material and the chemical reactions taking place. These two terms (η_t and J_0) are used to define the charge transfer resistance. Also depicted is the spreading resistance, R_s, which accounts for the net resistance encountered by a current spreading out from an electrode into a conductive solution. This term depends inversely on the geometric area of the electrode (not the actual area [85]). For completeness the values are $C_i = 2$ nF, $R_t = 165$ MΩ and $R_s = 30$ kΩ. R_{ITO} represents the resistance of the ITO track and is a function of the track width. Finally, the Warburg terms, R_w and C_w, are due to diffusion effects which take place at higher frequencies than are of interest here. The Warburg model [86] [87] is based on the assumption that a sinusoidal potential applied to the electrode will force a sinusoidally varying spatial concentration function on the ions participating in electrochemical reactions.

Measurements from the test array gave R_{ITO} values ranging from 75 kΩ for the 400 nm track, to 7 kΩ for the 10 μm wide track. Using the PSPICE circuit simulator, this circuit allows a comparison between theoretical and experimental values of impedance to be made and can then be used to predict future array characteristics.

Results from equivalent circuit model

A comparison using data taken from the test structure and the PSPICE simulations is shown in Figure 6.11. As before, the frequency ranges from 100 Hz to 100 kHz and the line widths of interest, in this case are 10 μm and 400 nm. The two data sets are shown to be in good agreement with the

model and it predicts well the impedance of the electrode-cell interface at 1 kHz.
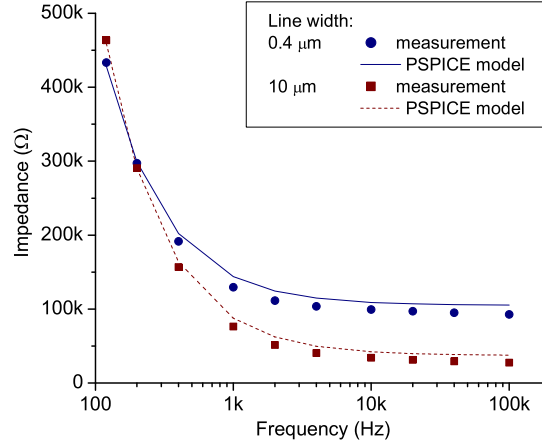
Figure 6.11: Comparison between PSPICE simulation and experimental data for impedance of 10 μm and 400 nm ITO tracks

It has been shown through these results that at 1 kHz, the impedance of the ITO traces down to a width of 400 nm is $\sim$200 kΩ. Since higher density arrays would require reduced line widths such as these, this is a significant result which promises the ability to fabricate arrays with thousands of electrodes spaced by 60 and 30 μm.

6.3 Applications

There are many scientific applications of the microelectrode arrays described in this thesis. Implications to the field of medicine could be significant as an understanding of how the retina processes the visual scene could conceivably lead to the manufacture of a retinal prosthesis for the blind [58] [88]. Such a device would be capable of imitating, through their electrical excitation,

the function of damaged or dead photoreceptor cells, caused by degenerative retinal diseases [20] [89], resulting in the restoration of sight. Also, although understanding retinal processing provides an interesting insight into the functions of this particular region of the brain, the microelectrode arrays used for the experiments described in Section 2.5 could be used to stimulate and record from other samples of brain tissue. In the following sections, however, direct applications of the high-density, large area, indium tin oxide microelectrode arrays, described in this thesis, are discussed.

6.3.1   Electrical stimulation

In the study of the behaviour of populations of neurons, it is desirable to have electrodes well matched in diameter and density to that of the neural network being studied. In particular, direct electrical stimulation studies of neural tissues would benefit greatly from arrays of small and durable stimulating microelectrodes, however, currently no technology exists to meet these requirements. Whilst arrays of 5 μm diameter, 60 μm spaced 61-platinum black electrodes have been used in cell stimulation experiments to deliver large current densities to neurons, they do not exhibit longevity and are required to be reformed post experiment [80]. Referring to the iridium oxide studies in Chapter 5, it was shown to be possible to form 5 μm diameter iridium oxide electrodes onto an ITO surface using an electrochemical activation technique. These electrodes were capable of providing a low impedance electrode/electrolyte interface ($\sim$200 kΩ at 1 kHz) and, most importantly, of delivering large enough charge densities for the direct stimulation of neurons (4 mC/cm^2). An interesting and beneficial application of this work to neuronal stimulation studies would be to form an array of these low impedance, high charge capacity, activated iridium oxide electrodes. Previously, irid-

ium electrodes were deposited on a 61-electrode array. The process used, however, could be adapted to accommodate higher density and larger area arrays. It would, therefore, be feasible to combine two technologies developed in this thesis: a state-of-the-art 30 μm spacing 519-electrode array with the developed iridium oxide films. Such a device could repeatedly stimulate populations of neurons at the highest spatial resolution, tissue coverage and durability available at present.

6.3.2 Cortical slice studies

The state-of-the-art 30 μm spacing 519-electrode array manufactured in this thesis has been very successfully employed in studies of mammalian retinal tissue. Whilst the planar, layered cellular organisation of the retina lends itself to recording from arrays of planar microelectrodes, the usefulness of these arrays are not restricted to recording and stimulating retinal cells. To further our understanding of how the brain functions, it is essential to study networks of neurons in the brain. This is a complex problem but studying slices of brain tissue is a first step in comprehending how brain cells communicate and store information. At the University of California, Santa Cruz, ongoing research on the neuronal processing, and in particular a phenomenon know as neuronal avalanches [90], of cortical slices has benefited from the spatial resolution and coverage offered by the microelectrode arrays fabricated in this thesis. Pilot experiments have, in fact, been performed using the 30 μm spacing array to record from and stimulate neurons in cultured rat cortex.

6.3.3 Retinal development

Another application of this 30 μm spacing 519-electrode array is to study, in unprecedented detail and coverage, the physiological properties of transgenic

mouse retina. In particular, retinal development could be more thoroughly investigated by firstly identifying a certain class of cell eg. direction selective and then monitoring these cells' development with time. The major goal of these experiments would be to target and understand the genes responsible for the incredibly well organised nature of cells in the retina.

Chapter 7

Conclusions

The work in this thesis has the potential to provide a major contribution to the study of retinal processing. The main aim was to fabricate a transparent, high density, large area array of microelectrodes for use in biological experiments. These experiments involve the read out of retinal ganglion cell responses simultaneously from hundreds of recording sites. The combination of size, density and coverage of the proposed electrode array are unprecedented. Fabricated onto a glass/ITO substrate, it has 519 hexagonally close packed electrodes with inter-electrode spacing of 30 μm and covers an area of 0.4 mm^2.

Arduous process development was required to achieve the successful fabrication of this device. Simultaneously reducing production time whilst increasing device quality and design flexibility, the existing process was adjusted to involve only electron beam lithography for the transfer of the device pattern onto the indium tin oxide surface. Initially, a combination of photolithography and electron beam lithography were involved in the manufacture of the devices. The new process was a significant step toward producing a high

quality microelectrode array as it greatly reduced the number of shorted channels. Another major advantage of the new technique was significantly decreased production time.

The main failure mechanism during the fabrication of these microelectrode arrays was the passivating silicon nitride layer which is deposited using a plasma enhanced chemical vapour deposition technique. A thick (2μm) layer is required to minimise coupling between the underlying ITO traces and the retinal cells positioned above the Si_3N_4. For a layer this thick, it is necessary to deposit very low stress Si_3N_4 and initially this caused many problems. The eventual transition to the SNF laboratories for this step of array fabrication improved the quality of the nitride, lowering the stress of the film whilst also allowing a thicker layer to be deposited in reduced time.

For use in the proposed biological experiments, strict boundaries exist for the electrical properties of these arrays. These were measured to confirm the device suitability for use. It was found that for well isolated, good quality electrodes, the inter-channel resistance was greater than 200 GΩ, inter-channel capacitance varied between 0.2 fF and 2 fF and the impedance across a platinised electrode was in the region of 200 kΩ. All of these properties are entirely suitable for the intended purpose of the array.

Pilot experiments were undertaken using macaque monkey retina and provided evidence of the 30 μm spacing 519-electrode array working very successfully as a high resolution, recording device. Retinal ganglion cell action potentials were recorded and electrophysiological images created which identified each cell over a larger number of electrodes and, as hoped, an increased

number of OFF-midget ganglion cells were detected. However, due to the many biological factors which can affect the outcome of an experiment, further experimentation is required using this device to quantify accurately its capabilities.

The existing process for the fabrication of 61-electrode arrays was also optimised. It now allows, using a select combination of photolithography, reactive ion etching, plasma and solvent cleaning, the transfer of the 61-electrode design onto the ITO surface exceptionally quickly and with a high success rate. This allows routine experimentation using these devices.

Also described in this thesis were investigations into adapting the previously described ITO microelectrode arrays into devices for direct electrical stimulation of neurons. Platinum black, the electrode/tissue interface used for recording experiments, was firstly studied. The additional characteristic, aside from impedance and inter-channel resistance and capacitance values, required of a cell stimulating electrode is that it can repeatedly provide large currents to tissue. With electrodes here measuring ~ 5 μm in diameter, this results in a high charge density and so it is necessary to calculate an electrode's charge capacity. On finding that the charge capacity of platinum black electrodes was lower than the ideal value [80], studies were undertaken on different forms of iridium oxide electrode.

Of the several iridium oxide film deposition techniques available, activated and electrodeposited iridium oxide films (AIROF and EIROF) were the most suitable for the devices being used here. Whilst less success was achieved electrodepositing iridium oxide, preliminary studies showed that well contained

5 μm diameter, low impedance and high charge capacity iridium oxide electrodes could be produced using an electrochemical "activation" technique. The electrode impedance was found to measure 50 % higher than typical platinum black electrodes but 300 kΩ is still entirely suitable for the electrode purposes. However, the AIROF charge capacity was calculated to be an order of magnitude greater than that of platinum black at $\sim$4 mC/cm^2. It was also found that the iridium films adhered well to the underlying ITO and were unmoved during solvent cleaning. Future studies would include using the activation technique to form a complete array of 61 low impedance, high charge capacity, 5 μm diameter iridium oxide electrodes which would be used in direct electrical stimulation experiments. Such experiments would provide more in depth detail of retinal cell processing.

Amongst development, characterisation and fabrication of working electrode arrays for both recording and electrical stimulation experiments, work was done to investigate the limits of this technology on array size and electrode density. An array was designed with 60 μm spacing 1027-electrodes. It was successfully fabricated, platinised and electrically characterised. The results showed this array to be worthy for biological use, however, a readout system with the correct pitch and number of channels, which does not currently exist, would be required for this array to be used. An array of 519 electrodes with unprecedented inter-electrode spacings of 15 μm was also fabricated. Due to time constraints, this array was not insulated with silicon nitride. However, the initial transfer of the pattern onto ITO, which is the most challenging step in the fabrication of this particular device as a consequence of 500 nm minimum feature size, was successful. The wires were unbroken and inter-channel resistance measurements proved good channel isolation.

An electrical model of the electrode/electrolyte was adapted and used to predict electrical characteristics of future higher density and larger area arrays and promised the feasibility of arrays of thousands of electrodes.

In conclusion, the work undertaken in this thesis has led to the development of a complicated process used for the successful fabrication of state-of-the-art transparent microelectrode arrays. This 30 μm spacing 519-electrode array is enabling the study of retinal processing and encoding of the visual scene in unprecedented detail. By recording the correlated activity of hundreds of neurons it has produced, in preliminary experiments, the most complete primate retina datasets available.

Bibliography

[1] A.L. Hodgkin and A.F. Huxley, 'A quantitative description of ion currents and its applications to conduction and excitation in nerve membranes', Journal of Physiology, Vol. 117, pp. 500-544, 1952

[2] D.H. Hubel and T.N. Wiesel, 'Receptive fields of single neurones in the cat's striate cortex', Journal of Physiology, Vol. 148, pp. 574-591, 1959

[3] Figure courtesy of http://www.esc13.net/socialstudies/neurons.htm

[4] Figure courtesy of http://www.oraculartree.com/hawkes_NoviceScientist3.html

[5] Y. Jimbo et al., 'A system for MEA-based multisite stimulation', IEEE Transactions on Biomedical Engineering, Vol. 50 (2), pp. 241-248, 2003

[6] Y. Jimbo and H.P.C. Robinson, 'Propagation of spontaneous synchronized activity in cortical slice cultures recorded by planar electrode arrays', Bioelectrochemistry, Vol. 51, pp. 107115, 2000

[7] K.D. Wise, J.B. Angell and A. Starr, 'An integrated-circuit approach to extracellular microelectrodes', IEEE Transactions on Biomedical Engineering, Vol. 17, pp. 238-247, 1975

[8] G.W. Gross et al., 'A new fixed array multimicroelectrode system designed for long-term monitoring of extracellular single unit neuronal activity *in vitro*', Neuroscience Letters, Vol. 6, pp. 101105, 1977

[9] G.W. Gross et al., 'Transparent indium-tin oxide electrode patterns for extracellular, multisite recording in neuronal cultures', Journal of Neuroscience Methods, Vol. 15, pp. 243-252, 1985

[10] G.W Gross et al., 'Stimulation of monolayer networks in culture through thin film indium-tin oxide recording electrodes', Journal of Neuroscience Methods, Vol. 50, pp. 131143, 1993

[11] J. Pine et al., 'Studying mammalian neurons *in vitro* with multielectrode arrays', Engineering in Medicine and Biology Society, Vol. 4, pp. 3686-3689, 2003

[12] D.A. Borkholder et al., 'Microelectrode arrays for stimualation of neural slice preparations', Journal of Neuroscience Methods, Vol. 77 (1), pp. 61-66, 1997

[13] G.T.A. Kovaks et al., 'Silicon-substrate microelectrode arrays for parallel recording of neural activity in peripheral and cranial nerves', IEEE Transactions on Biomedical Engineering, Vol. 41 (6), pp. 567-577, 1994

[14] L. Berdondini et al., 'High-density microelectrode arrays for electrophysiological activity imaging of neuronal networks', Electronics, Circuits and Systems, Vol. 3, pp. 1239-1242, 2001

[15] K.D. Wise et al., 'Wireless implantable microsystems: High-density electronic interfaces to the nervous system', Proceedings of the IEEE, Vol. 92 (1), pp. 76-97, 2004

BIBLIOGRAPHY

[16] P.A House et al., 'Acute microelectrode array implantation into human neocortex: preliminary technique and histological considerations', Neurosurgical Focus, Vol. 20 (5), pp. 1-4, 2006

[17] Santa Cruz Institute for Particle Physics, University of California Santa Cruz, California, http://scipp.ucsc.edu/groups/retina

[18] AGH University of Science and Technology, Krakow, Poland, http://www.ftj.agh.edu.pl/zej

[19] Salk Institute for Biological Studies, San Deigo, California, http://www.salk.edu/faculty/faculty/details.php?id=10

[20] R.W. Rodieck, 'The first steps in seeing', Sinauer Associates, pp. 38-55, 1998

[21] J.E. Dowling, 'The retina: An approachable part of the brain', Cambridge, MA, The Belknap Press of Harvard University Press, 1987

[22] SPIE - The International Society for Optical Engineering, http://photonicsclusters.com/history.html

[23] http://www.unhas.ac.id/ rhiza/saintis/haitham.html

[24] Figure courtesy of http://www.biologydaily.com

[25] Encyclopedia Britannica Macropedia, Sensory Reception, Britannica Inc., 1997

[26] R.G. Michels et al., 'Retinal detachment', The C.V. Mosby Company, 1990

[27] Figure courtesy of the Institute for Biological Information Processing http://www.fz-juelich.de/ibi/ibi-1/Photoreception

[28] B. Borwein, 'Scanning electron microscopy in retinal research', Scanning Electron Microscopy, (1), pp. 279-301, 1985

[29] S.G. Hormuzdi et al., 'Electrical synapses: a dynamic signaling system that shapes the activity of neuronal networks', Biochimica et Biophysica Acta, Vol. 1662 (1-2), pp. 113-37, 2004

[30] E.R. Kandel, J.H. Schwartz, T.M. Jessell, 'Principles of Neural Science', 4th edition, New York, McGraw-Hill, 2000

[31] P. Sterling and G. Matthews, 'Structure and function of ribbon synapses', Trends in Neurosciences, Vol. 28 (1), pp. 20-29, 2005

[32] W. Baehr and K. Palczewski, 'Photoreceptors and calcium', Springer, pp. 1-20, 2002

[33] D.M. Dacey, 'The mosaic of midget ganglion cells in the human retina', Journal of Neuroscience, Vol. 13, pp. 5334-5355, 1993

[34] R.A. Jacoby et al., 'Diffuse bipolar cells provide input to OFF parasol ganglion cells in the macaque retina', Journal of Comparative Neurology, Vol. 416, pp. 6-18, 2000

[35] E. Callaway, 'Structure and function of parallel pathways in the primate early visual system', Journal of Physiology, Vol. 566 (1), pp. 13-19, 2005

[36] A.M. Litke et al., 'Large-scale imaging of retinal output activity', Nuclear Instruments and Methods in Physics Research A, Vol. 501, pp. 298-307, 2003

[37] A.M. Litke and M. Meister, 'The retinal readout array', Nuclear Instruments and Methods in Physics Research, Vol. 310 (A), pp. 389-394, 1991

[38] W. Dabrowski et al., 'A low noise multichannel integrated circuit for recording neuronal signals using microelectrode arrays', Biosensors and Bioelectronics, Vol. 19, pp. 749-761, 2004

[39] A.M. Litke et al., 'What Does the Eye Tell the Brain?: Development of a System for the Large Scale Recording of Retinal Output Activity', IEEE Transactions on Nuclear Science, (2003)

[40] D. Gunning et al., '30 μm Spacing 519-Electrode Arrays for *In vitro* Retinal Studies', submitted to National Instruments and Methods, (2004)

[41] W. Dabrowski et al., 'Development of front-end ASICs for imaging neuronal activity in live tissue', Nuclear Instruments and Methods in Physics Research A, Vol. 541, pp. 405-411, 2005

[42] Stanford Nanofabrication Facility: http://snf.stanford.edu

[43] James Watt Nanofabrication Centre: http://www.elec.gla.ac.uk/jwnc

[44] E.J. Chichilnisky and R. Kalmar, 'Functional asymmetries in ON and OFF ganglion cells of macaque retina', Investigative Ophthalmology and Visual Science, Vol. 42 (4), pp. , 2001

[45] A. Ames and F. Nesbitt, '*In vitro* retina as an experimental model of the central nervous system', Journal of Neurochemistry, Vol. 37, pp. 867, 1981

[46] E.J. Chichilnisky et al., 'A simple white noise analysis of neuronal light responses', Network: Computation in Neural Systems, Vol. 12, pp. 199-213, 2001

[47] H.M. Sakai, 'White-noise analysis in neurophysiology', Physiological Reviews, Vol. 72 (2), pp. 491-505, 1992

[48] M.S. Lewicki, 'A review of methods for spike sorting: the detection and classification of nerual action potentials', Network: Computation in Neural Systems, Vol. 9, pp. R53-R78, 1998

[49] L.I. Smith, 'A tutorial on principal components analysis', http://csnet.otago.ac.nz/cosc453/student_tutorials/principal_components.pdf, 2002

[50] Thin Film Devices inc. website: http://www.tfdinc.com

[51] S.A. Campbell, 'The science and technology of microelectronic fabrication', Oxford University Press, New York, 2001

[52] S.M. Sze, 'Semiconductor Devices, Physics and Technology', Wiley, New York, 1985

[53] G.E. Moore, 'Cramming More Components onto Integrated Circuits', Electronics, Vol. 38 (8), pp. 114-117, 1965

[54] S.A. Bashar, 'Study of Indium Tin Oxide (ITO) for Novel Optoelectronic Devices', PhD thesis, Kings College London, 1998

[55] I. Adesida et al., 'Etching of Indium Tin Oxide in Methane/Hydrogen Plasmas', Journal of Vacuum Science Technology, Vol. 9 (6), 1991

[56] G. Schmitt et al., 'Passivation and corrosion of microelectrode arrays', Materials and Corrosion, Vol. 51, pp. 20-25, 2000

[57] M. Martynuik et al., 'Determination of residual stress in low temperature PECVD silicon nitride thin films', International Society for Optical Engineering Proceedings Series, Vol. 5276, pp. 451-462, 2003

[58] D.R. Merrill et al., 'Electrical stimulation of excitable tissue: design of efficacious and safe protocols', Journal of Neuroscience Methods, Vol. 141, pp. 171-198, 2005

[59] J.D. Weiland and D.J. Anderson, 'Chronic neural stimulation with thin-film, iridium oxide electrodes', IEEE Transactions on Biomedical Engineering, Vol. 47 (7), pp. 911-918, 2000

[60] P.R. Troyk et al., '"Safe" charge-injection waveforms for iridium oxide (AIROF) microelectrodes', Proceedings of the 26th Annual International Conference of the IEEE EMBS, 2004

[61] S. Cogan et al., '*In Vitro* comparison of the charge-injection limits of activated iridium oxide (AIROF) and platinum-iridium microelectrodes', IEEE Transactions on Biomedical Engineering, Vol. 52 (9), 2005

[62] R.D Meyer et al., 'Electrodeposited iridium oxide for neural stimulation and recording electrodes', IEEE Transactions on Neural Systems and Rehabilitation Engineering, Vol. 9 (1), pp. 2-11, 2001

[63] S.A.M. Marzouk et al., 'Electrodeposited iridium oxide pH electrode for measurement of extracellular myocardial acidosis during acute ischemia', Analytical Chemistry, Vol. 70, pp. 5054-5061, 1998

[64] T. Ohtsuka and K. Kunimatsu, 'In situ infrared spectroscopy of iridium oxide', Journal of the Electrochemical Society, Vol. 134, pp. 3090, 1987

[65] R. Kotz et al., 'Anodic iridium oxide films: XPS-studies of oxidation state changes and O_2-evolution', Journal of the Electrochemical Society, Vol. 131, pp. 72-77, 1984

[66] W.F. Agnew et al., 'Histopathologic evaluation of prolonged intracortical electrical stimulation', Experimental Neurology, Vol. 92, pp. 162-185, 1986

[67] L.S. Robblee et al., 'Activated Ir: An electrode suitable for reversible charge injection in saline solution', Journal of the Electrochemical Society, Vol. 130, pp. 731-733, 1983

[68] P.G. Pickup, 'A model for anodic hydrous oxide growth at iridium', Journal of Electroanalytical Chemistry, Vol. 220, pp. 83-100, 1987

[69] M. Huppauff, 'Valency and structure of iridium in anodic iridium oxide films', Journal of the Electrochemical Society, Vol. 140, pp. 598602, 1993

[70] X. Beebe and T.L. Rose, 'Charge injection limits of activated iridium oxide electrode with 0.2 ms pulses in bicarbonate buffered saline', IEEE Transactions on Biomedical Engineering, Vol. 35, pp. 494-496, 1988

[71] S.B. Brummer and M.J. Turner, 'Electrical stimulation of the nervous system: The principle of safe charge injection with noble metal electrodes', Bioelectrochemical Bioengineering, Vol. 2, pp. 13-25, 1975

[72] D. Prutchi and M. Norris, 'Design and development of medical electronic instrumentation', Wiley, pp. 326-334, 2005

[73] J.D. Klein et al., 'Morphology and charge capacity of sputtered iridium oxide films', Journal of Vacuum Science Technology, Vol. 7 (5), pp.3043-3047, 1989

[74] E. Slavcheva et al., 'Sputtered iridium oxide films as charge injection material for functional electrostimulation', Journal of the Electrochemical Society, Vol. 151, pp. E226-237, 2004

BIBLIOGRAPHY

[75] K. Yamanaka, 'Anodically electrodeposited iridium oxide films (AEIROF) from alkaline solutions for electrochromic display devices', Japanese Journal of Applied Physics, Vol. 28 (4), pp. 632-637, 1989

[76] A. Blau et al., 'Characterization and optimization of microelectrode arrays for in vivo nerve signal recording and stimulation', Biosensors and Bioelectronics, Vol. 12 (9-10), pp. 883-892, 1997

[77] University of Michigan Center for Neural Communication Technology, http://www.cnct.engin.umich.edu/www/probe4_activation.html

[78] D.A. Skoog, F.J. Holler, T.A. Nieman, Principles of Instrumental Analysis, 5th Edition, Saunders College Publishing, pp. 654-656, (1992)

[79] M. Noel, K.I. Vasu, Cyclic Voltammetry and the Frontiers of Electrochemistry, Aspect Publications Ltd., Chap. 2,3, (1990)

[80] C. Sekirnjak et al., 'Electrical stimulation of mammalian retinal ganglion cells with multielectrode arrays', Journal of Neurophysiology, Vol. 95, pp. 3311-3327, 2006

[81] X. Liu et al., 'Stability of the interface between neural tissue and chronically implanted intracortical microelectrodes', IEEE Transactions on Rehabilitation Engineering, Vol. 7 (3), pp. 315-326, 1999

[82] A.J. Bard and L.R. Faulkner, 'Electrochemical methods', Wiley, New York, 1980

[83] G.T.A Kovacs, 'Microelectrode models for neural interfaces', Enabling Technologies for Cultured Neural Networks, Academic Press, New York, pp. 121-165, 1994

[84] D.A. Borkholder, 'Cell based biosensors using microelectrodes', Dissertation, Department of Electrical Engineering, Stanford University, 1998

[85] D.A. Robinson, 'The electrical properties of metal microelectrodes', Proceedings of IEEE, Vol. 56 (6), pp. 1065-1071, 1968

[86] E. Warburg, Annalen der Physik und Chemie, Vol. 67, pp. 493-499, 1899

[87] E. Warburg, Annalen der Physik, Vol. 6, pp. 125-135, 1901

[88] J.I. Loewenstein, S.R. Montezuma and J.F. Rizzo, 'Outer retinal degeneration: An electronic retinal prosthesis as a treatment strategy', Archives of Ophthalmology, Vol. 122, pp. 587-596, 2004

[89] S. Haddad et al., 'The genetics of age-related macular degeneration: A review of progress to date', Survey of Ophthalmology, Vol. 51 (4), pp. 316-363, 2006

[90] J.M. Beggs and D. Plenz, 'Neuronal avalanches are diverse and precise activity patterns that are stable for many hours in cortical slice cultures', The Journal of Neuroscience, Vol. 24 (22), pp. 5216 5229, 2004